

**A Novel Adaptive Mismatch Cancellation  
System for Quadrature IF Radio Receivers**

by

Li Yu

A thesis submitted to the Faculty of Graduate Studies and Research  
in partial fulfillment of the requirements for the degree of Master of Engineering

Ottawa-Carleton Institute for Electrical Engineering,

Department of Electronics,

Carleton University,

Ottawa, Ontario, Canada

© Li Yu 1997

The undersigned recommended to the Faculty of Graduate Studies  
and Research acceptance of this thesis

“A novel Adaptive Mismatch Cancellation System for  
Quadrature IF Radio Receivers”

submitted by Li Yu ( B.Eng.) in partial fulfillment of the  
requirements for the degree of Master of Engineering

---

Thesis Supervisor

Professor Martin Snelgrove

---

Chairman, Department of Electronics

Professor Jim Wight

Carleton University

Oct.8 1997

---

## *Abstract*

This thesis investigates and resolves I/Q imbalances between the input paths of quadrature IF receivers. These mismatches along the paths result in the image interference aliasing into the desired signal band, thus reducing the dynamic range and degrading the performance of the receivers. I/Q errors occur because of gain and phase imbalances between quadrature mixers. They are also caused by capacitor mismatches in A/Ds which are designed to be identical for each input path.

This thesis presents a novel and feasible DSP solution for the I/Q mismatch problems. The system includes a novel complex LMS algorithm and a modified adaptive noise canceler (signal separator) to separate the desired signal and the image noise caused by the mismatch. The noise canceler can also solve the signal leakage problem, which is that the noise reference has the signal components.

This system was implemented in a Xilinx FPGA and an Analog Devices DSP chip. It was tested with a complex IF receiver which includes an analog front end and a complex sigma delta modulator. Both simulation results and test results show a dramatic attenuation of the image noise. Extending applications of the system to double sampling systems and N-path systems further indicates the robustness and feasibility of this novel adaptive mismatch cancellation system.

---

## *Acknowledgments*

I wish to express my gratitude to my supervisor Professor Martin Snelgrove for his support and guidance during the course of my M. Eng. studies at Carleton University.

I also like to thank:

Ashok Swaminathan, for providing his platform chips and assisting me with testing.

Peter Nyasulu, for sharing his knowledge on Xilinx FPGA design tools.

Philip Lauzon, for laying out the test boards.

and the rest of the radio group for their help.

Thanks to Philsar's Edward MacRobbie, for preparing and filing the preliminary disclosure patent on this work.

The financial and technical support of TRIO is gratefully acknowledged.

Most of all, thanks to my parents for their constant encouragement and support.

---

# Table of Contents

<b>Chapter 1 Introduction .....</b>	<b>1</b>
1.1. Motivation and Introduction .....	1
1.2. Contributions .....	3
1.3. Thesis Outline .....	4
<b>Chapter 2 Complex IF Receivers .....</b>	<b>6</b>
2.1. Introduction .....	6
2.2. Complex Filters .....	6
2.3. Complex Sigma-Delta Modulators .....	9
2.3.1. Architecture of a Fourth Order Complex Sigma Delta A/D .....	9
2.3.2. Advantages of Complex Bandpass Sigma-Delta Modulators .....	10
2.3.3. Mismatch Problem of I/Q Systems .....	11
2.4. Complex IF Receiver .....	14
2.4.1. Structure of a Single IF Receiver .....	14
2.4.2. Mismatch Problems .....	14
2.4.2.1 Gain and Phase Imbalance .....	15
2.4.2.2 Coefficient Mismatch .....	20
2.4.3. Interference .....	24
2.4.4. Examples .....	26
2.5. Conclusion .....	34
<b>Chapter 3 An Adaptive Algorithm for I/Q Channel Mismatch Cancellation</b>	<b>36</b>
3.1. Introduction .....	36
3.2. Previous Solutions .....	37
3.2.1. Off-Line Adjustment .....	37
3.2.2. Hilbert Transform .....	39
3.2.3. An Improved Sigma Delta Modulator Structure .....	40
3.3. An Adaptive Noise Canceler System .....	44
3.4. A Modified Adaptive Noise Canceler Model .....	46
3.4.1. Problems in the Classic Model .....	47

---

3.4.2. Improved Model .....	48
3.5. Complex LMS Algorithm .....	50
3.5.1. A Basic Complex LMS Algorithm .....	50
3.5.2. A Modified Algorithm .....	51
3.5.3. Decimation Filtering .....	52
3.6. A Simulink Model for the Complex A/D and the Modified Algorithm ...	56
3.7. Simulation Results .....	58
3.8. Further Application in Double Sampling Systems .....	61
3.8.1. A Gain Mismatch in Double Sampling Systems .....	63
3.8.2. Uneven Clock Phases in Double Sampling Systems .....	65
3.9. Conclusion .....	66
<b>Chapter 4 A Real Time Implementation and Further Applications .....</b>	<b>68</b>
4.1. Introduction .....	68
4.2. A real-time Implementation .....	68
4.2.1. RF Front End .....	69
4.2.2. Complex Sigma Delta Modulator .....	69
4.2.3. Decimation Filters and Interface to the DSP Board .....	72
4.2.4. Analog Devices ASDP 21020 .....	76
4.2.5. ASIC Option .....	77
4.3. Clock Rate Matching on the Interfaces .....	77
4.4. Performance of the real-time implementation .....	78
4.4.1. Experimental Results .....	78
4.4.2. Analysis of Experimental Results .....	79
4.4.3. SNR Versus Step size .....	82
4.4.4. Orders of Adaptive filters Versus SNR .....	85
4.4.5. Location of Interference .....	87
4.5. Conclusion .....	89
<b>Chapter 5 Conclusion and Future Work .....</b>	<b>90</b>
5.1. Summary .....	90
5.2. Conclusion .....	91
5.3. Future Work .....	92
5.3.1. ASIC Approach .....	92
5.3.2. N-path Systems .....	92

---

---

*APPENDIX A Assembly Code for the Novel Adaptive Algorithm .....100*

*APPENDIX B Coefficient Mismatch Effects in Single-pole Complex  
Filters .....106*

*APPENDIX C Power Inversion .....108*

---

## *List of Tables*

<i>Table 2.1 Receiver Parameters</i> .....	26
<i>Table 2.2 Desired signal and interference</i> .....	31

---

## *List of Figures*

<i>Figure 1.1: Architecture of a radio receiver</i> .....	2
<i>Figure 2.1: Complex filter block diagram</i> .....	7
<i>Figure 2.2: Mismatch model of the complex filter</i> .....	8
<i>Figure 2.3: Block diagram of a sigma-delta modulator</i> .....	10
<i>Figure 2.4: NTF frequency responses and zero-pole plots</i> .....	12
<i>Figure 2.5: Output spectra of a fourth-order sigma delta modulator</i> .....	13
<i>Figure 2.6: Single IF receiver structure</i> .....	15
<i>Figure 2.7: Output of balanced I and Q channels:</i> .....	17
<i>Figure 2.8: Output of imbalance I and Q channels</i> .....	18
<i>Figure 2.9: Degradation as a function of gain and phase imbalance</i> .....	19
<i>Figure 2.10: Complex pole realization</i> .....	21
<i>Figure 2.11: Mismatch model for the single-pole complex filter</i> .....	22
<i>Figure 2.12: Pole-zero plot, signal and image response plots of a single-pole complex filter</i>	23
<i>Figure 2.13: Degradation as a function of frequencies for 1% coefficients mismatch</i> .....	24
<i>Figure 2.14: Degradation as a function of frequencies and coefficients mismatch</i> .....	25
<i>Figure 2.15: Simulated output spectrum of the complex sigma delta modulator <math>I3+jQ3</math> without mismatch and without image interferences</i> .....	28
<i>Figure 2.16: Magnitude response of <math>I5+jQ5</math></i> .....	28
<i>Figure 2.17: Simulated output spectrum of the complex sigma delta modulator with 1% mismatch but without image interferences</i> .....	29
<i>Figure 2.18: Magnitude response of <math>I5+jQ5</math></i> .....	30
<i>Figure 2.19: Output spectra of the complex sigma delta modulator</i> .....	31
<i>Figure 2.20: Magnitude response of <math>I5+jQ5</math></i> .....	32
<i>Figure 2.21: Comparison of the eye diagrams between the input signal and the received signal: no mismatch, but with interferer, the eye diagram is unaffected by the interferer</i> .....	33
<i>Figure 2.22: Output spectra with mismatch</i> .....	34
<i>Figure 2.23: Eye diagrams of the degraded I, Q signal</i> .....	35
<i>Figure 3.1: A digital receiver with Hilbert Transform</i> .....	40
<i>Figure 3.2: Zero/pole constellations for the regular and improved complex NTFs</i> .....	40
<i>Figure 3.3: Power spectrum of a fourth order complex sigma delta modulator</i> .....	41

---

Figure 3.4: Power spectra of an improved fourth order complex sigma delta modulator .....	42
Figure 3.5: Power spectra for two fourth order complex bandpass sigma delta modulators with simultaneous image interference and 1% mismatches .....	43
Figure 3.6: Adaptive noise cancellation model .....	45
Figure 3.7: Modified adaptive noise cancellation model .....	49
Figure 3.8: Block diagram of the mismatch cancellation system (using bandpass filters) .....	53
Figure 3.9: Output spectrum after the mismatch cancellation .....	54
Figure 3.10: Block diagram of a CIC decimation filter .....	55
Figure 3.11: Matlab module and signal spectrum in each stage .....	57
Figure 3.12: Output spectra before and after using the mismatch cancellation system .....	58
Figure 3.13 : Output magnitude responses before and after the mismatch cancellation system .....	59
Figure 3.14: Eye diagrams before and after mismatch cancellation .....	60
Figure 3.15: Coefficients of the adaptive filter .....	61
Figure 3.16: Double sampling circuit model .....	62
Figure 3.17: Double sampling mismatch cancellation model .....	63
Figure 3.18: Ideal case .....	64
Figure 3.19 : Magnitude response with 5% gain mismatch in a double sampling sigma delta A/D .....	65
Figure 3.20: Magnitude response after mismatch cancellation system .....	66
Figure 4.1: Hardware system for testing .....	70
Figure 4.2: STF and NTF magnitude responses of a fourth order complex modulator .....	71
Figure 4.3: Real time structure of the decimation filter .....	73
Figure 4.4: Implementation of the decimation filter .....	74
Figure 4.5: ADSP-21020 memory read cycle .....	75
Figure 4.6: State diagram of the interface .....	76
Figure 4.7: Magnitude responses of the receiver output- before and after mismatch cancellation (Experimental) .....	80
Figure 4.8: Eye diagrams for I and Q channels- before and after mismatch cancellation (Experimental) .....	81
Figure 4.9: The adaptive transversal FIR filter .....	82
Figure 4.10: SNR versus stepsize (Experimental) .....	83
Figure 4.11: Coefficient convergencies for and (Experimental) .....	84
Figure 4.12: SNR versus orders of adaptive filters (Experimental) .....	87
Figure 4.13: Coefficients of the adaptive filter with the image interference at different frequencies (Experimental) .....	88

---

---

*Figure 5.1: N-path system model* .....92  
*Figure C.1 : Adaptive noise canceler with signal components leaking into the reference input.* .....108

---

## *Glossary of Terms*

STF	Signal Transfer Function
NTF	Noise Transfer Function
I	In-phase
Q	Quadrature-phase
ISI	Intersymbol Interference
SAW	Surface Acoustic Wave
MSE	Mean Square Error
LMS	Least Mean Square
DSP	Digital Signal Processing
LNA	Low Noise Amplifier
RF	Radio Frequency
IF	Intermediate Frequency
OSR	Oversampling Ratio
FPGA	Field Programmable Gate Array
CIC	Cascaded Integrator Comb
BiCMOS	Bipolar Complementary Metal Oxide Semiconductor
ASIC	Application Specific Integrated Circuit
GMSK	Gaussian Minimum Shift Keying
DFE	Decision Feedback Equalizer

# *Chapter 1*

---

## *Introduction*

Digital receivers with quadrature IF (Intermediate Frequency) architectures have been known for many years. This architecture has gained a great deal of interest recently as a potential candidate for use in single-chip digital radio receivers [Bollinger90][Schultes90]. But it is vulnerable to mismatch. Any gain or phase imbalance between the in-phase (I) and quadrature phase (Q) paths in the system causes an image noise to be aliased into the passband of the signal. This problem is investigated and a novel solution is developed in this thesis.

### **1.1 Motivation and Introduction**

Fig. 1.1 shows the general structure of a modern quadrature digital wireless receiver. The desired signal is transmitted at  $\omega_{LO} - \omega_{IF}$  and the receiver is unfortunately sensitive to image interference at a frequency  $\omega_{LO} + \omega_{IF}$ . In general, radio designers must reject image interferers by about 80~100 dB [Long96]. One way to get this performance is to filter the image out before the mixing stage (at point A). But for a low IF, this filter must be very selective and so becomes extremely expensive. Another method is to use I/Q mixing or image reject mixing [Macedo96] (at point B). This second technique has recently become important because high performance filtering is harder to integrate than mixers. The problem with this structure is that it is vulnerable to gain and phase errors in the LO (local oscillator), mixer, A/D and filters, which cause image

“leakage”, typical degrading the performance of receivers to rejection of only about 30 dB even with careful design. In this thesis, we attempt to improve the SNR by 10~20 dB in DSP. In the example to be given, we still use the image rejection filter at point A but with easier specifications.

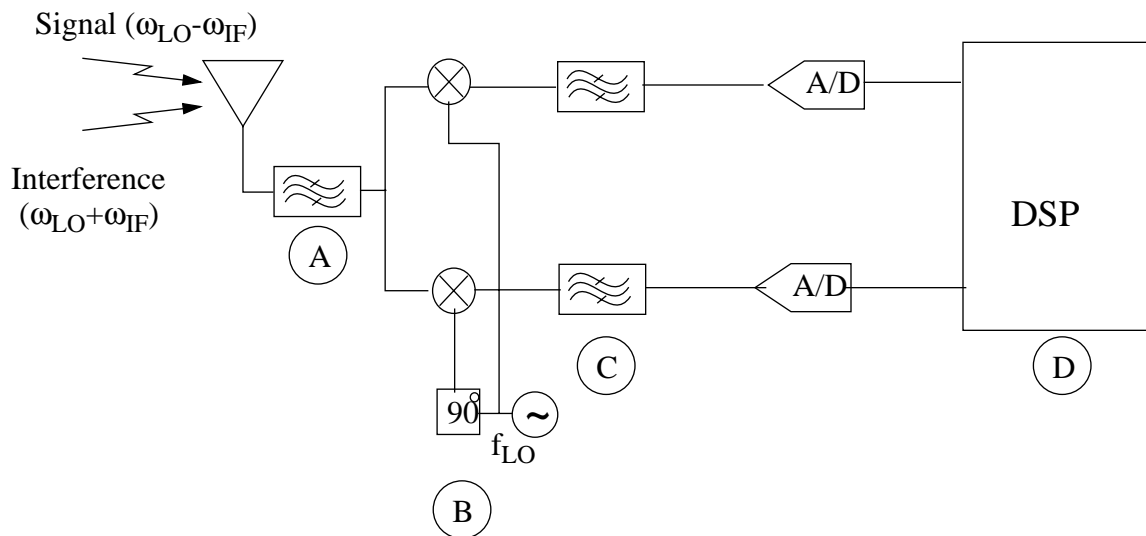


*Fig. 1.1 Architecture of a radio receiver*

In Chapter 2, we introduce a model of a complex IF receiver. The model includes an RF (Radio Frequency) front end with quadrature mixers and a two-input sigma delta analog-to-digital converter (A/D) as analog portions. It is difficult to achieve good balance between the I and Q paths due to the imperfection of the analog components. Both the RF front end and the A/D can introduce imbalance.

Many approaches for the correction of I/Q channel imbalance have been proposed using both analog and digital methods. Modifying the analog circuitry [Wiesbauer96], careful layout [Abdennadher92] and making the circuit more robust are the analog solutions [Swaminathan96a] [Jantzi96][Wiesbauer96]. Using off-line compensation of channel imbalances is a digital solution

---

introduced in [Carlson86][Schwartz90]. Other digital approaches such as using the Hilbert transform to generate I/Q signals in the digital domain are presented in [Trees68][Churchill81][Shenoi95].

In this thesis, a novel robust adaptive mismatch cancellation system is introduced. The new system uses a new complex Least Mean Square (LMS) algorithm and a modified adaptive noise cancellation model to compensate the SNR degradation due to the mismatch between the I and Q paths.

Both simulation and experimental results will be presented to confirm the feasibility of the algorithm and the system described. Finally, a real-time implementation of the system will be presented.

## 1.2 Contributions

This thesis addresses I/Q channel mismatch problems in digital receivers and proposes a novel and feasible DSP (Digital Signal Processing) solution for them. The core contribution is to show how to correct analog mismatches using the DSP technique. A preliminary disclosure for a patent on this work was filed in August 1997 [Snelgrove97]. The contributions are as follows:

1. A novel solution is found for problems caused by I/Q mismatches in quadrature receivers [Yu97][Snelgrove97].

Without modifying the analog design or using tedious correction procedures, this thesis shows how to use a novel adaptive DSP system to improve the SNR and therefore enlarge the dynamic range of digital receivers.

2. We show how to model and fix mismatch problems in the practical situation where the desired signal leaks into the noise reference [Yu97][Snelgrove97].

This system includes a new complex LMS algorithm and a modified classic adaptive noise cancellation system to separate the desired signal and the image noise.

3. A real-time implementation of a single IF complex receiver including the mismatch cancellation system is developed [Yu97][Snelgrove97].

The proposed mismatch canceler runs on a DSP chip. The implementation also includes decimation filters for the complex sigma delta A/D and the interface to the DSP chip.

4. We extend the proposed mismatch cancellation system to double sampling applications and N-path systems such as beamforming applications [Snelgrove97].

The presented system can be used in many applications other than I/Q systems. Mismatch and clock offset in double sampling systems are analogous to the mismatch in I/Q systems. With a small modification, our system can easily handle these problems. The implemented system can be further applied to N-path applications.

### **1.3 Thesis Outline**

This thesis is divided into five chapters and three appendices. Chapter 1 presented an introduction to I/Q channel mismatch problems and the contributions of the thesis.

The structure of a complex IF receiver and its performance degradation due to the imbalance between the I and Q paths are introduced in Chapter 2. I/Q mismatch problems are investigated and concepts such as complex filters, gain and phase imbalances are presented.

A novel DSP system to compensate the receiver performance degradation caused by the I/Q mismatch is developed in Chapter 3. This chapter introduces the novel adaptive algorithm and the mismatch cancellation system. Previous work done on compensation of the SNR degradation for quadrature systems is reviewed. Simulation results are also included in Chapter 3.

In Chapter 4, a real-time implementation of a complex IF receiver with the adaptive mismatch canceler is proposed. The novel adaptive algorithm is implemented in a DSP chip. The performance of the system is discussed with the experimental results. Extended applications of the system are introduced in this chapter.

Chapter 5 concludes the thesis.

Appendix A shows the assembly code implemented in the Analog Devices ADSP-21020 chip.

Appendix B is the derivation of mismatch phenomenon of a single-pole complex filter.

Appendix C is the derivation of the power inversion formula.

---

## Chapter 2

---

### *Complex IF Receivers*

#### 2.1 Introduction

In this chapter, the basic structure of a complex IF receiver system (I/Q system) is introduced. The way mismatch affects the performance of the receiver is also discussed.

In Section 2.2, the theory of the complex filter, its structure and mismatch effects are introduced. In Section 2.3, the complex sigma delta modulator and its mismatch effects are discussed. Based on the complex sigma delta modulator, a complex IF receiver is constructed and the performance degradation due to the I/Q channel mismatches in the whole receiver system is investigated in Section 2.4.

#### 2.2 Complex Filters

Complex filters are the basic components in complex systems (I/Q systems). A complex filter is a filter that has a transfer function with complex coefficients. It can, however, be modeled with several cross-coupled real filters [Allen85][Swaminathan96a][Jantzi96]. This is shown in Fig. 2.1 where the real part of the output  $Y_{re}(z)$  is the sum of the real part of the input  $X_{re}(z)$  fed through  $T_{Re1}(z)$  and the imaginary part of the input  $X_{im}(z)$  fed through  $T_{Im2}(z)$ ; the imaginary part of the output  $Y_{im}(z)$  is the sum of the real part of the input  $X_{re}(z)$  fed through  $T_{Im1}(z)$  and the

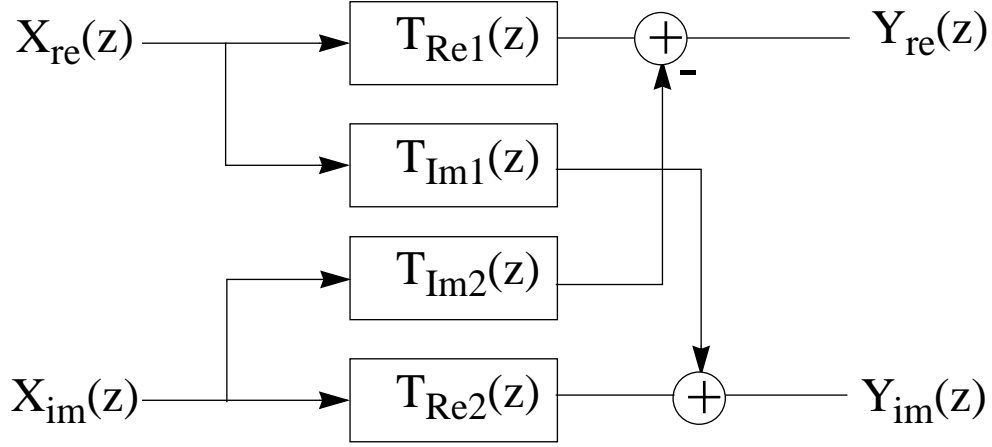


Fig. 2.1 Complex filter block diagram

imaginary part of the input  $X_{im}(z)$  fed through  $T_{Re2}(z)$ . In the ideal case,  $T_{Re1}(z) = T_{Re2}(z) = T_{Re}(z)$  and  $T_{Im1}(z) = T_{Im2}(z) = T_{Im}(z)$ , thus the transfer function of the complex filter is  $T_{nom}(z) = T_{Re}(z) + jT_{Im}(z)$ . Due to imbalances or coefficient variation in the transfer functions in the system, the two real-part transfer functions are not equal in practical situations and neither are the two imaginary-part transfer functions. Therefore, the complex filter no longer simply realizes a complex transfer function. It has been shown in [Allen85] that the transfer function of the mismatched filter can be written as a nominal term, a common-mode error term and a differential-error term.

$$Y(z) = T_{nom}(z)X(z) + \Delta T_{cm}X(z) + \Delta T_{diff}\overline{X(z)} \quad \text{Eq. (2.1)}$$

where  $\overline{X(z)}$  is the complex conjugate of  $X(z)$ ,

$$\Delta T_{cm} = \left[ \frac{T_{Re1}(z) + T_{Re2}(z)}{2} - T_{Re,nom}(z) \right] + j \left[ \frac{T_{Im1}(z) + T_{Im2}(z)}{2} - T_{Im,nom}(z) \right] \quad \text{Eq. (2.2)}$$

and

$$\Delta T_{diff} = \left[ \frac{T_{Re1}(z) - T_{Re2}(z)}{2} \right] + j \left[ \frac{T_{Im1}(z) - T_{Im2}(z)}{2} \right]. \quad \text{Eq. (2.3)}$$

The differential error  $\Delta T_{diff}$  models differential changes between  $T_{Re1}(z)$  and  $T_{Re2}(z)$  as well as between  $T_{Im1}(z)$  and  $T_{Im2}(z)$ . It adds an error term which is a function of the complex conjugate of the input function. This is called image aliasing because it aliases signals between positive frequencies and the corresponding negative frequencies. On the other hand, the common-mode error  $\Delta T_{cm}$  is used to model common changes in  $T_{Re1}(z)$  and  $T_{Re2}(z)$  as well as in  $T_{Im1}(z)$  and  $T_{Im2}(z)$ .  $\Delta T_{cm}$  can be ignored because it is usually small compared to the  $T_{nom}(z)$ . Fig. 2.2 shows a mismatch model of a complex filter.  $\overline{(\cdot)}$  represents the complex conjugate operation. We

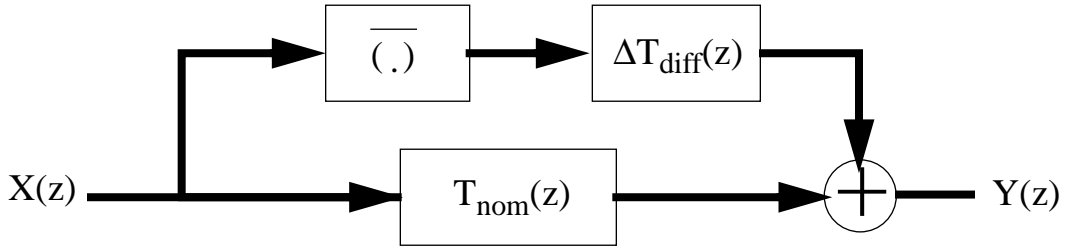


Fig. 2.2 Mismatch model of the complex filter

will show how to cancel the image due to the  $\Delta T_{diff}$  path in Chapter 3.

In the next section, we will see that the differential error term is always the main concern in the complex system and it degrades the performance of the system dramatically. We will use complex sigma delta A/Ds in the rest of the thesis.

---

## 2.3 Complex Sigma-Delta Modulators

From the previous section, we know the structure of a complex filter. Based on the complex filter theory, complex modulators can be built which have wider bandwidth than real modulators[Swaminathan96a][Jantzi94][Swaminathan97][Jantzi96][Aziz95]. In this thesis, only complex sigma delta modulators are discussed.

Sigma-delta modulation is a modulation scheme based on sigma delta A/D conversion technology. Oversampling and noise shaping are the characteristics of the sigma delta modulators[Candy92]. The oversampling method has the advantages of reduced complexity and higher SNR over the Nyquist sampling method for A/D and D/A conversion. Nyquist samplers require a complicated and high-precision analog lowpass filter (often called an anti-aliasing filter) to limit the maximum frequency input to the A/D which is vulnerable to noise and interference. On the other hand, oversampling converters can use simple and relatively high-tolerance analog components, by taking advantage of the VLSI technology suited for providing fast and complex digital circuits.

The noise transfer function in sigma-delta modulators is a highpass filter. Thus, quantization noise is shaped out of the band of interest. This is therefore called noise shaping.

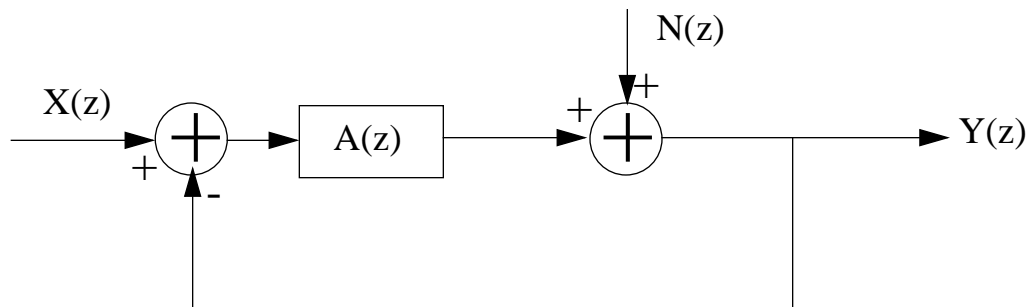
### 2.3.1 Architecture of a Fourth Order Complex Sigma Delta A/D

The sigma-delta model shown in Fig. 2.3 includes the signal transfer function (STF) and the noise transfer function (NTF). The summing node to the right of  $A(z)$  represents a quantizer. It is here that sampling occurs and quantization noise is added into the model.

The STF is defined as the transfer function between the input  $X(z)$  and the output  $Y(z)$  when  $N(z) = 0$ , while the NTF is defined as the transfer function between the quantization noise

$N(z)$  and the output  $Y(z)$  when  $X(z) = 0$ . For example, in the first order low pass sigma delta modulator,  $A(z)$  is an integrator. As the loop integrates the error between the sampled signal and the input signal, it low-pass filters the signal and high-pass filters the noise. In other words, the signal is left unchanged as long as its frequency content doesn't exceed the filter's cut-off frequency, but the sigma delta loop pushes the noise into a higher frequency band. For the bandpass sigma delta modulator, the quantization noise will be pushed out of band.

In sigma-delta modulator designs, the number of zeros in the NTF at a certain frequency controls the depth of the notch in that frequency. The more the zeros, the deeper the notch and the better the performance.



$$\text{Signal Transfer Function: } \frac{Y(z)}{X(z)} = \frac{A(z)}{1 + A(z)} \quad (\text{when } N(z) = 0)$$

$$\text{Noise Transfer Function: } \frac{Y(z)}{N(z)} = \frac{1}{1 + A(z)} \quad (\text{when } X(z) = 0)$$

*Fig. 2.3 Block diagram of a sigma-delta modulator*

### **2.3.2 Advantages of Complex Bandpass Sigma-Delta Modulators**

A complex bandpass sigma-delta modulator is a bandpass sigma-delta modulator which has a complex NTF. A complex NTF can achieve better performance than a real NTF for a given

order or numbers of zeros [Aziz95], because the depth of the notch depends on the number of the zeros in the band of interest, and because a complex NTF is not constrained to realize the zeros in complex conjugate pairs, all its zeros can be put in the band of interest. For example, Fig. 2.4 shows the frequency response of a fourth order complex NTF, a fourth order real NTF as well as an eighth order real NTF. We can see that the fourth order complex filter has almost the same bandwidth as the eighth order real NTF in the real frequency band but is more stable [Swaminathan97]. In terms of complexity, using the fourth-order real NTF would involve two modulators (for I and Q) for a total of eight integrators, the same complexity as the fourth-order complex case [Swaminathan96b].

### 2.3.3 Mismatch Problem of I/Q Systems

For I and Q systems, there is always a big concern about mismatch. Any imbalances between the two paths, such as component mismatch or gain/phase error in the mixer, means that there is a differential error between the two channels [Swaminathan96a][Tsui95]. Signals or noise at the image frequency will alias into the band of interest. For complex bandpass sigma-delta modulators, this situation is more serious because their frequency responses are asymmetric and the notches at the image band are usually much shallower than their real parts. Fig. 2.5 shows the output spectrum of a complex bandpass sigma-delta modulator ( $f_s=80\text{MHz}$ ) with and without a 1% coefficient mismatch in  $A(z)$  [Swaminathan97]. Coefficient mismatch refers to the coefficient differences between  $T_{\text{Re}1}(z)$  and  $T_{\text{Re}2}(z)$ , as well as  $T_{\text{Im}1}(z)$  and  $T_{\text{Im}2}(z)$ . In switched-capacitor circuits, these coefficients are implemented with capacitors. Thus, coefficient mismatch is caused by the imperfection of the capacitors.

It can be seen that with a 1% coefficient mismatch the SNR is degraded by 35 dB.

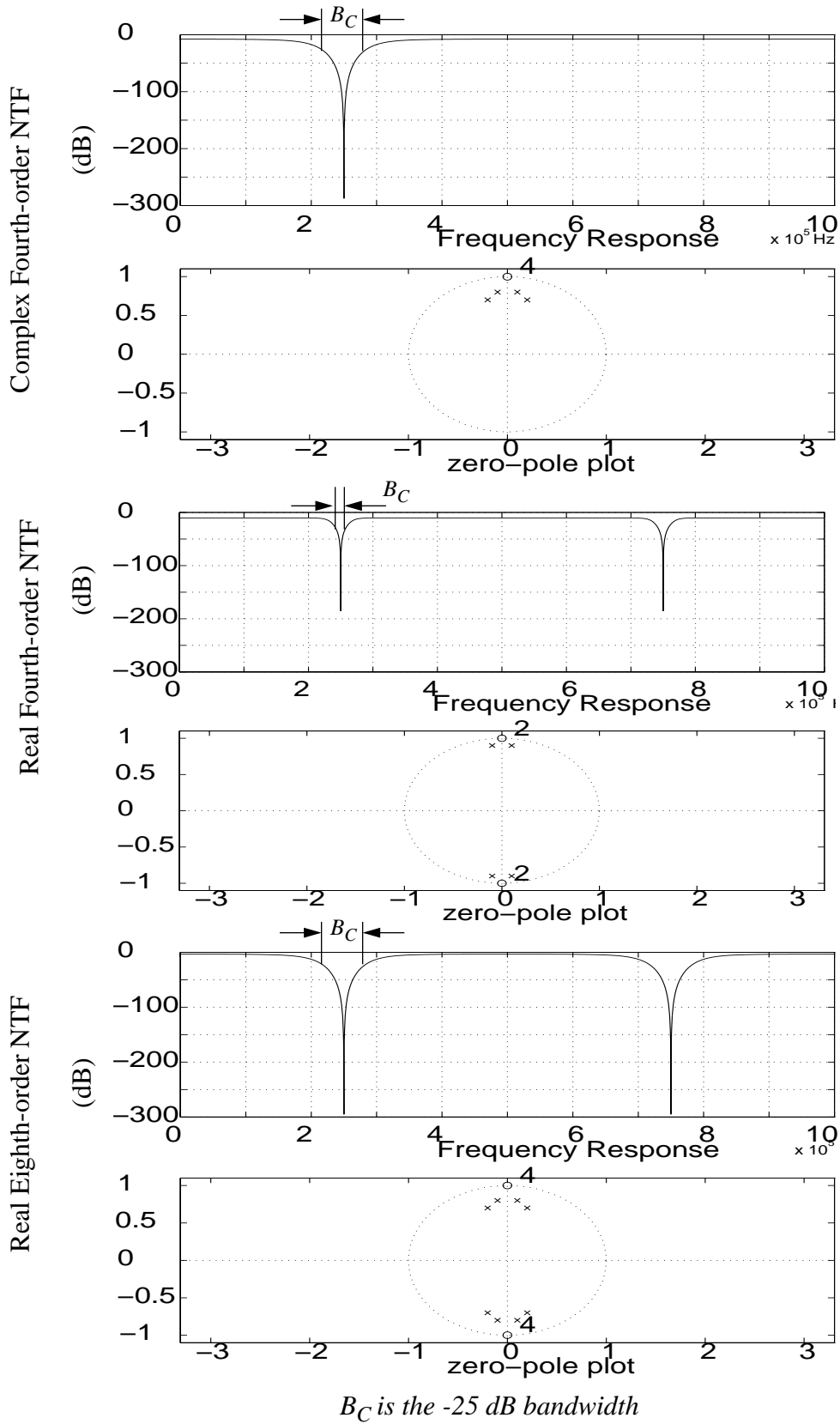
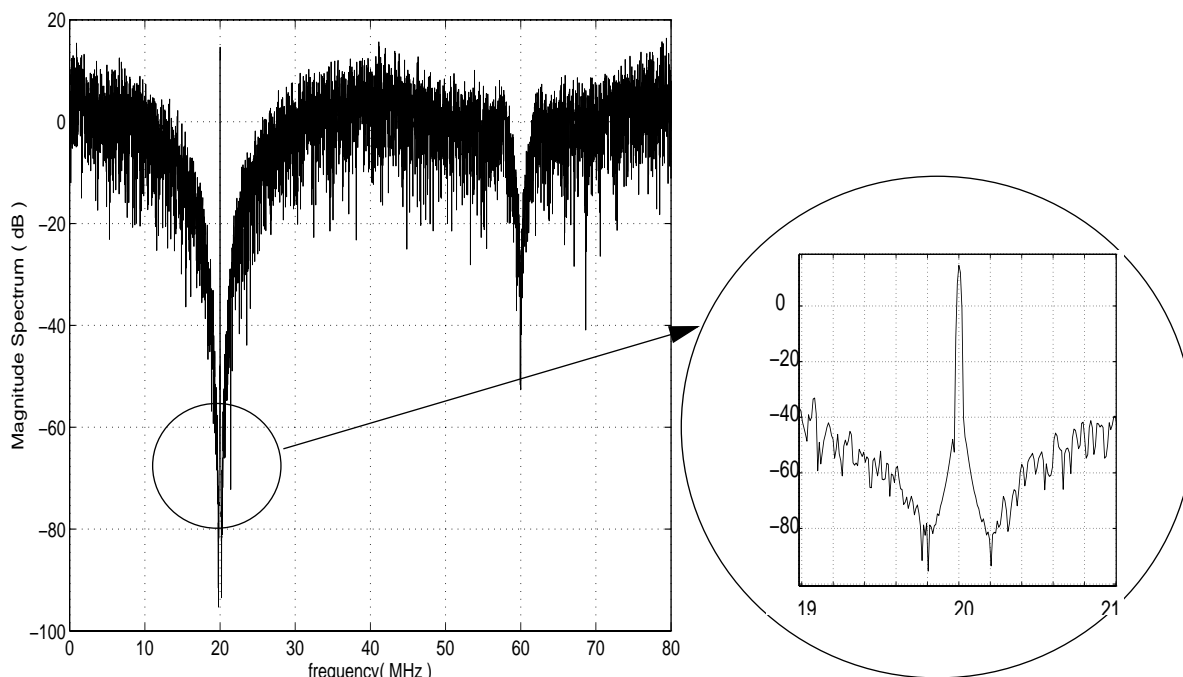
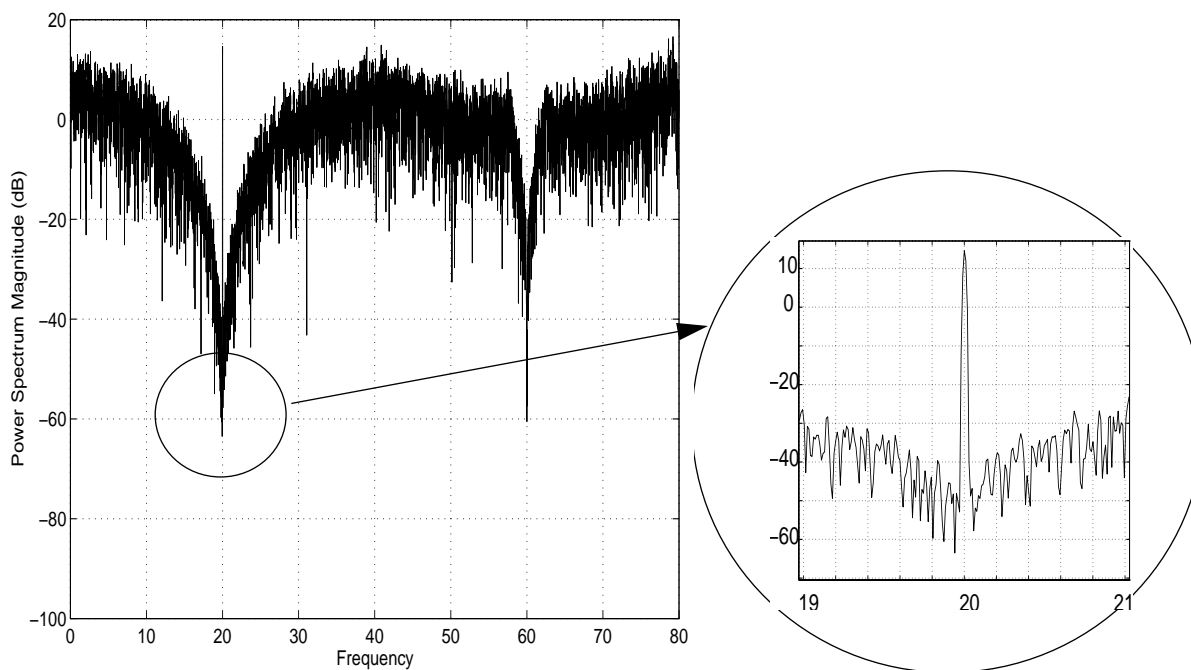


Fig. 2.4 NTF frequency responses and zero-pole plots



(a) ideal case (SNR = 100dB)



(b) with 1% coefficient mismatch (SNR=65 dB)

Fig. 2.5 Output spectra of a fourth-order sigma delta modulator

---

## 2.4 Complex IF Receiver

### 2.4.1 Structure of a Single IF Receiver

Based on the complex sigma-delta modulator introduced in the previous section, we can build a single IF receiver. The structure of the receiver is shown in Fig. 2.6 [Stetzler95] [Swaminathan96b] [Vieria95]. We use the digital complex sampling technique [Saulnier90], also called digital quadrature demodulation, in the demodulation process of this quadrature IF receiver. Digital complex sampling is a technique which uses IF sampling to produce baseband I and Q signals. The IF signal is sampled at approximately four times the IF center frequency and the samples are sorted into I and Q data streams. The quadrature sinusoids used to demodulate the IF signal simply become sequences of  $(1, 0, -1, 0, \dots)$  and  $(0, 1, 0, -1, \dots)$  respectively. This can be easily implemented without using multipliers, which results in minimal hardware [Schreier90].

$I_1$  and  $Q_1$ , which are the same at this point, are RF signals which are at  $1.9GHz$  according to the PCS standard.  $I_2$  and  $Q_2$  are IF signals which are generated through mixing  $I_1$  and  $Q_1$  with  $f_{LO}$ .  $I_3$  and  $Q_3$  are quantized versions of  $I_2$  and  $Q_2$  represented as 1-bit streams. Using digital quadrature demodulation,  $I_4$  and  $Q_4$  are baseband signals but still 1-bit streams at a high sampling rate. After decimation filtering,  $I_5$  and  $Q_5$  are n-bit streams at a Nyquist sampling rate.

### 2.4.2 Mismatch Problems

The outputs  $I_3$  and  $Q_3$  of the two paths should have the same amplitude and 90 degree phase difference. But mismatches can occur at many locations in the receiver shown in Fig. 2.6. For example, in the RF front end, the main component is the mixer. It uses two sinusoids at a RF frequency nominally equal in amplitude, with a 90 degrees phase difference. In practice these two

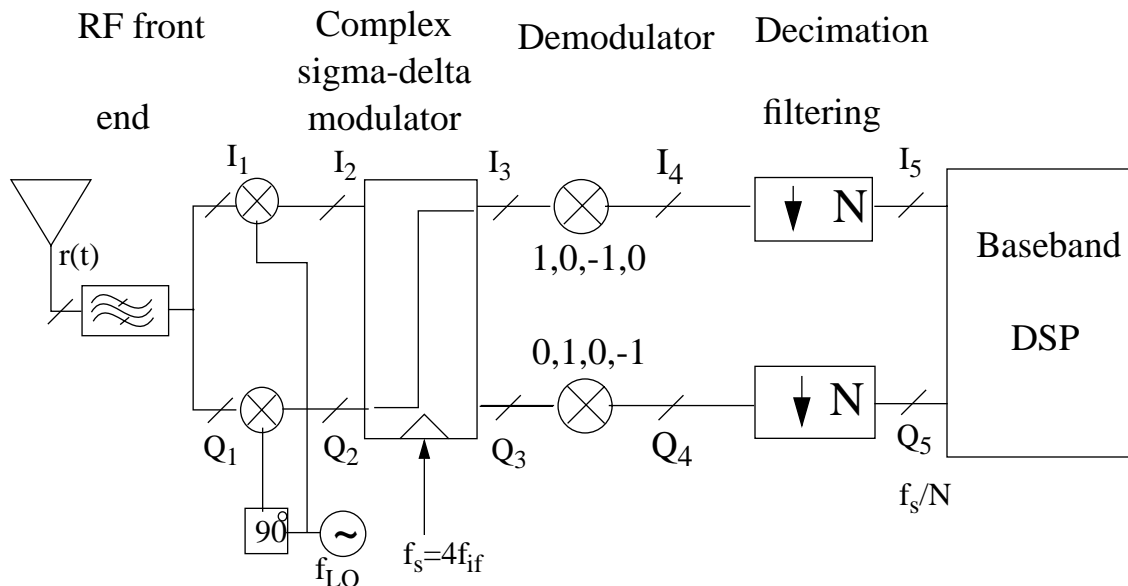


Fig. 2.6 Single IF receiver structure

sinusoids are always unbalanced because high precision phase matching is difficult to achieve in analog circuitry. The effect of this imbalance is to generate an image, which can limit the dynamic range of a receiver [Tsui95].

In addition to gain or phase imbalances in the mixer, capacitor mismatch is also a big concern in the analog system. Coefficients in the transfer functions are realized by capacitors in switched-capacitor circuits, so capacitor mismatch will result in coefficient mismatch. As shown in Fig. 2.2, with the coefficient mismatch in the transfer functions of the complex sigma delta modulator, the image noise will be aliased into the signal band through the upper path in the model.

#### 2.4.2.1 Gain and Phase Imbalance

The following is an example that explains the generation of an image signal due to the imbalance of the two paths.

Assume  $I_2$  and  $Q_2$  are  $\cos(2\pi f_{if}t)$  and  $\sin(2\pi f_{if}t)$ , so the complex expression of the input is

$$e^{j2\pi f_{if}t} = \cos(2\pi f_{if}t) + j \sin(2\pi f_{if}t)$$

The Fourier transforms of  $\cos(2\pi f_{if}t)$  and  $\sin(2\pi f_{if}t)$  can be written as

$$F[\cos(2\pi f_{if}t)] = \frac{\delta(f - f_{if}) + \delta(f + f_{if})}{2}$$

$$F[\sin(2\pi f_{if}t)] = \frac{\delta(f - f_{if}) - \delta(f + f_{if})}{2j}$$

where  $\delta(\cdot)$  is the delta function.

The Fourier transform of  $e^{j2\pi f_{if}t}$  can be combined as

$$F[e^{j2\pi f_{if}t}] = \frac{1}{2}[\delta(f - f_{if}) + \delta(f + f_{if}) + \delta(f - f_{if}) - \delta(f + f_{if})] = \delta(f - f_{if})$$

The negative frequency components  $\delta(f + f_{if})$  cancel each other. Only the positive frequency components  $\delta(f - f_{if})$  are left. These results are shown in Fig. 2.7.

From the structure of the IF receiver shown in Fig. 2.6, the quadrature mixer is a crucial component which can cause imbalances between the I/Q paths. If there is a gain difference between the two mixers, the two outputs of  $I_2$  and  $Q_2$  will not have the same amplitude. For example, suppose  $I_2 = \cos(2\pi f_{if}t)$  and  $Q_2 = 0.8\sin(2\pi f_{if}t)$ . The negative frequency components of the combined result will not cancel each other exactly. There will be an output in the negative frequency component position, as shown in Fig. 2.8. In a receiver design, the image of a strong signal can limit the dynamic range of the receiver because the weak signal must be higher than the image in order to be detected.

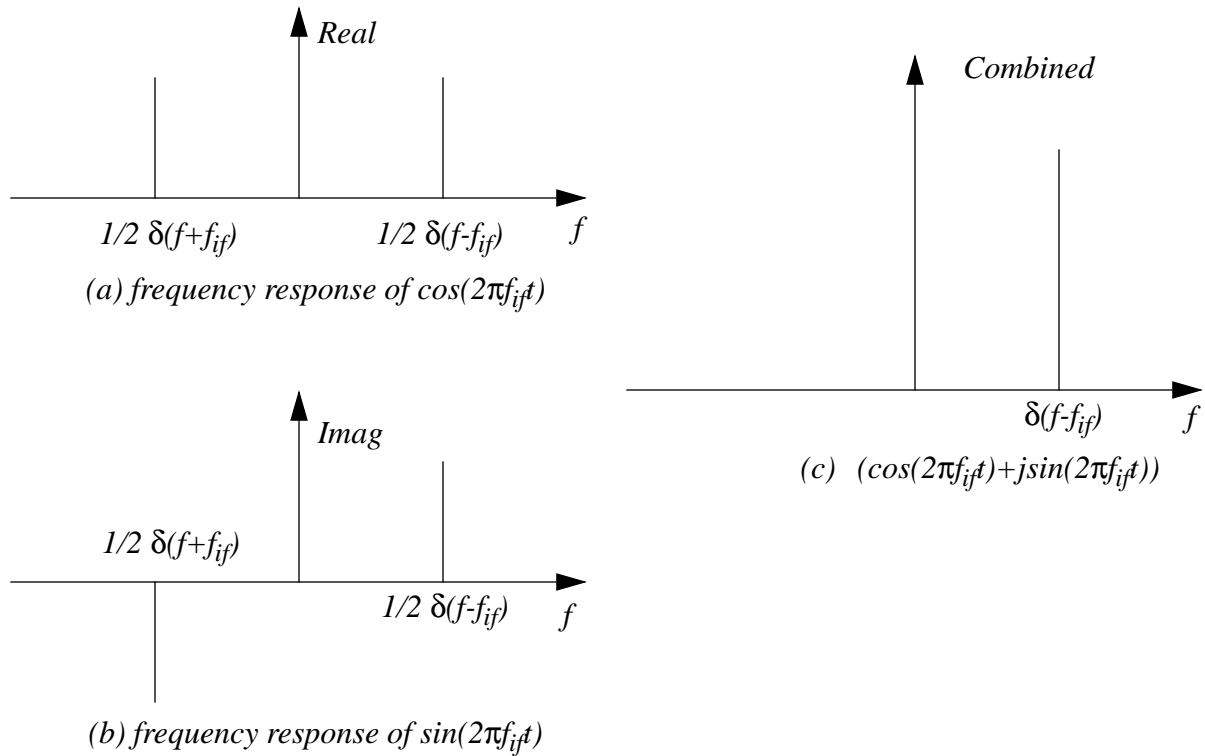


Fig. 2.7 Output of balanced I and Q channels:

The mixer can not only have gain imbalances, but can also introduce a phase imbalance, which means the phase difference between  $I_2$  and  $Q_2$  is not exactly 90 degrees. Thus, in general, the two outputs  $I_2$  and  $Q_2$  can be expressed as

$$\begin{aligned}
 s(t) &= \cos(2\pi f_{if}t) + j(1+k)\sin(2\pi f_{if}t + \theta) \\
 &= \frac{1}{2}[e^{j2\pi f_{if}t} + e^{-j2\pi f_{if}t}] + \frac{(1+k)}{2}[e^{j(2\pi f_{if}t + \theta)} - e^{-j(2\pi f_{if}t + \theta)}] \\
 &= \frac{1}{2}[e^{j2\pi f_{if}t}(1 + (1+k)e^{j\theta})] + \frac{1}{2}[e^{-j2\pi f_{if}t}(1 - (1+k)e^{-j\theta})] \quad \text{Eq. (2.4)}
 \end{aligned}$$

Where  $f_{if}$  is the IF frequency,  $k$  is the gain imbalance, and  $\theta$  is the phase imbalance. In this example, the cosine path is assumed to be perfect and the sine path has all the imbalance.

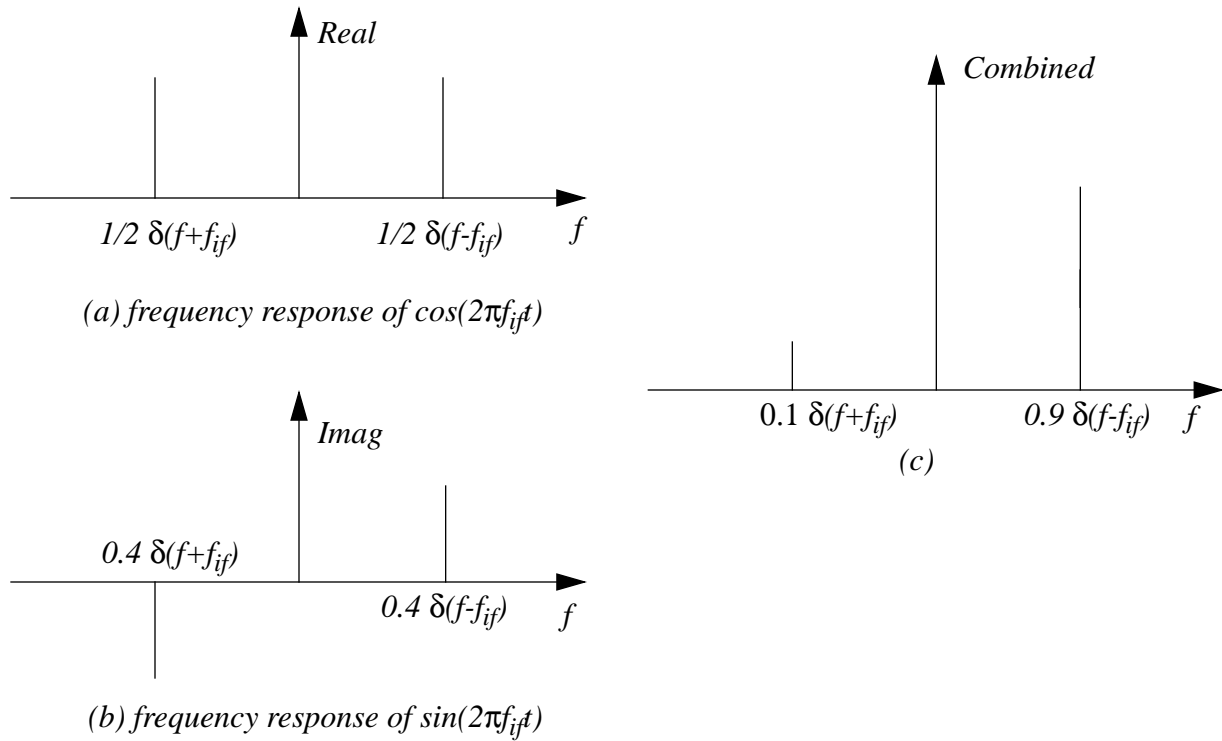


Fig. 2.8 Output of imbalance I and Q channels

According to Eq. (2.4), the corresponding amplitudes of the signal and image are  $1 + (1 + k)e^{j\theta}$  and  $1 - (1 + k)e^{-j\theta}$ , respectively. Image rejection is defined as the ratio of the gain of the desired signal to the gain of the image signal.

The power of the signal and the image can be expressed as

$$A_s^2 = 1 + (1 + k)^2 + 2(1 + k)\cos\theta = 2 + k^2 + 2k(1 + \cos\theta) + 2\cos\theta$$

$$A_i^2 = 1 + (1 + k)^2 - 2(1 + k)\cos\theta = 2 + k^2 + 2k(1 - \cos\theta) - 2\cos\theta$$

and the image rejection can be written in decibels

$$10\log\left(\frac{A_s}{A_i}\right)^2 = 10\log\frac{2 + k^2 + 2k(1 + \cos\theta) + 2\cos\theta}{2 + k^2 + 2k(1 - \cos\theta) - 2\cos\theta} \quad \text{Eq. (2.5)}$$

The result is displayed in Fig. 2.9. It can be seen that as the gain and/or the phase

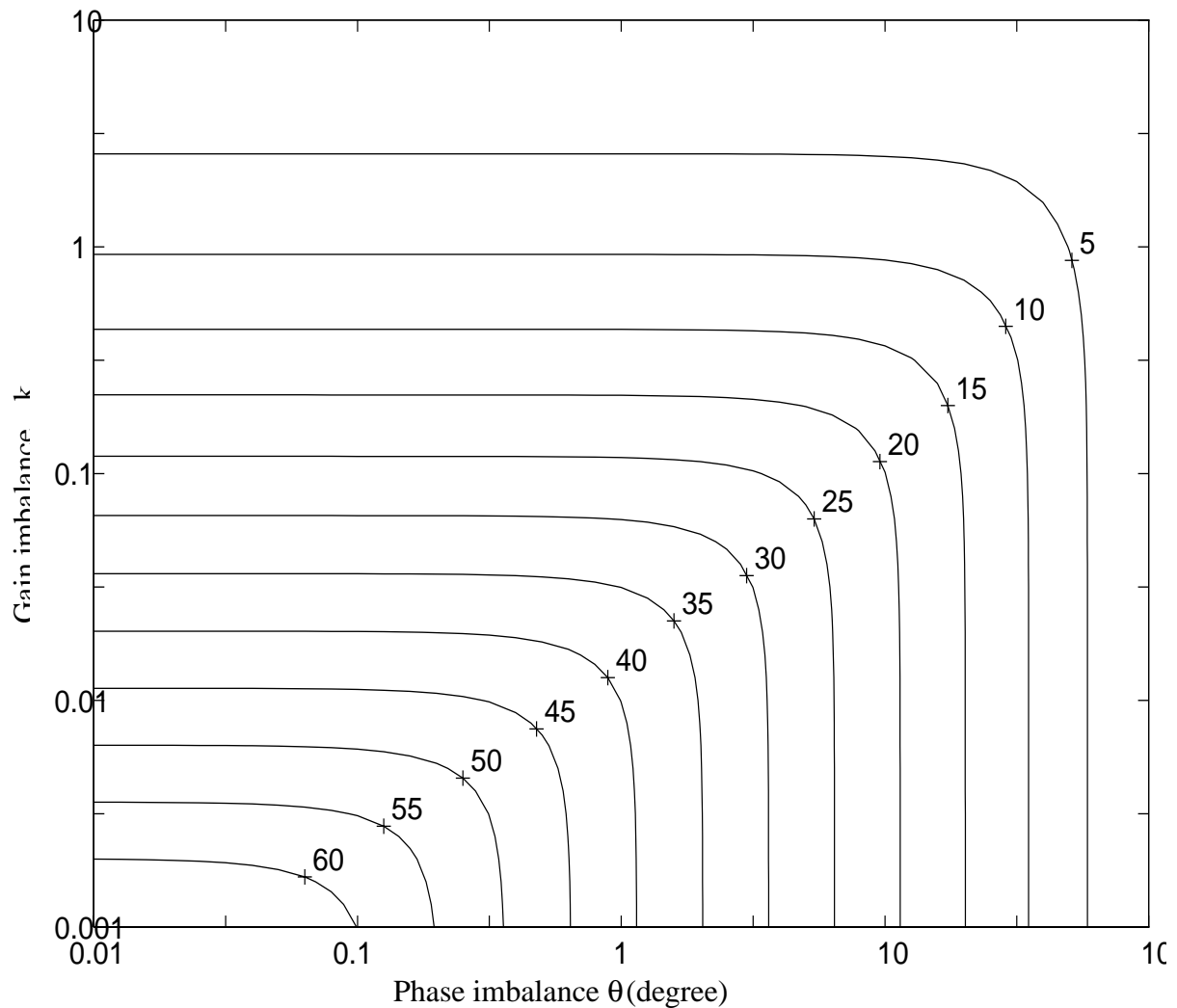


*Fig. 2.9 Degradation as a function of gain and phase imbalance*

imbalances get larger, image rejection decreases. With a  $2^\circ$  phase imbalance, the image rejection is only about 35 dB. In order to build a receiver that has an image rejection more than 50 dB, the gain imbalance has to be less than 0.6% and the phase imbalance can not exceed  $0.4^\circ$ .

### 2.4.2.2 Coefficient Mismatch

Coefficient differences in transfer functions of a filter or a sigma delta modulator can be modeled as producing gain and phase imbalances that vary with frequency.

The embedded filter in the feedback loop of the complex bandpass sigma delta modulator ( $A(z)$  in Fig. 2.3) contains a number of complex integrators. These complex integrators are simple complex filters with one complex pole that lies on the unit circle.

The transfer function of a single pole complex filter can be represented as

$$H(z) = \frac{1}{z - a - jb} \quad , \text{ or } \quad H(z) = \frac{z - a + jb}{(z - a)^2 + b^2}$$

$$\text{Pole} = a + jb$$

An efficient realization [Snelgrove82] of this complex filter is shown in Fig. 2.10(a). This network can be constructed using real blocks in the two-channel system shown in Fig. 2.10(b).

The  $\frac{1}{z-1}$  blocks are simply delaying type switched-capacitor integrators, and thus a complex pole is easily created in switched-capacitor technology by way of two cross-coupled integrators [Jantzi94]. If there is capacitor mismatch in the circuit, the complex filter coefficients “a” and “b” in the different paths are no longer equal as shown in Fig. 2.11.  $\epsilon_a/a$  and  $\epsilon_b/b$  are relative coefficient mismatch.

According to the model shown in Fig. 2.2, the output in Fig. 2.11 can be represented as

$$V_{out}(z) = T_{nom}(z)V_{in}(z) + \Delta T_{diff}(z)\overline{V_{in}(z)} \quad \text{Eq. (2.6)}$$

where

$$T_{nom}(z) = \frac{1}{z - a - jb}$$

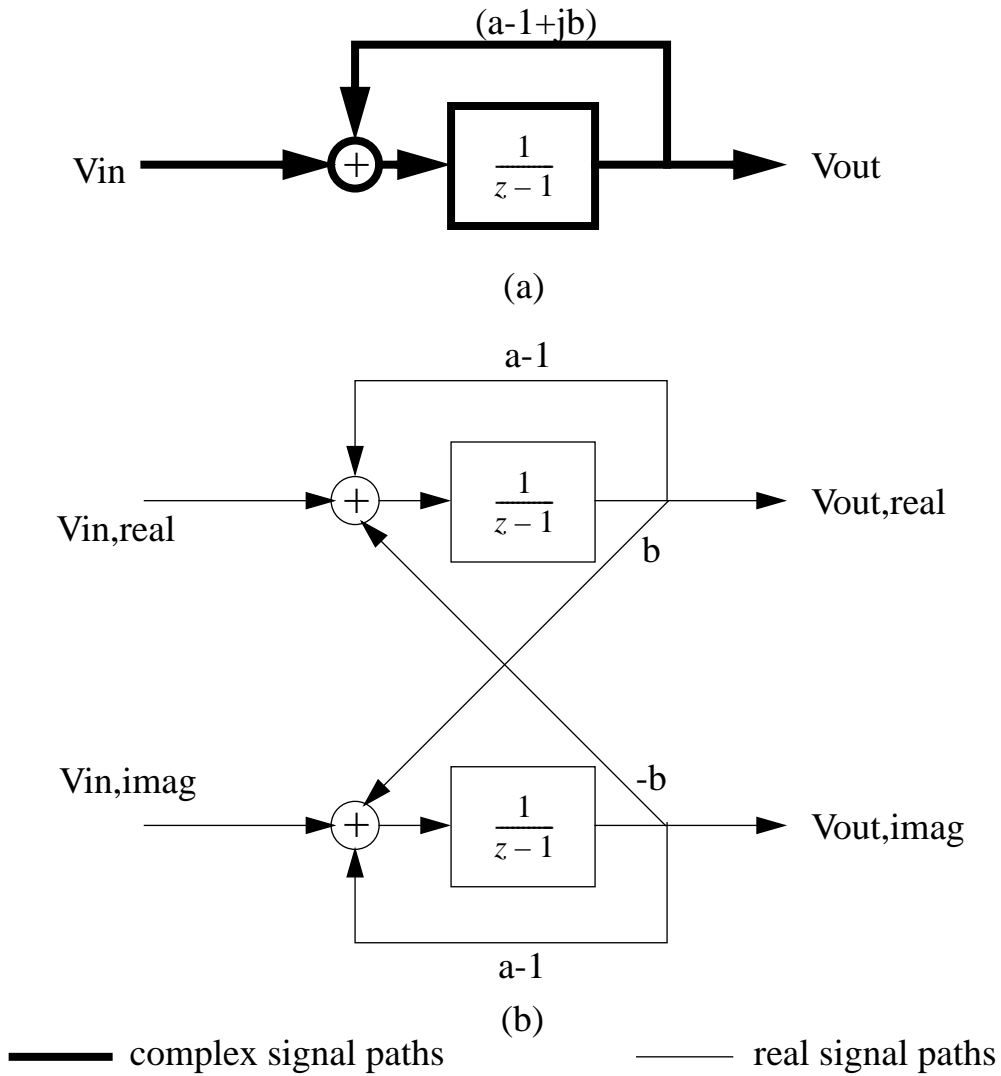


*Fig. 2.10 Complex pole realization*

and

$$\Delta T_{diff} \approx \frac{(\epsilon_a + j\epsilon_b)/2}{(z - a - j\sigma)(z - a + j\sigma)}. \quad \text{Eq. (2.7)}$$

where  $\sigma^2 = b^2 - (\epsilon_a/2)^2 - (\epsilon_b/2)^2$ .

The derivation of Eq. (2.7) is shown in APPENDIX B. The image transfer function  $\Delta T_{diff}$

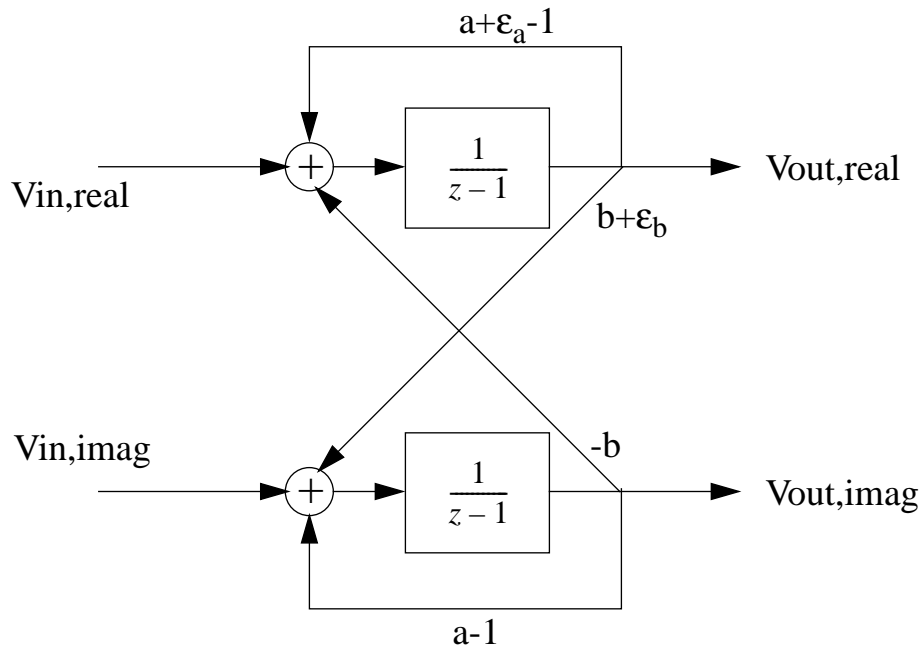


Fig. 2.11 Mismatch model for the single-pole complex filter

has nearly the same pole as the complex filter,  $T_{nom}$ , but also has the conjugate pole, and has a gain directly related to the coefficient mismatches. A simple example of the complex bandpass filter is shown in Fig. 2.12, which has a single pole located at  $(-0.1, 0.8)$ . This complex filter's pole-zero plot is shown in Fig. 2.12(a) and its signal response and image response are shown in Fig. 2.12(b) and Fig. 2.12(c) respectively. In this example,  $\epsilon_a/a = 1\%$ ,  $\epsilon_b/b = 1\%$ . The signal response has a peak at  $\omega = \pi/2 + 0.1244$ <sup>1</sup> as shown in Fig. 2.12(b). The image response has peaks at both  $\omega = \pi/2 + 0.1244$  and  $\omega = 3\pi/2 - 0.1244$  as shown in Fig. 2.12(c).

It can be seen from Eq. (2.6) that the output not only has the input component, which is the desired signal, but also includes the complex conjugate of the input, which is the image noise. Define image rejection as the ratio of the in-band gain, which is the gain of the desired signal, to

---

1.  $\text{atan}\left(\frac{1}{8}\right) = 0.1244$

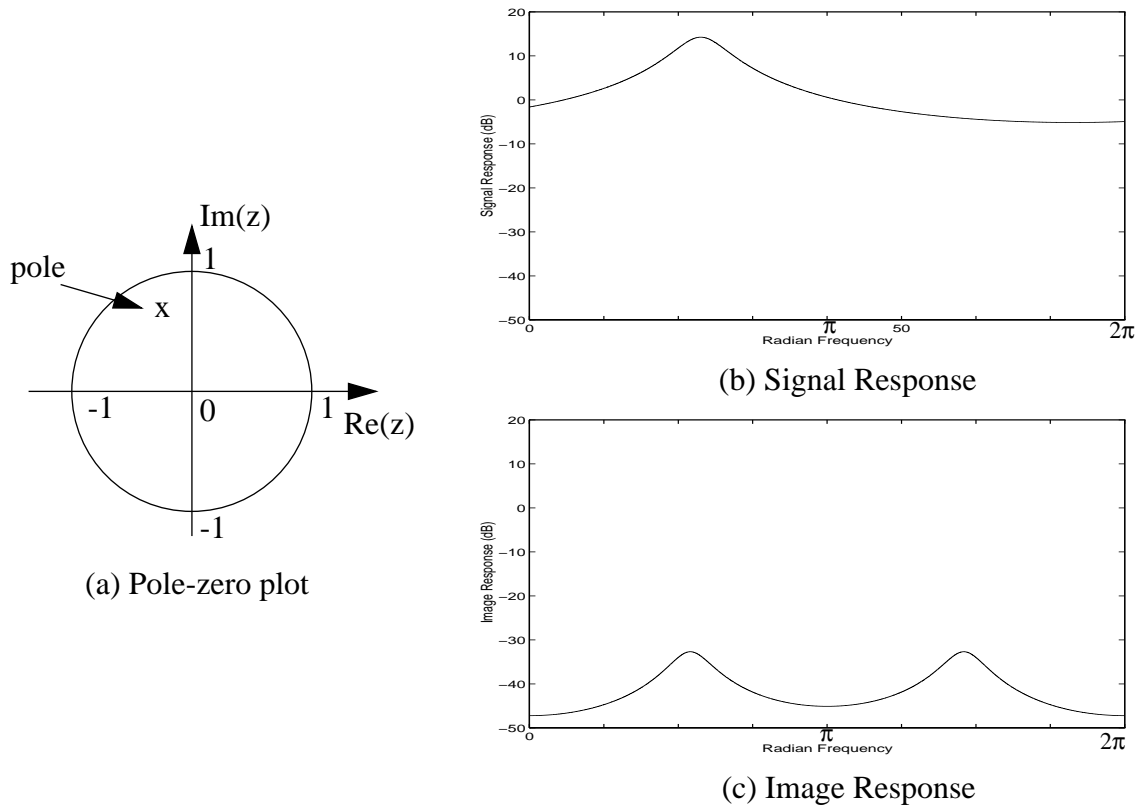
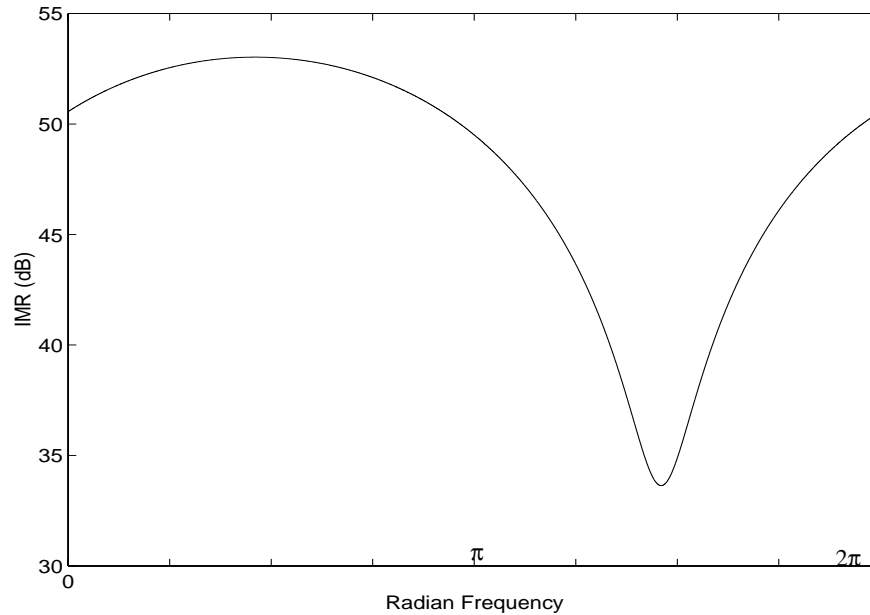


Fig. 2.12 Pole-zero plot, signal and image response plots of a single-pole complex filter

the image-band gain, which is the gain of the image noise. Image rejection indicates how effectively a complex filter passes in-band inputs relative to inputs in the image band. The image rejection expressed in decibels is:

$$\begin{aligned}
 IMR &= 10\log\left(\left|\frac{T_{nom}(z)}{\Delta T_{diff}(z)}\right|^2\right) \approx 20\log\left(\left|\frac{\frac{1}{z-a-jb}}{(\epsilon_a + j\epsilon_b)/2}\right|\right) \\
 &= 20\log\left|\frac{z-a+j\sigma}{(\epsilon_a + j\epsilon_b)/2}\right| = 10\log\frac{(z-a)^2 + \sigma^2}{(\epsilon_a^2 + \epsilon_b^2)/4} \quad \text{Eq. (2.8)}
 \end{aligned}$$

It can be seen that the image rejection varies with frequency. In this example, the image rejection shown in Eq. (2.8) is displayed in Fig. 2.13. It shows that with 1% coefficient mismatch,



*Fig. 2.13 Degradation as a function of frequencies for 1% coefficients mismatch*

the worst-case image rejection occurs at  $\omega = 3\pi/2 - 0.1244$  and is only about 34 dB. The best-case image rejection at signal frequency  $\omega = \pi/2 + 0.1244$  is 52 dB. Thus, interference exactly at  $\omega = 3\pi/2 - 0.1244$  will cause the biggest problem because it gets the least attenuation before it aliases into the signal band.

Fig. 2.14 shows how image rejection changes with relative coefficient mismatch. With smaller mismatch (less than 0.2%), the image rejection is almost constant in the whole band. While as the mismatch increases, the image rejection at the image frequency of the passband gets worse. If we want to get the image rejection of more than 40 dB at the image frequency, the coefficient mismatch has to be less than 0.8%.

### 2.4.3 Interference

During the mixing stage, the desired signal at  $f_{RF}$  is mixed with local oscillator signal at

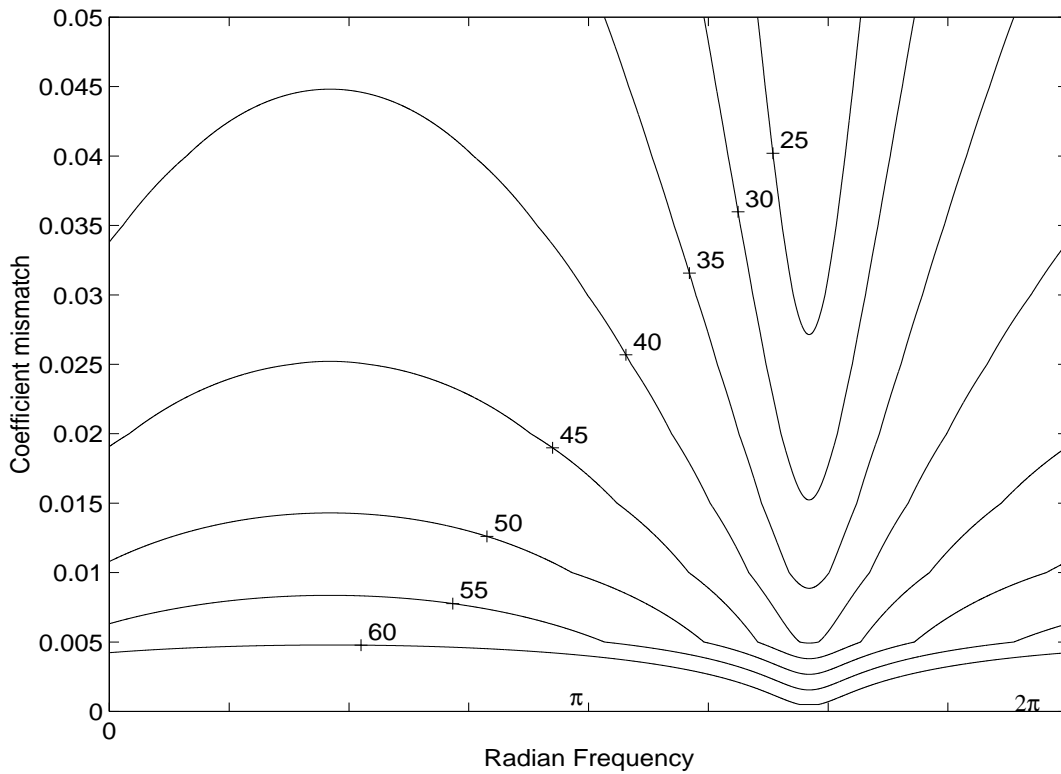


Fig. 2.14 Degradation as a function of frequencies and coefficients mismatch

$f_{LO}$  to produce an IF signal at  $f_{IF} = f_{LO} - f_{RF}$ . However, some signals at a certain frequency,  $f_{\text{image}}$  can be mixed with  $f_{LO}$  to produce an image interference at  $-f_{IF}$ .

Assume in the receiver system shown in Fig. 2.6, the received signal  $r(t)$  can be expressed as:

$$r(t) = r_D(t) + r_I(t)$$

where  $r_D(t)$  is the desired signal at  $f_{RF}$  expressed as Eq. (2.9) and  $r_I(t)$  is the interference signal at  $f_{\text{image}}$  expressed as Eq. (2.10).

$$r_D(t) = \alpha(t) \cos(2\pi f_{RF} t) \quad \text{Eq. (2.9)}$$

$$r_I(t) = \beta(t) \cos(2\pi f_{\text{image}} t + \Delta\phi) \quad \text{Eq. (2.10)}$$

So the signals  $I_2$  and  $Q_2$  can be written as

$$I_2 = r(t) \cos(2\pi f_{LO} t) = r_D(t) \cos(2\pi f_{LO} t) + r_I(t) \cos(2\pi f_{LO} t) \quad \text{Eq. (2.11)}$$

$$Q_2 = r(t) \sin(2\pi f_{LO} t) = r_D(t) \sin(2\pi f_{LO} t) + r_I(t) \sin(2\pi f_{LO} t) \quad \text{Eq. (2.12)}$$

After substituting Eq. (2.9) and Eq. (2.10) into Eq. (2.11) and Eq. (2.12), removing the high frequency terms,  $I_2$  and  $Q_2$  can be expressed as

$$\begin{aligned} I_2 &= \frac{1}{2} \alpha(t) \cos(2\pi(f_{LO} - f_{RF})t) + \frac{1}{2} \beta(t) \cos(2\pi(f_{LO} - f_{image})t - \Delta\phi) \quad \text{Eq. (2.13)} \\ &= \frac{1}{2} \alpha(t) \cos(2\pi f_{IF} t) + \frac{1}{2} \beta(t) \cos(-2\pi f_{IF} t - \Delta\phi) \end{aligned}$$

$$\begin{aligned} Q_2 &= \frac{1}{2} \alpha(t) \sin(2\pi(f_{LO} - f_{RF})t) + \frac{1}{2} \beta(t) \sin(2\pi(f_{LO} - f_{image})t - \Delta\phi) \quad \text{Eq. (2.14)} \\ &= \frac{1}{2} \alpha(t) \sin(2\pi f_{IF} t) + \frac{1}{2} \beta(t) \sin(-2\pi f_{IF} t - \Delta\phi) \end{aligned}$$

If we have interference at  $f_{RF} + 2f_{IF}$ , after mixing, image interference appears at  $-f_{IF}$ .

When there is no mismatch between the two paths, this image interference has no effect on the performance of the system. But if there is a gain, phase or coefficient imbalance in any part of the system, this image interference will alias into the desired signal band as discussed in Section 2.4.1 and Section 2.4.2.2. This will limit the selectivity of the receiver.

#### 2.4.4 Examples

To study the mismatch phenomenon in a single IF receiver, this thesis proposes a

**Table 2.1 Receiver Parameters**

Parameter	Value
RF Frequency	1.9GHz

**Table 2.1 Receiver Parameters**

Parameter	Value
LO $f_{lo}$	1.91GHz
Sampling Frequency $f_s$	40MHz
Modulation Scheme	GMSK
Data rate	270.833 kb/s
BT <sup>a</sup>	0.3
Decimation rate	64

a. Bandwidth - Time product. B is the 3 dB bandwidth of the Gaussian filter and T is the symbol period. BT=0.3 is specified in the GSM standard.

technique and analyzes, simulates and builds a prototype. The test example is based on DCS-1800 (GSM-like) in the receiver proposed by Swaminathan [Swaminathan96b]. The architecture of the receiver shown in Fig. 2.6. Table 2.1 shows the parameters used in the receiver. The signal bandwidth after decimation filtering is about 312.5 kHz, which can be used in a GSM receiver [Rappaport96]. The data rate in the GSM standard is 270.833 kb/s.

**Case 1: no interference signal at  $f_{RF} + 2f_{IF}$**  Fig. 2.15 shows the output spectrum of the complex modulator,  $I_3 + jQ_3$ , when there is no image interference and the I and Q paths are perfectly balanced. It can be seen that there is no image interference at  $-10MHz$ . The SNR is about 80 dB in the 625 kHz bandwidth. Fig. 2.16 is the spectrum of the received signal after decimation,  $I_5 + jQ_5$ , which shows that the received signal is contained in the band  $-312.5$  to  $312.5kHz$ . The SNR of the received signal after decimation is about 63 dB.

Fig. 2.17 shows the output spectrum of the complex modulator,  $I_3 + jQ_3$ , without an image interferer but with 1% mismatch between the two paths. It can be seen that the signal tone is only 60 dB in the 625 kHz bandwidth due to the image aliasing which increases the noise floor.

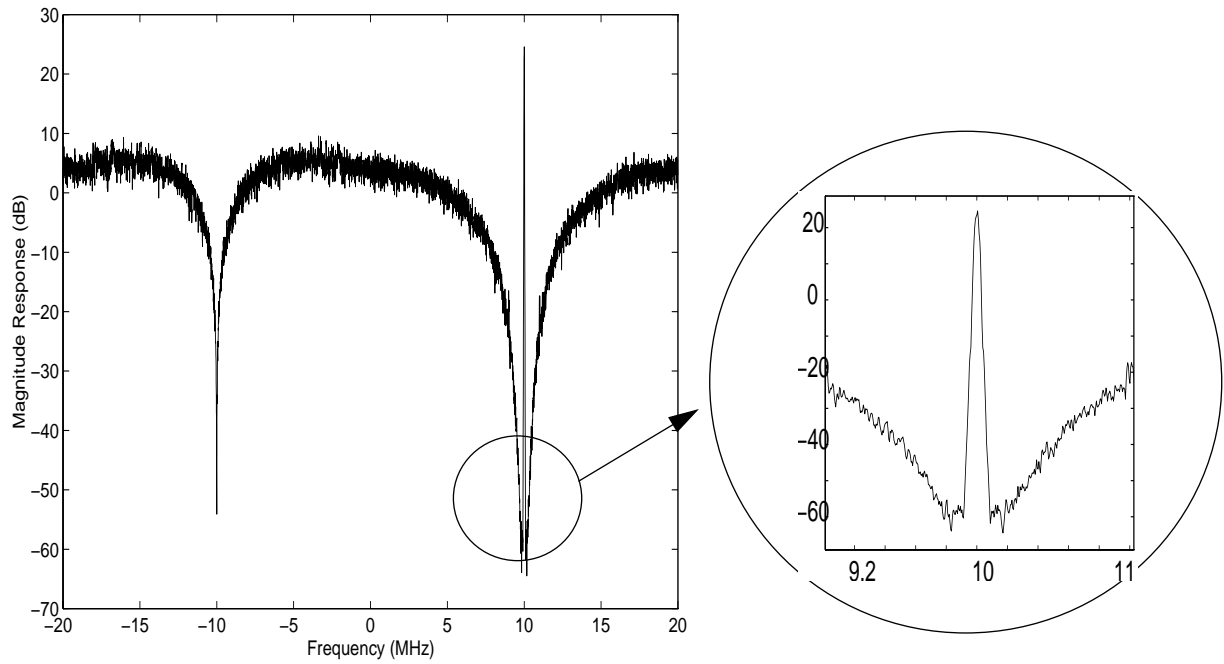


*Fig. 2.15 Simulated output spectrum of the complex sigma delta modulator  $I_3+jQ_3$  without mismatch and without image interferences*

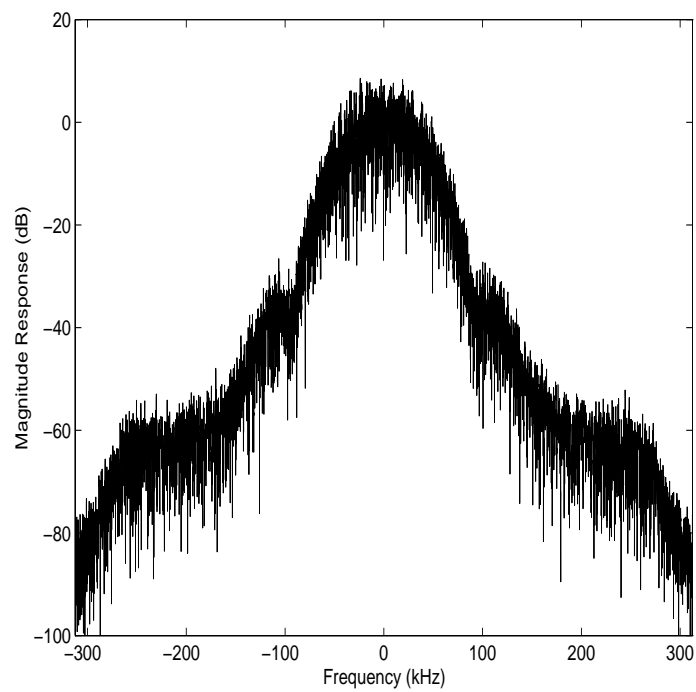


*Fig. 2.16 Magnitude response of  $I_5+jQ_5$*

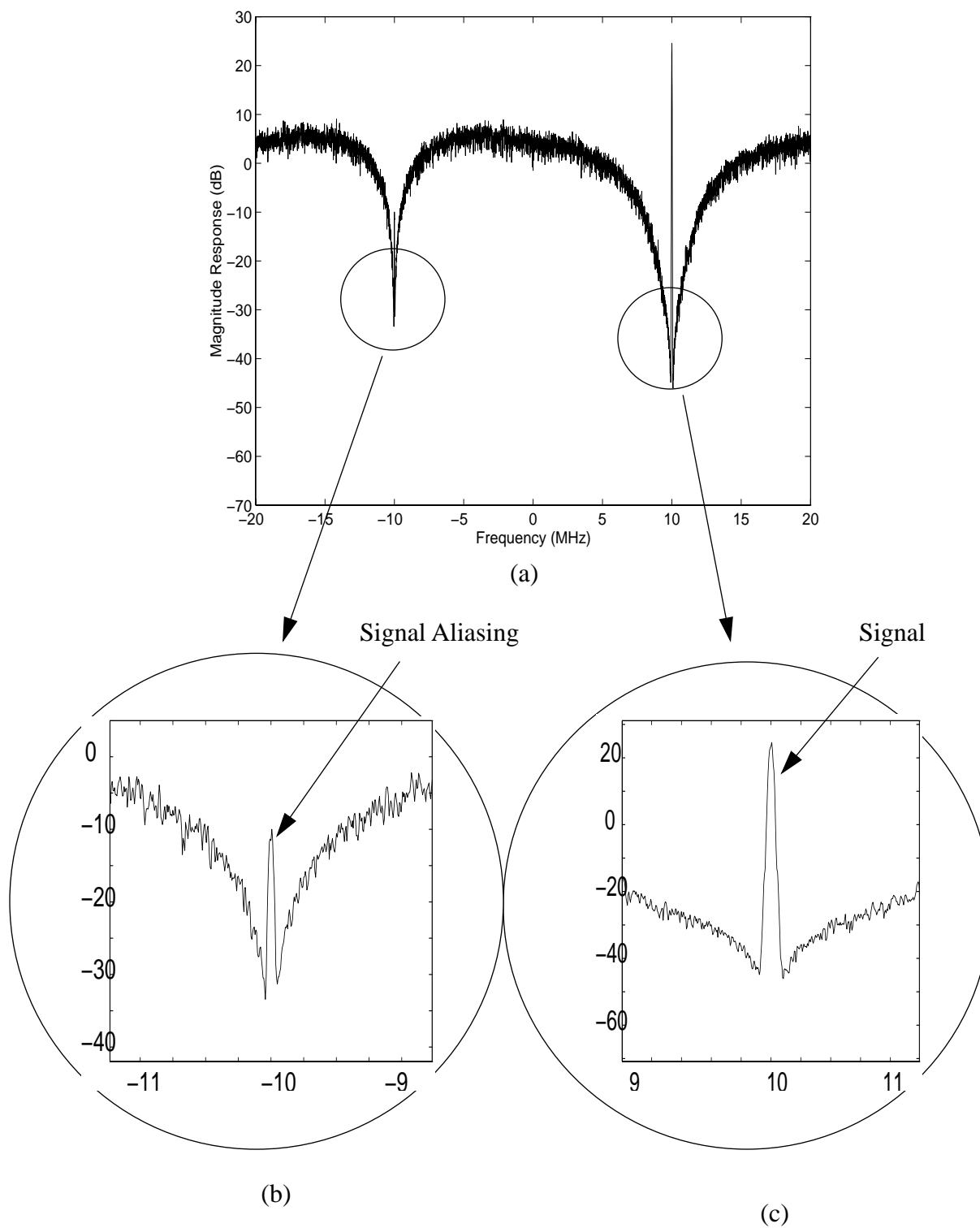


*Fig. 2.17 Simulated output spectrum of the complex sigma delta modulator with 1% mismatch but without image interferences*

There is also a tone at  $-10\text{MHz}$  because the signal aliases into the image band at the same time as the image noise aliases into the desired signal band. Image noise in this case is only the quantization noise because there is no image interference at the input.

The magnitude response of the received signal after decimation is shown in Fig. 2.18. It can be seen that the noise floor is moved up. The SNR is 42 dB which represents about 20 dB degradation compared with Fig. 2.16.

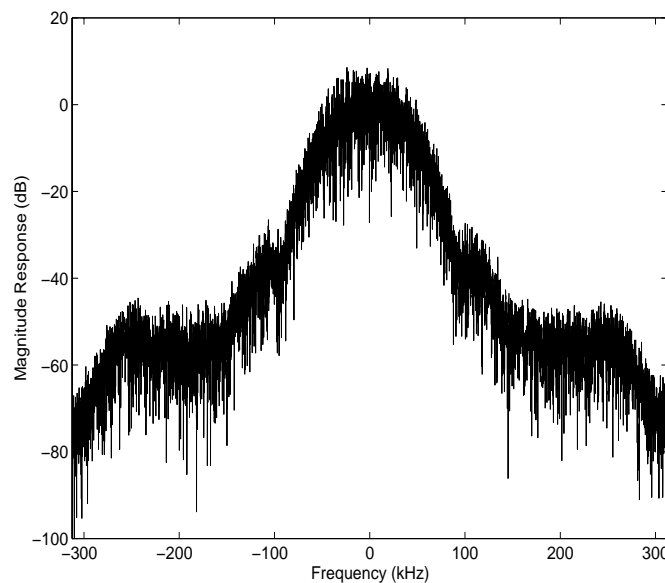


Fig. 2.18 Magnitude response of  $I_5 + jQ_5$

**Case 2: an interference signal exists at  $f_{RF} + 2f_{IF}$** —The desired signal and interference signal for our example are respectively shown in Table 2.2. Fig. 2.19 is the spectrum of the output of the sigma delta modulator,  $I_3 + jQ_3$ , with the desired signal and its image interference, when there is no mismatch between I and Q paths. An expanded frequency response in the band of interest (9~11MHz) is shown next to it. The desired signal tone is at 10MHz after being mixed from the RF down to the IF band. The interference signal is at  $-10\text{MHz}$ . The SNR is about 76 dB

as in case 1 without mismatch (Fig. 2.15) which shows the image interference has very little effect in the desired signal band when the I and Q paths are perfectly balanced.

**Table 2.2 Desired signal and interference**

desired signal		interference	
modulation scheme	GMSK	modulation scheme	FM
bit rate	270.833 kb/s	bandwidth	100kHz
carrier frequency	1.9GHz	carrier frequency	1.9202GHz

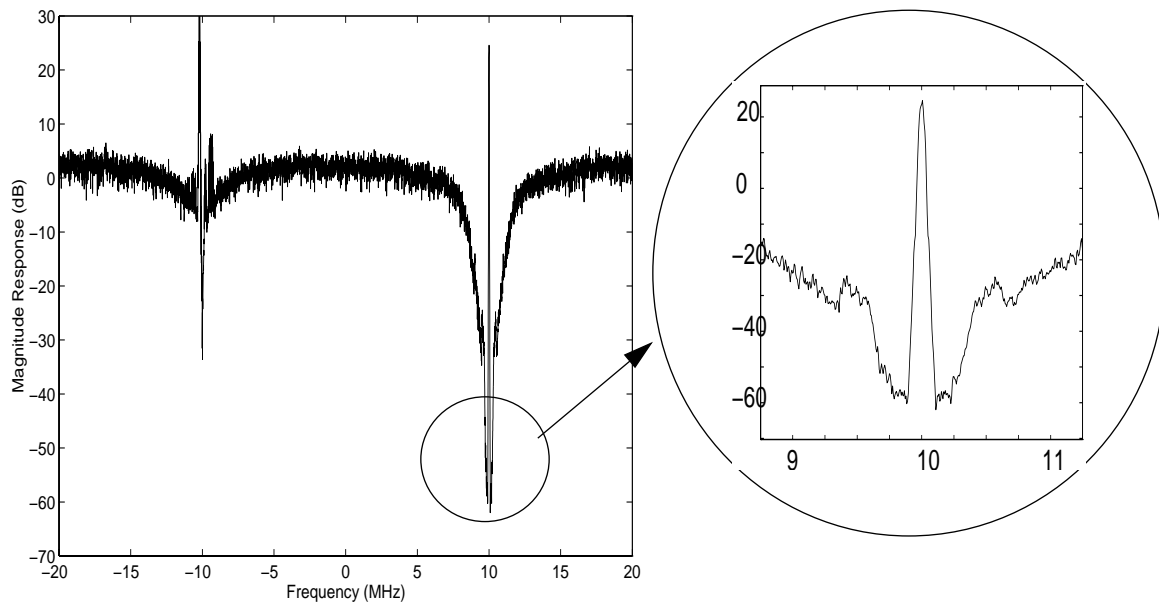


*Fig. 2.19 Output spectra of the complex sigma delta modulator*

Fig. 2.20 is the spectrum of the received signal after decimation, and is the same as Fig. 2.16. This demonstrates that when the I and Q paths are perfectly balanced, the image interferer has no effect on system performance.

Fig. 2.21(a) is the eye diagram of the transmitted baseband signal and Fig. 2.21(b) is the eye diagram of the received signal. It can be seen that the received signal is a delayed version of the input signal. For this ideal case, the interference has no effect.

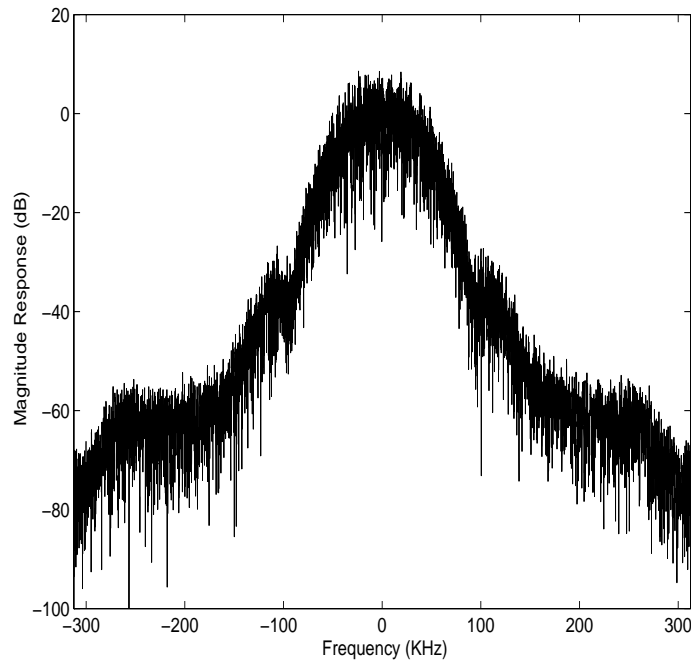
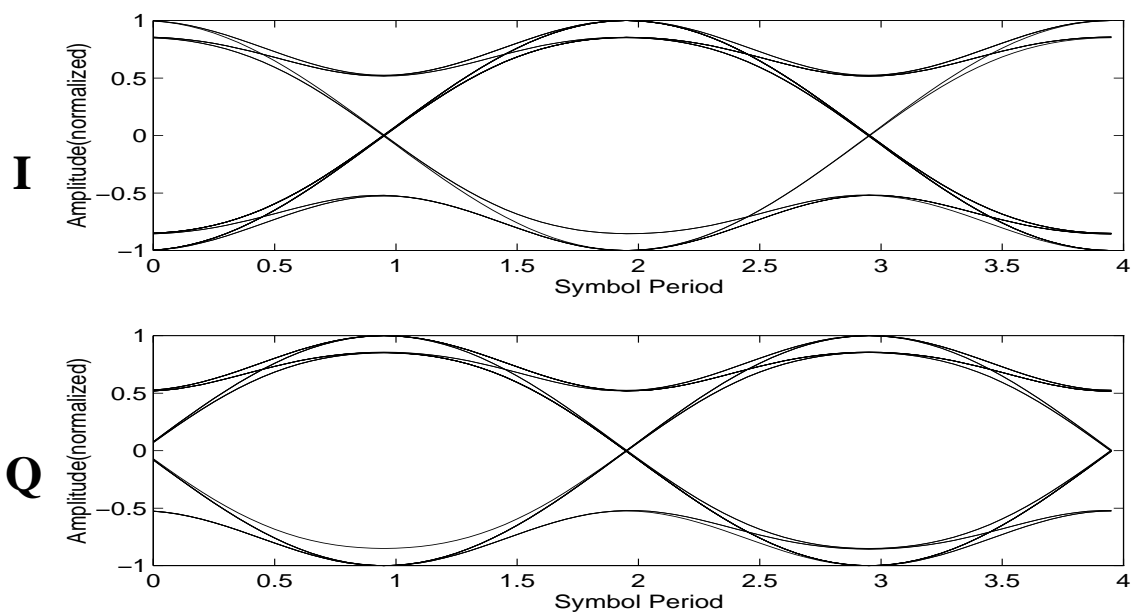


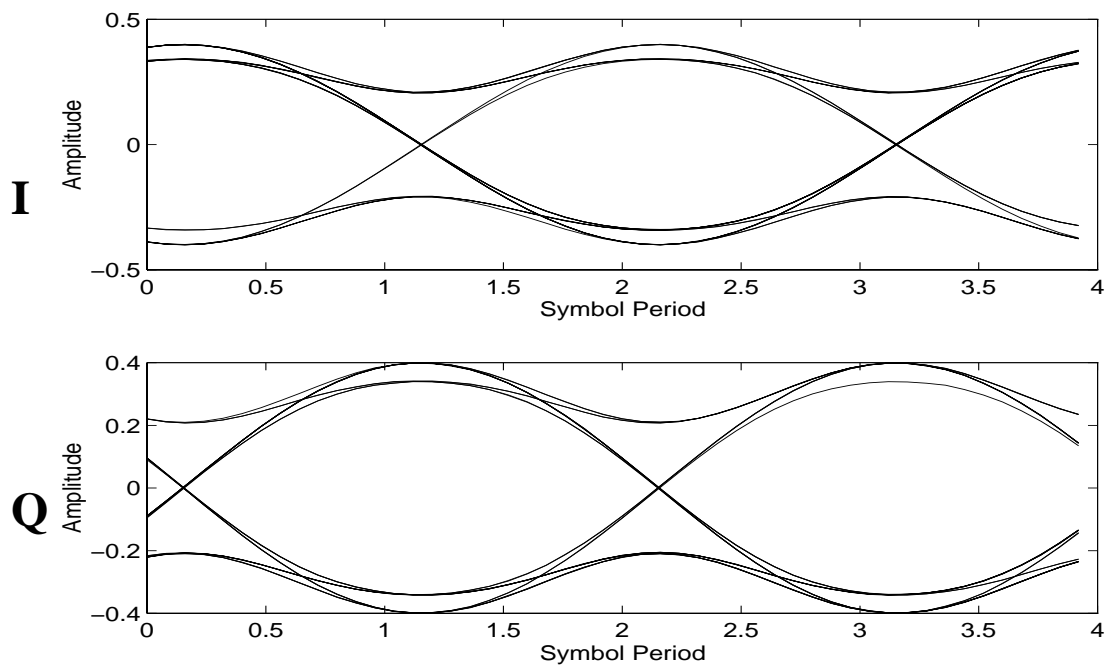
*Fig. 2.20 Magnitude response of  $I_5+jQ_5$*

Comparing Fig. 2.22(a) and Fig. 2.19(a), it can be seen that with mismatches between the I and Q paths, not only is the noise floor increased, but also the FM interference is aliased into the region 10.15~10.25 MHz. The recovered baseband signal is shown in Fig. 2.22(b), which shows the image aliasing located in the band 150~250kHz. The SNR is about 30 dB which represents a degradation of more than 30 dB compared to the ideal case. The spectra shown in Fig. 2.22 are obtained with the interference offset by 200kHz so that the reader can distinguish it from the GMSK signal. In this case, of course, conventional filtering could remove it and the problem would not be serious. We will show more results with no offset in the interference in Chapter 3.

Fig. 2.23 shows the eye diagrams of the corrupted signal. It can be seen that the eyes are modulated by the image interference. The performance degradation is obvious.



(a) Eye diagram of the input signal



(b) Eye diagram of the received signal

Fig. 2.21 Comparison of the eye diagrams between the input signal and the received signal: no mismatch, but with interferer, the eye diagram is unaffected by the interferer

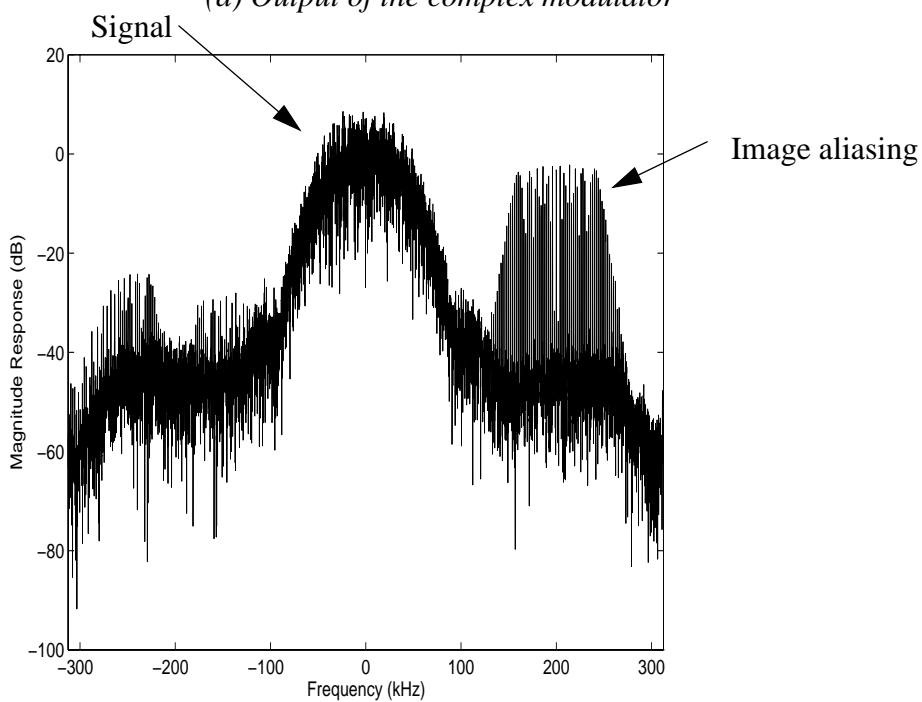
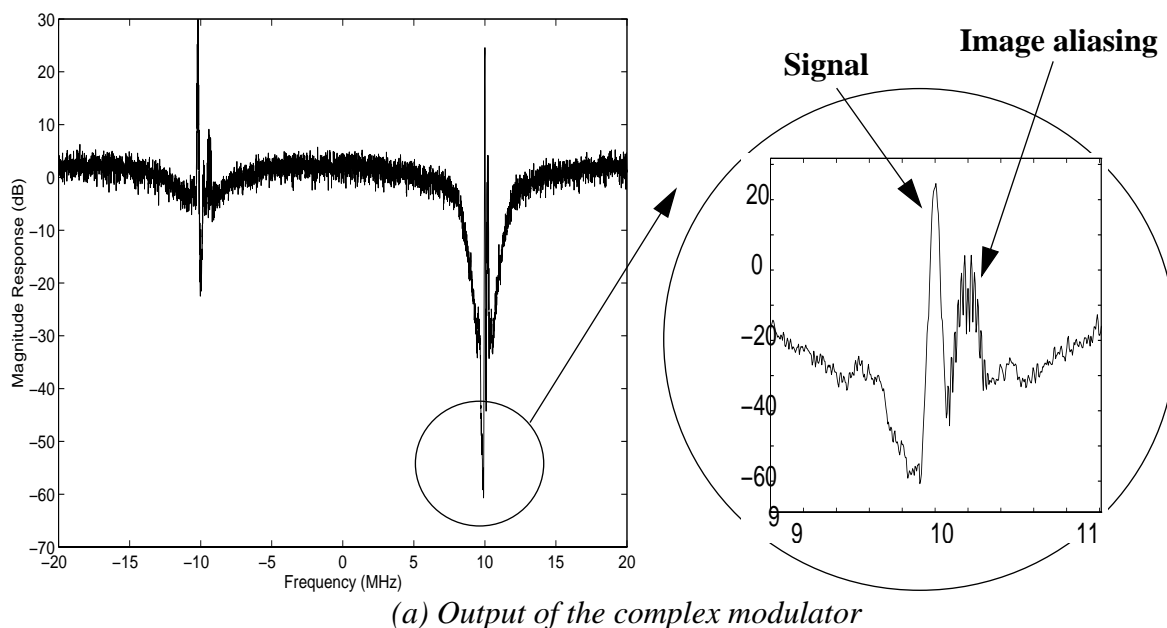
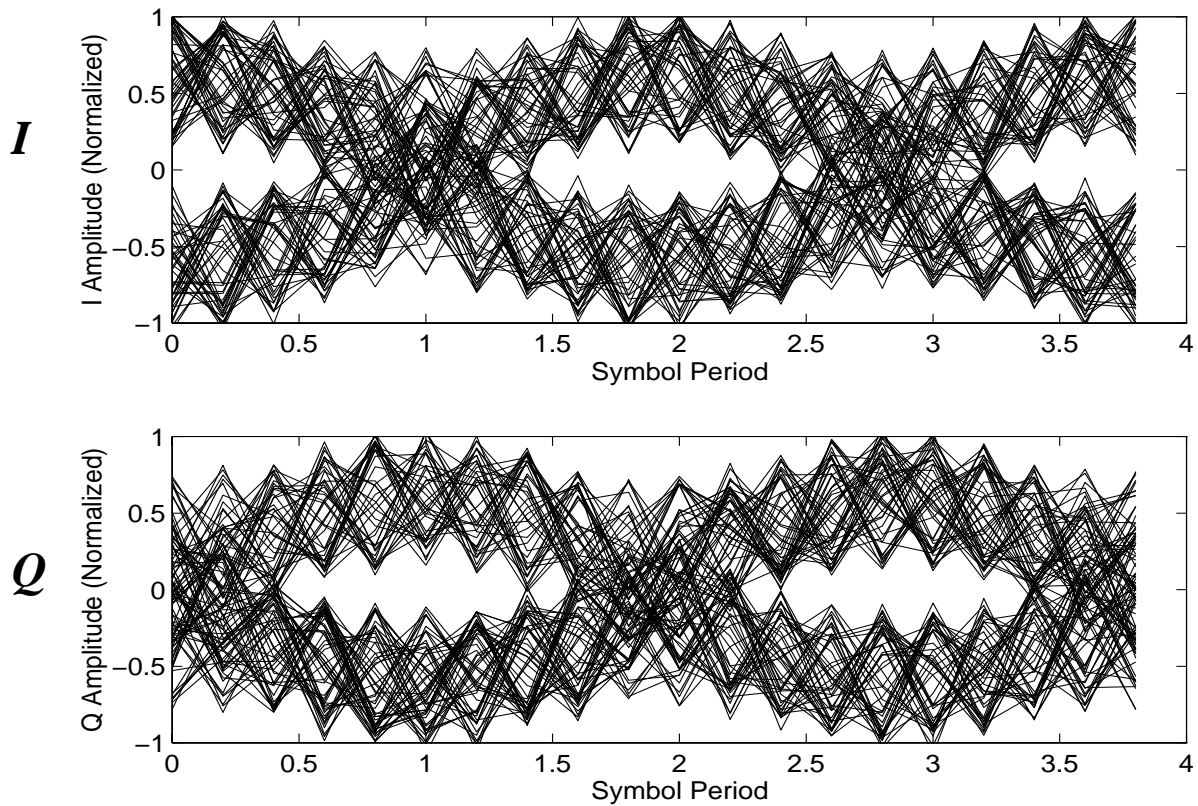


Fig. 2.22 Output spectra with mismatch

## 2.5 Conclusion

The theories of complex filters and complex sigma delta modulators have been introduced



*Fig. 2.23 Eye diagrams of the degraded I, Q signal*

in this chapter. Based on the complex sigma delta modulator, a single IF receiver is constructed.

I and Q channel mismatch problems and their effects are discussed. Mismatches due to imperfection of analog circuitry, such as gain or phase imbalances introduced by mixers, or coefficient mismatch introduced by the complex modulator, can limit the selectivity of the receiver.

## *Chapter 3*

---

### *An Adaptive Algorithm for I/Q Channel Mismatch Cancellation*

#### **3.1 Introduction**

In the previous chapter, we analyzed the mismatch problems in the complex system. In this chapter, we are going to present a novel DSP solution for this problem. Using a modified adaptive noise cancellation model and a new adaptive algorithm, the degradation due to the I/Q channel mismatch can be effectively compensated.

In Section 3.2, the previous solutions for the I/Q channel mismatch problems are introduced. The classic adaptive noise cancellation system will be reviewed in Section 3.3. It is explained in Section 3.4 that directly applying the classic adaptive noise cancellation model to the I/Q channel mismatch problem will not improve the performance of the system. Thus, a modified noise canceler model is introduced. The LMS (Least Mean Square) algorithm has been chosen for this application because of its simplicity and stability. The new complex LMS algorithm is discussed in Section 3.5. The MATLAB simulink model of the entire system is shown and explained in Section 3.6 [MATLABa][MATLABb][Oppenheim94]. An experimental receiver using this technique will be presented in Chapter 4.

An extension of the technique, which applies the algorithm to double sampling systems is also analyzed and discussed.

## 3.2 Previous Solutions

In quadrature sampling systems, the I/Q channel mismatch problem is always a big concern. A large amount of work has been done to minimize the degradation due to the channel mismatch. In this section, different solutions will be introduced.

### 3.2.1 Off-Line Adjustment

If the imbalance of the two paths can be measured, it can be corrected. The correction scheme is through the Gram-Schmidt procedure, which produces an orthonormal basis from an arbitrary set of vectors [Trees68][Carlson86][Schwartz90]. In [Churchill81], Churchill presented a method that uses the Gram-Schmidt procedure to correct I/Q problems. The results will be presented here.

In order to simplify this discussion, assume that both the amplitude error and the phase error are in the Q path. The I and Q outputs of the mixer in the RF front end can be expressed as:

$$\begin{aligned} I_2 &= A \cos(2\pi f_{IF}t) \\ Q_2 &= (1+k)A \sin(2\pi f_{IF}t + \theta) \end{aligned} \quad \text{Eq. (3.1)}$$

where  $k$  represents the amplitude imbalance and  $\theta$  represents the phase imbalance. The corrected outputs  $I_2'$  and  $Q_2'$  can be written in matrix form as

$$\begin{bmatrix} I_2' \\ Q_2' \end{bmatrix} = \begin{bmatrix} E_G & 0 \\ P & 1 \end{bmatrix} \begin{bmatrix} I_2 \\ Q_2 \end{bmatrix} \quad \text{Eq. (3.2)}$$

where  $I_2'$  and  $Q_2'$  are orthogonal and balanced.

For the case of Eq. (3.1), E and P are

$$\begin{aligned} E_G &= (1 + k)\cos\theta \\ P &= -(1 + k)\sin\theta \end{aligned} \quad \text{Eq. (3.3)}$$

If the values in Eq. (3.3) are substituted into Eq. (3.2), the results are

$$\begin{aligned} I_2' &= (1 + k)A\cos\theta\cos(2\pi f_{IF}t) \\ Q_2' &= (1 + k)A\cos\theta\sin(2\pi f_{IF}t) \end{aligned} \quad \text{Eq. (3.4)}$$

which indicates that the two outputs have the same amplitudes and they are  $90^\circ$  out of phase.

To correct the errors we must find the imbalance and then generate the correction coefficients in the above equation. This correction can be accomplished by using a test signal of frequency  $f$ . The sampling frequency is four times the input frequency, which means  $f_s = 4f$ . Only four samples are required to calculate the correction coefficients. The output of the I/Q paths can be written in a complex form as

$$s_t(t) = A\cos(2\pi ft + \varphi) + j(1 + k)A\sin(2\pi ft + \varphi + \theta) \quad \text{Eq. (3.5)}$$

where  $\varphi$  is the initial phase of the input signal. And the four samples are

$$\begin{aligned} s_t(0) &= A\cos\varphi + j(1 + k)A\sin(\varphi + \theta) \\ s_t(1) &= -A\cos\varphi + j(1 + k)A\sin(\varphi + \theta) \\ s_t(2) &= -A\cos\varphi - j(1 + k)A\sin(\varphi + \theta) \\ s_t(3) &= A\cos\varphi - j(1 + k)A\sin(\varphi + \theta) \end{aligned} \quad \text{Eq. (3.6)}$$

The Fourier transform of  $s_t(t)$  can be written as

$$S_t(m) = \sum_{n=0}^{N-1} s_t(t)e^{-j2\pi nm/N} \quad \text{Eq. (3.7)}$$

Since the input frequency is  $f$  and the input is sampled at  $4f$  and only four samples are obtained, in the frequency domain  $S_t(m)$  has only four outputs. Three of the four frequency components are as follows:  $S_t(0)$  is the dc component,  $S_t(1)$  is the input frequency, and  $S_t(3)$  is the image.

From the frequency domain outputs at test signal frequency  $S_t(1)$  and at the image frequency  $S_t(3)$ , the coefficients  $E_G$  and  $P$  for correction of gain and phase errors can be obtained:

$$E_G = 1 - \operatorname{Re} \left[ \frac{2S_t(3)}{S_t^*(1) + S_t(3)} \right]$$

$$P = -\operatorname{Im} \left[ \frac{2S_t(3)}{S_t^*(1) + S_t(3)} \right] \quad \text{Eq. (3.8)}$$

This correction can be applied one frequency at a time. When the I and Q channels cover a wide bandwidth, the imbalance is a function of frequency. This method might be impractical to apply because it needs an off-line test input and can not track time variation.

### 3.2.2 Hilbert Transform

A solution mentioned in [Tsui95] is to move the generation of I and Q signals to the digital domain by using the Hilbert transform [Carlson86] [Lee94] [Oppenheim89] [Oppenheim83] [Sabin95]. The structure of this kind of receiver is shown in Fig. 3.1. In this approach, the data for one channel (say the I channel) are obtained from a single path A/D converter, while the data of the Q channel are generated by processing the I channel data through a Hilbert filter. Since the Q channel data are generated digitally, the imbalance between the outputs of the I and Q channels can be kept at a minimum.

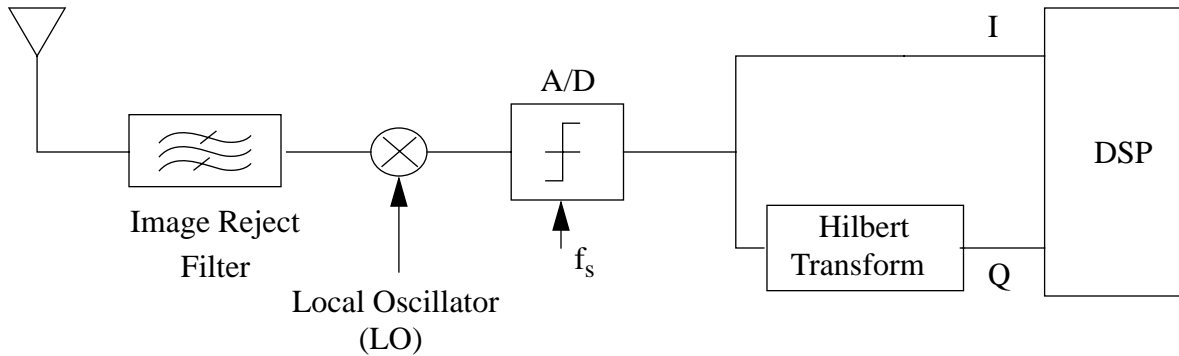


Fig. 3.1 A digital receiver with Hilbert Transform

One of the major disadvantages of this approach is that the operating speed is limited by the complexity of Hilbert filters. In order to get balanced I and Q signals, a high order filter is needed to perform the Hilbert transform. The resulting solution has high power consumption, low processing speed and high hardware complexity. More importantly, the system now has a single-path mixer and therefore relies entirely on a filter to control the image at  $f_{RF} \pm 2f_{IF}$ .

### 3.2.3 An Improved Sigma Delta Modulator Structure

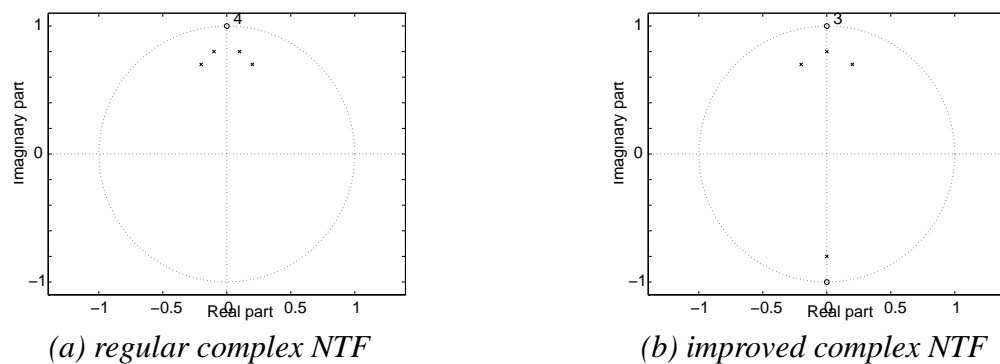
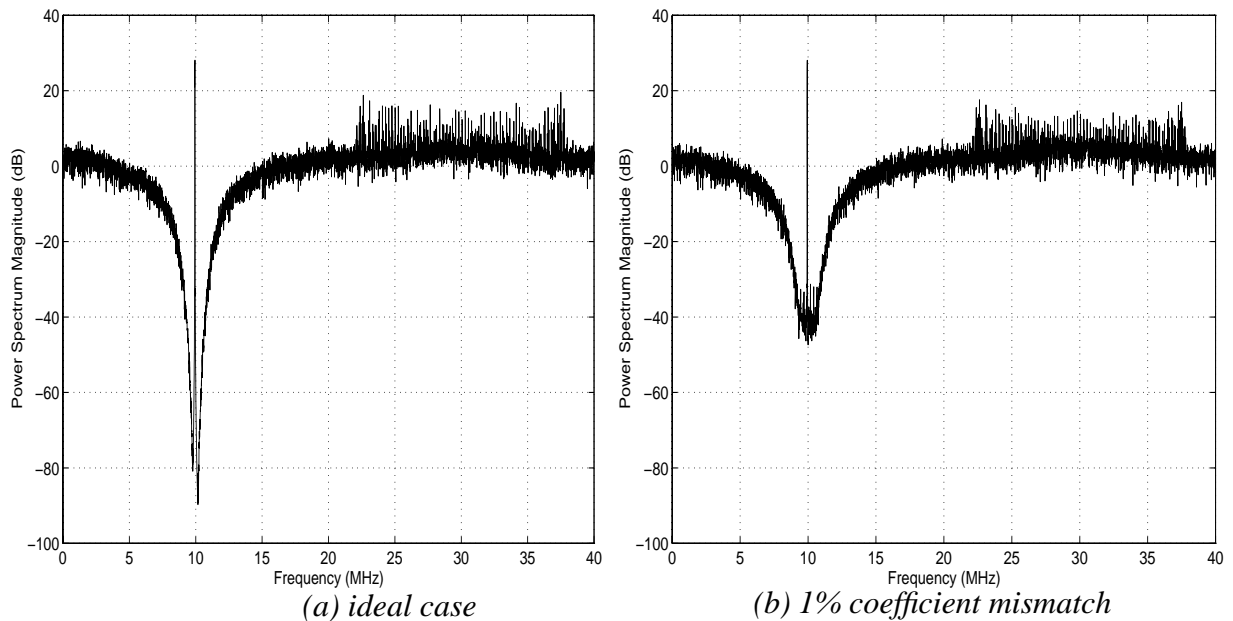


Fig. 3.2 Zero/pole constellations for the regular and improved complex NTFs

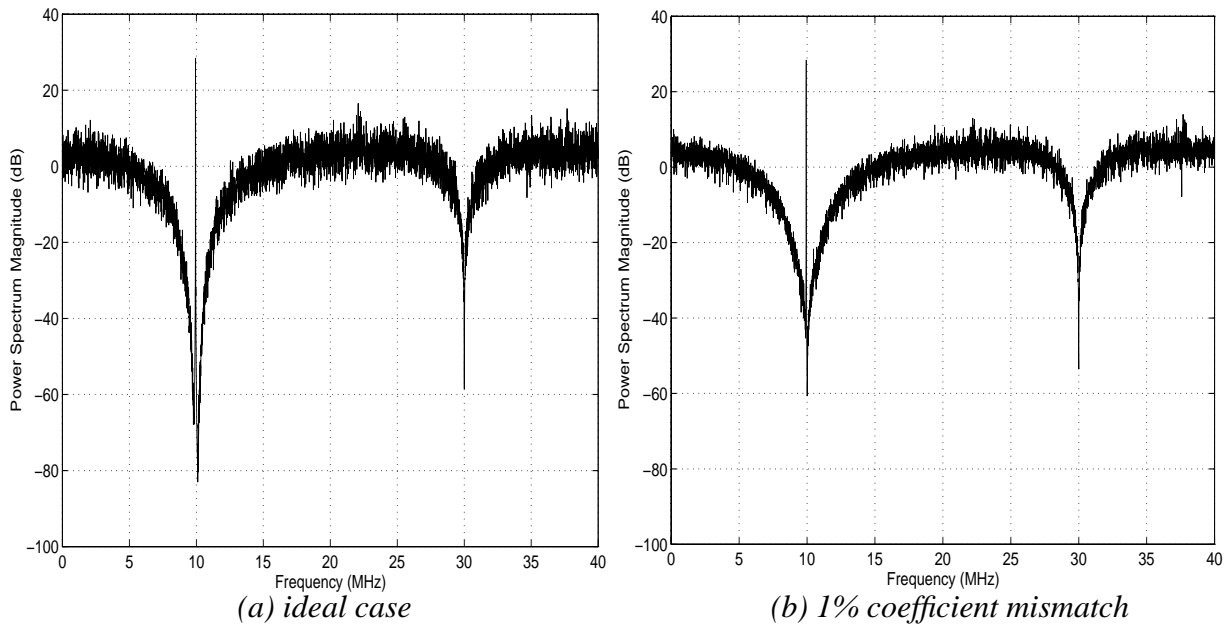
Another technique to compensate for part of the performance degradation due to mismatch in complex sigma delta modulators. One of the NTF notches is placed in the quantizer's

own image band, which provides some attenuation of the image band noise before it aliases into the desired signal band [Jantzi96]. An example of this method is pictured in Fig. 3.2. The NTF shown in Fig. 3.2(a) has all four notches in the real band, while the NTF shown in Fig. 3.2(b) has one of its four notches placed in the image band. The frequency responses of these two NTF are shown in Fig. 3.3 and Fig. 3.4 respectively. For comparison, an ideal frequency response and one with 1% coefficient mismatch are placed next to each other. We can see that the SNR degradation in the complex sigma delta modulator which has all four notches in the real band is about 45 dB, while the SNR degradation in the other modulator, which has one notch placed in the image band, is only about 20 dB.



*Fig. 3.3 Power spectrum of a fourth order complex sigma delta modulator*

Thus, this method is extremely effective in maintaining a mismatched modulator's SNR, but we notice that the quantization noise floor in Fig. 3.4(a) is about 15 dB higher than in Fig. 3.3(a) because there are only three zeros in-band (in the real band) rather than four zeros (compare



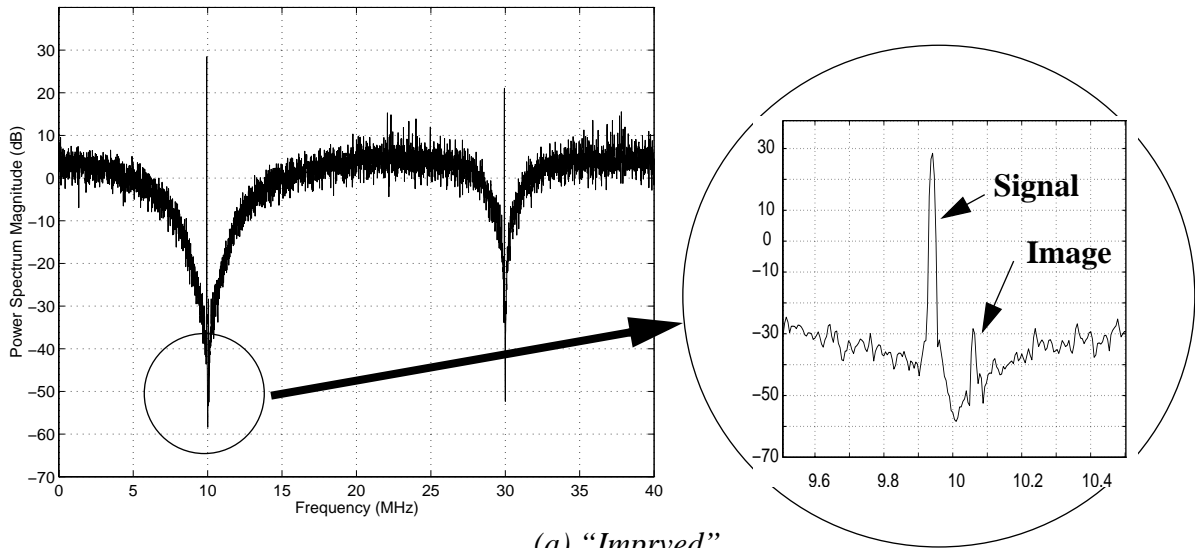
*Fig. 3.4 Power spectra of an improved fourth order complex sigma delta modulator*

Fig. 3.2(a) and (b)).

Moreover, this kind of improvement does not have much effect on the interference that exists at the image frequency because it involves only the transfer functions for quantization noise. From Fig. 3.5(a) (the fourth order complex modulator with one zero in the image band), we can see that the image interference tone is attenuated by 50 dB when it aliases back to the band of interest with 1% coefficient mismatch while in Fig. 3.5(b) (the fourth order complex modulator with all the zeros in band), the degradation is also around 50 dB. So there is no advantage in the improved structure for input image interference. It is explained as follows. The output of the complex sigma delta modulator  $Y$  can be simply expressed as:

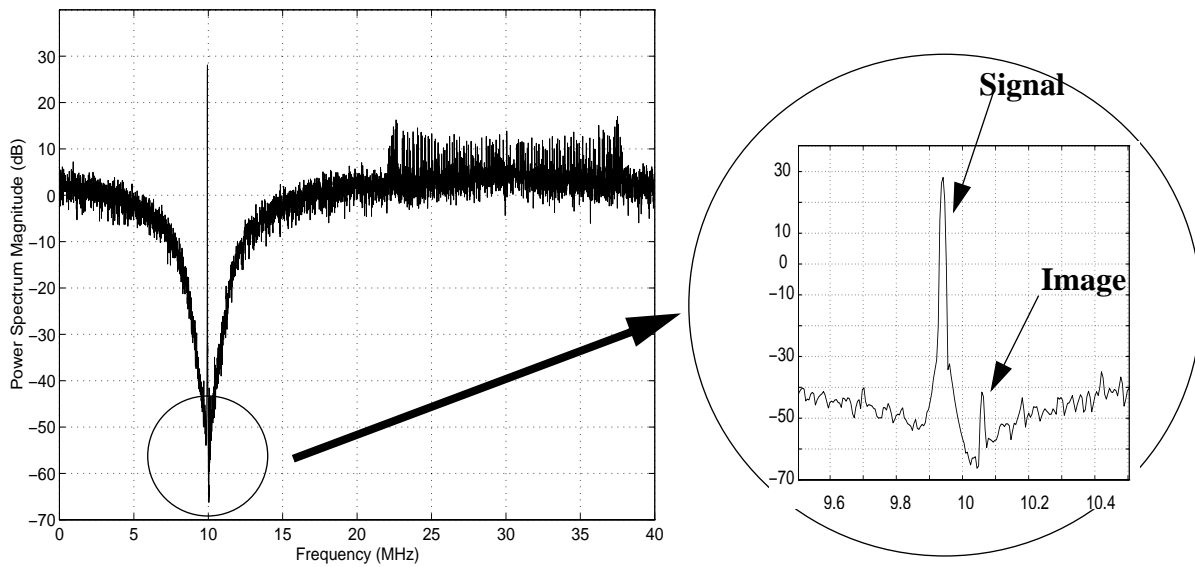
$$Y = GX + HE \quad \text{Eq. (3.9)}$$

where  $X$  is the input of the complex sigma delta modulator,  $E$  is the quantization noise,  $G$  is the STF (signal transfer function) and  $H$  is the NTF (noise transfer function).



(a) "Improved"

Modulator with one NTF zero in the image band



(b) "Regular"

Modulator with no NTF zeros in the image band

Fig. 3.5 Power spectra for two fourth order complex bandpass sigma delta modulators with simultaneous image interference and 1% mismatches

When there is a mismatch, Eq. (3.9) can be written as:

$$Y = GX + \Delta G_{diff} \bar{X} + HE + \Delta H_{diff} \bar{E} \quad \text{Eq. (3.10)}$$

where  $\bar{(\cdot)}$  is the complex conjugate,  $\Delta G_{diff}$  and  $\Delta H_{diff}$  are the differential error term of transfer

functions  $G$  and  $H$  respectively.

By placing one of the four notches in the image band, only  $H$  has been improved such that  $\bar{E}$  gets attenuated by  $\Delta H_{diff}$  before it aliases into the signal band. The other differential error term  $\Delta G_{diff} \bar{X}$  has not been considered. If there is a strong interference at the image frequency, image aliasing due to this term cannot be ignored.

Next, we are going to introduce a new method to improve the SNR in the unbalanced I/Q system. The method uses the fact that the analog circuitry error can be compensated in the digital world. It takes advantage of the complex system and uses the adaptive noise cancellation model to get best performances.

### 3.3 An Adaptive Noise Canceler System

The usual method of recovering a signal corrupted by additive noise or interference is to pass the degraded signal through a filter that can suppress the noise while leaving the signal relatively unchanged. Filters used for this purpose can be fixed or adaptive. The design of fixed filters must be based on prior knowledge of both the signal and the interference which is not the case in most applications. On the other hand, adaptive filters are able to adjust their own parameters automatically and their design requires much less prior knowledge of signal or interference characteristics.

The adaptive noise-cancellation concept is shown in Fig. 3.6. A signal is transmitted over a channel to a sensor that receives the signal  $s$  plus an uncorrelated noise,  $n_0$ . The combined signal and noise,  $s+n_0$ , form the *primary input* of the canceler.

A second sensor receives a noise  $n_1$  which is uncorrelated with the signal  $s$  but is

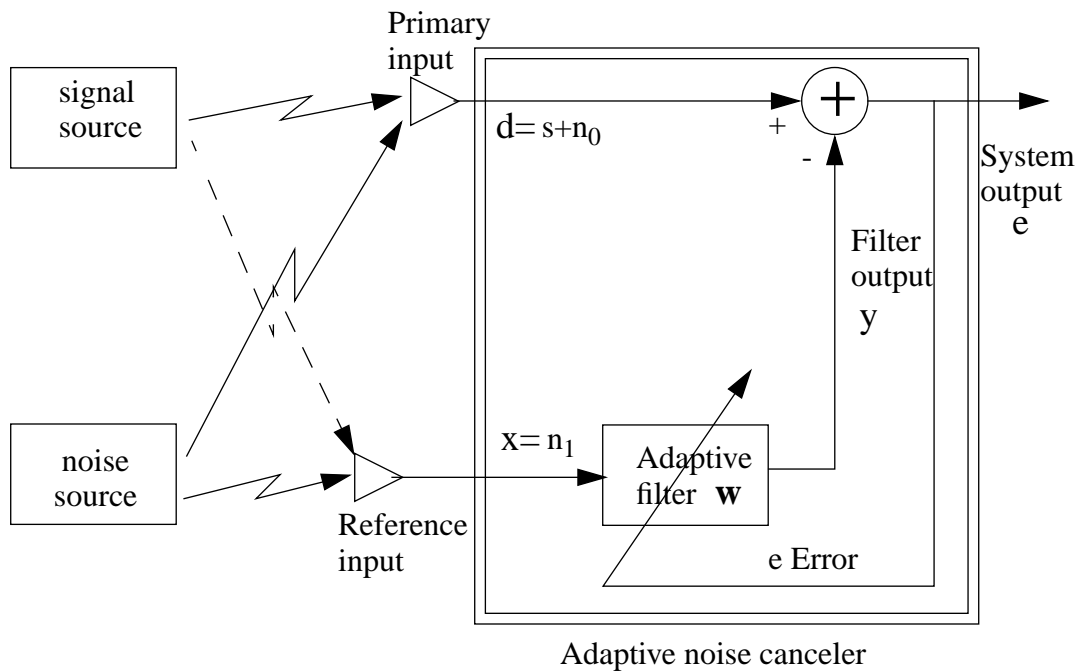


Fig. 3.6 Adaptive noise cancellation model

correlated in some unknown way with the noise  $n_0$ . This sensor provides the *reference input* to the canceler. The noise  $n_1$  is filtered to produce an output  $y$  that is a close replica of  $n_0$ . This output is subtracted from the *primary input*  $s+n_0$  to produce the system output,  $e$ , which is equal to  $s+n_0-y$ .

If one knew the characteristics of the channels over which the noise was transmitted to the primary and reference sensors, one could, in general, design a fixed filter capable of changing  $n_1$  into  $y=n_0$ . The filter output could then be subtracted from the *primary input*, and the system output would be the signal alone.

Since, however, the characteristics of transmission paths are assumed to be unknown or known only approximately and are not of a fixed nature, the use of a fixed filter is not feasible. Moreover, even if a fixed filter were feasible, its characteristics would have to be adjusted with a precision difficult to attain, and the slightest error could result in increased output noise power.

In the system shown in Fig. 3.6, the *reference input* is processed by an adaptive filter that automatically adjusts its own impulse response through an adaptive algorithm [Widrow85] [Leon94] such as LMS (least mean square) to the transfer function between  $n_1$  and  $n_0$ . Thus with the proper algorithm, the filter can operate under changing conditions and can readjust itself continuously to minimize the error signal.

### 3.4 A Modified Adaptive Noise Canceler Model

How do we fit this model to our complex system to minimize the image noise due to channel mismatches?

In our system shown in Fig. 2.2 of Chapter 2, the noise or interference we are trying to eliminate comes from the differential error term. The perfect *reference input* signal would be the complex conjugate of the input signal  $X(z)$ . We have to notice that the input signal for the complex modulator is an analog signal and it will not be available as the *reference input* in the DSP system. The only way we can get the digitized complex conjugate of the input signal is from the output signal of the modulator. To simplify the equation, we use a complex representation, therefore, all the variables and transfer functions in the following expressions are complex. The output of the modulator  $Y(z)$  can be expressed as

$$Y = GX + \Delta G_{diff} \bar{X} + HE + \Delta H_{diff} \bar{E}. \quad \text{Eq. (3.11)}$$

where  $X$  is the input of the complex sigma delta modulator,  $E$  is the quantization noise,  $G$  is the STF (signal transfer function) and  $H$  is the NTF (noise transfer function).  $\Delta G_{diff}$  and  $\Delta H_{diff}$  are the differential error term of transfer functions  $G$  and  $H$  respectively. So that,

$$\bar{Y} = \overline{GX(z)} + \overline{\Delta G_{diff} X(z)} + \overline{HE(z)} + \overline{\Delta H_{diff} E(z)} \quad \text{Eq. (3.12)}$$

### 3.4.1 Problems in the Classic Model

If we choose  $\overline{Y(z)}$  as the *reference input*, it can be seen from Eq. (3.12) that  $\overline{Y(z)}$  not only has the component of the complex conjugates of the desired signal,  $\overline{X(z)}$ , but also the desired signal itself,  $X(z)$ , which means directly applying the algorithm will not only suppress the image noise but also attenuate the signal itself. The SNR improvement is impaired because this biases the filter coefficients. This phenomenon in adaptive signal processing is called *signal leakage* and it is represented by the dotted line in Fig. 3.6 [Widrow85].

According to Widrow et.al [Widrow85], assuming the noises in *primary* and *reference inputs* are mutually correlated, the SNR at the noise-canceller output, which is  $e$  in Fig. 3.6, is simply the reciprocal at all frequencies of the SNR at the *reference input*, which is  $x$ . The derivation of this formula is presented in Appendix C.

$$\rho_{out}(z) = \frac{1}{\rho_{ref}(z)} \quad [47] \quad \text{Eq. (3.13)}$$

where  $\rho_{out}(z)$  is the signal-to-noise ratio at the output and  $\rho_{ref}(z)$  is the signal-to-noise ratio at the *reference input*. This process in Eq. (3.13) is called *power inversion* [47].

Smaller signal leakage means there is less signal component at the *reference input*. The SNR density ratio  $\rho_{ref}$  is smaller. The output SNR will be larger.

For our system, the *primary input* is the output of the complex filter with the image aliasing,  $Y(z)$ . The signal is  $X(z)$  and the image noise is  $\overline{X(z)}$ . Thus, the SNR at the *primary input* is

$$\rho_{primary}(z) = \left| \frac{G(z)}{\Delta G_{diff}(z)} \right|$$

where  $\rho_{\text{primary}}(z)$  is the signal-to-noise ratio at the *primary input*. While the complex conjugate of the output is assigned as the *reference input*, the SNR at the *reference input* is

$$\rho_{\text{ref}}(z) = \left| \frac{\Delta G_{\text{diff}}(z)}{G(z)} \right| = \left| \frac{\Delta G_{\text{diff}}(z)}{G(z)} \right|$$

According to Eq. (3.13), the SNR at the adaptive noise canceler output is

$$\rho_{\text{out}}(z) = \frac{1}{\rho_{\text{ref}}(z)} = \left| \frac{G(z)}{\Delta G_{\text{diff}}(z)} \right| = \rho_{\text{primary}}(z)$$

If the classic adaptive noise cancellation system is connected after the complex filter, the output of the system has the same SNR as the output of the complex filter, which means the power of the image noise over the power of the desired signal is unchanged. There is then no point in adding the adaptive noise cancellation system.

### 3.4.2 Improved Model

The derivation above shows that we need to modify the classic noise canceler to a signal separator, which can separate the desired signal and the noise reference and get a “clean” signal and reference. “Clean” means they are uncorrelated to each other.

The classic noise canceler model in Fig. 3.6 is based on the correlation between the *reference input*  $n_1$  and  $n_0$  of the *primary input*. The adaptive filter models this correlation function. Now the reference input has some signal components that are correlated with the desired signal  $s$ . The modified model also considers this correlation and adds another adaptive filter modeling this correlation function. The modified system is called a signal separation system.

The signal separation system is shown in Fig. 3.7 [Compernelle95]. Here, we assume that two signals  $y_1(n)$ ,  $y_2(n)$  can be written as:

$$y_i(k) = s_i(k) + \mathbf{h}_i(k) \otimes s_j(k) \quad i = 1, 2 \quad j = 2, 1 \quad \text{Eq. (3.14)}$$

where  $s_1(k)$  and  $s_2(k)$  are uncorrelated. Both  $y_1(k)$  and  $y_2(k)$  have  $s_1(k)$  and  $s_2(k)$  components.

" $\otimes$ " represents convolution. The signal leakage problem can be modeled by Eq. (3.14).

The aim for the modified noise cancellation system is to obtain signal estimates  $u_i(k)$  by adaptive filtering of  $y_i(k)$ . The bold parts in Fig. 3.7 show differences between the improved

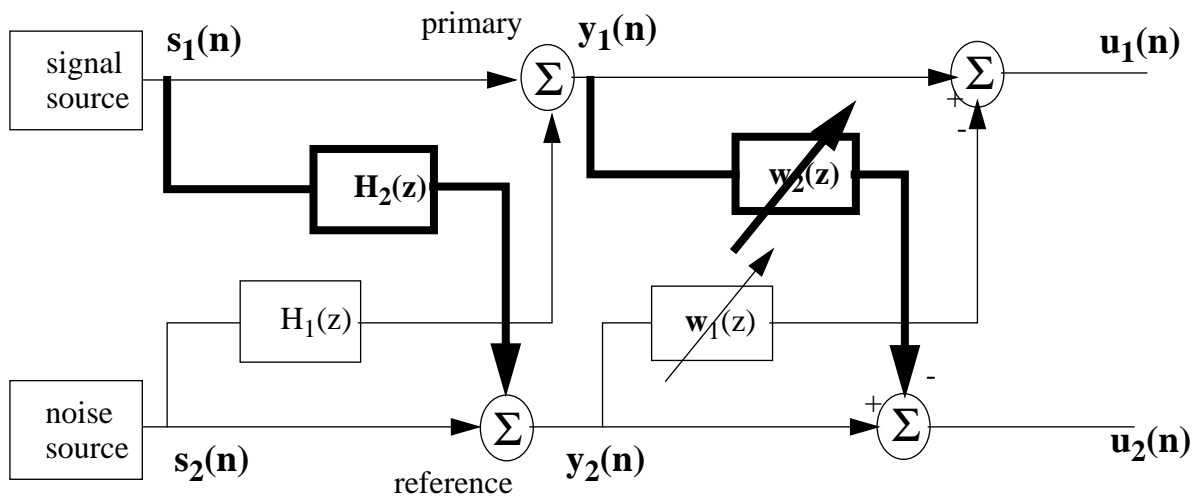


Fig. 3.7 Modified adaptive noise cancellation model

model and the traditional noise canceler.

The signal estimates  $u_i(k)$  can be written as:

$$u_i(k) = y_i(k) - \mathbf{w}_i^T(k) \otimes y_j(k) \quad i = 1, 2 \quad j = 2, 1 \quad \text{Eq. (3.15)}$$

where  $\mathbf{w}_i(k)$  is the coefficients of the adaptive filters which is expressed as:

$$\mathbf{w}_i(k) = [w_i^{(k)}(0)w_i^{(k)}(1)\dots w_i^{(k)}(L_i - 1)]^T$$

and  $L_i$  is the order of the adaptive filter,

$$\mathbf{y}_i(k) = [y_i(k)y_i(k-1)\dots y_i(k-L_i+1)]^T,$$

The coefficients' updates are:

$$w_1^{(k+1)}(m) = w_1^{(k)}(m) + \mu_1 u_1(k) u_2(k-m) \quad m = 0 \dots (L_1 - 1) \quad \text{Eq. (3.16)}$$

$$w_2^{(k+1)}(n) = w_2^{(k)}(n) + \mu_2 u_2(k) u_1(k-n) \quad n = 0 \dots (L_2 - 1)$$

Eq. (3.16) uses “ $u_2$ ” where a simple noise canceller would use “ $y_2$ ”. The signal leakage term has been cancelled in “ $u_2$ ” so that updates for  $\mathbf{w}_1$  are not biased by it.

## 3.5 Complex LMS Algorithm

### 3.5.1 A Basic Complex LMS Algorithm

The adaptive algorithm chosen here is the LMS algorithm, because of its simplicity, hardware efficiency and stability [Widrow85]. More sophisticated algorithms converge and track more rapidly, but typical mismatch mechanisms depending on device ratios and temperature differences do not need to be tracked very rapidly. Because the systems we are dealing with here are complex systems, the complex LMS algorithm will be introduced next.

Assume that all the signal and transfer function notations are shown in Fig. 3.6 and they are complex. The complex error and desired response required to adapt both the real and imaginary weights are given by [Widrow71].

$$e(k) = e_R(k) + je_I(k)$$

$$d(k) = d_R(k) + jd_I(k) \quad \text{Eq. (3.17)}$$

The complex output  $y$  is correspondingly given by

$$y(k) = y_R(k) + jy_I(k) \quad \text{Eq. (3.18)}$$

And it can be written as:

$$y(k) = \mathbf{w}^T(k) \otimes \mathbf{x}(k)$$

The system output  $e$  can be written as:

$$e(k) = d(k) - \mathbf{x}^T(k) \otimes \mathbf{w}(k)$$

The coefficients' update equations can be written as:

$$\mathbf{w}(k+1) = \mathbf{w}(k) + 2\mu e(k) \overline{\mathbf{x}(k)}$$

where  $\mu$  is the stepsize which controls the speed, stability and ultimate performance of adaptation.

The coefficients of the adaptive filter are  $\mathbf{w}(k)$ .

$$\mathbf{w}(k) = \mathbf{w}_R(k) + j \cdot \mathbf{w}_I(k)$$

where

$$\mathbf{w}_R(k) = [w_R^{(k)}(0)w_R^{(k)}(1)\dots w_R^{(k)}(L-1)]^T$$

$$\mathbf{w}_I(k) = [w_I^{(k)}(0)w_I^{(k)}(1)\dots w_I^{(k)}(L-1)]^T$$

$L$  is the order of the adaptive filter.

### 3.5.2 A Modified Algorithm

Based on the modified model proposed in Section 3.4.2 and the complex LMS algorithm introduced in Section 3.5.1, the modified complex LMS algorithm can be expressed as follows.

All expressions of the variables or adaptive filters follow the notations in Fig. 3.7.

The system outputs  $u_i(k) = u_{iR}(k) + ju_{iI}(k)$ , can be expressed as

$$u_i(k) = y_i(k) - \mathbf{y}_j^T(k) \otimes \mathbf{w}_i(k) \quad i = 1, 2 \quad j = 2, 1 \quad \text{Eq. (3.19)}$$

The *primary input* vector  $\mathbf{y}_1(k)$  and the *reference input* vector  $\mathbf{y}_2(k)$  are written as:

$$\mathbf{y}_i(k) = \mathbf{y}_{iR}(k) + j \cdot \mathbf{y}_{iI}(k) \quad i = 1, 2$$

The coefficient update equation can be written as:

$$\mathbf{w}_i(k+1) = \mathbf{w}_i(k) + 2\mu_i u_i(k) \overline{\mathbf{u}_j(k)} \quad i = 1, 2 \quad j = 2, 1 \quad \text{Eq. (3.20)}$$

$\mu_i$  are the stepsize which control the speed and stability of adaptation of the real part and imaginary part of the coefficients respectively. The system outputs, the “clean” signal and noise vectors are  $\mathbf{u}_i(k) = \mathbf{u}_{iR}(k) + j\mathbf{u}_{iI}(k)$ .

The coefficients of the adaptive filters are

$$\mathbf{w}_i(k) = \mathbf{w}_{iR}(k) + j \cdot \mathbf{w}_{iI}(k)$$

where

$$\mathbf{w}_{iR}(k) = [w_{iR}^{(k)}(0)w_{iR}^{(k)}(1)\dots w_{iR}^{(k)}(L_i - 1)]^T$$

$$\mathbf{w}_{iI}(k) = [w_{iI}^{(k)}(0)w_{iI}^{(k)}(1)\dots w_{iI}^{(k)}(L_i - 1)]^T$$

$L_i$  is the orders of the adaptive filters.

### 3.5.3 Decimation Filtering

Sigma delta modulators have noise shaping characteristics, that is, the quantization noise can be shaped out of the band of interest. We can see from Fig. 2.5(b) that the out of band quantization noise is much larger than the image noise due to mismatches. If we directly apply the outputs from the sigma delta modulator to the noise cancellation system, the *primary input* contains a large amount of quantization noise which is uncorrelated with the interference signal, and the out of band quantization noise floor can be higher than the interference level. This will

make the coefficients in the adaptive filter converge to zeros instead of converging to the coefficients that can eliminate the mismatch.

One way to solve this problem is to use bandpass filters to obtain only the information in the band of interest. The system architecture is shown in Fig. 3.8. The bandpass filters are added

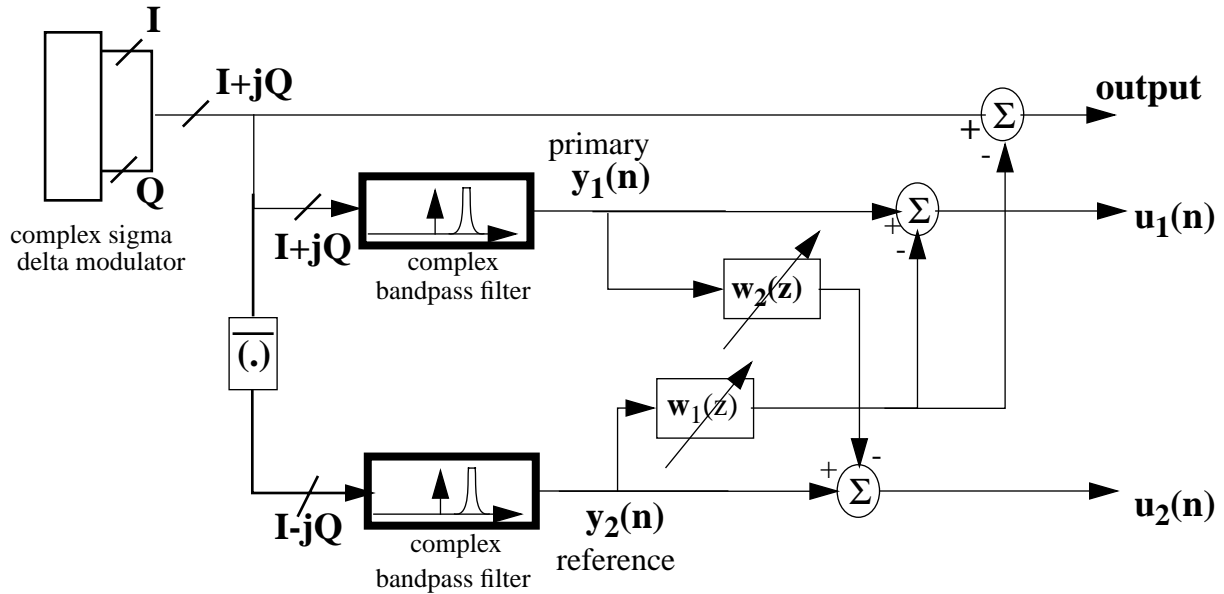
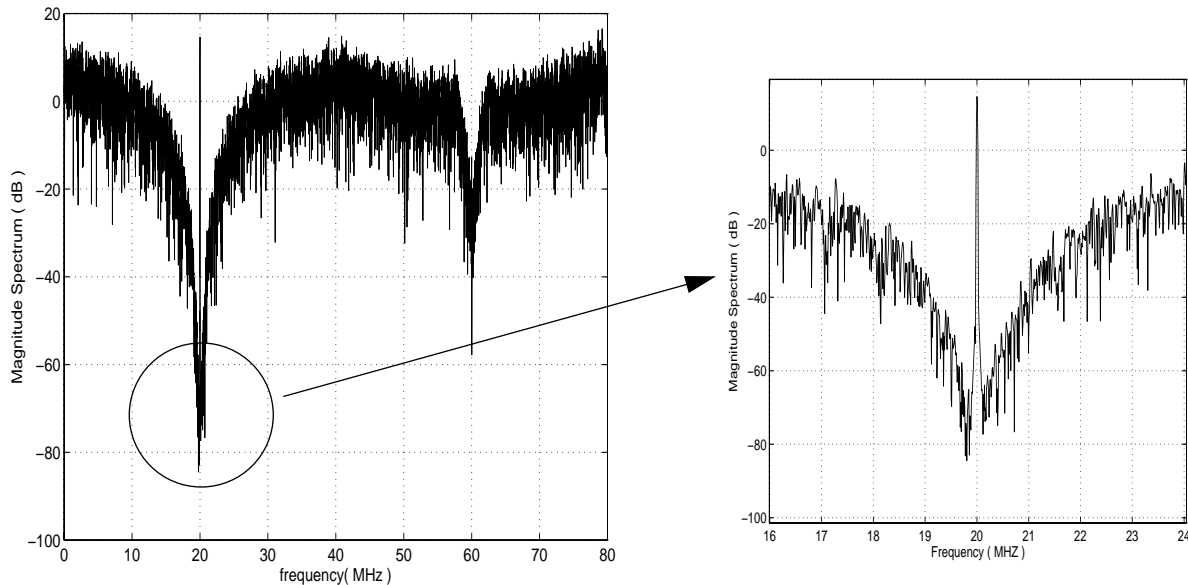


Fig. 3.8 Block diagram of the mismatch cancellation system (using bandpass filters)

before the mismatch cancellation system. Fig. 3.9 shows the simulation result of applying the new algorithm to the previous example in Fig. 2.5 with 1% coefficient mismatch. We can see the noise floor is brought down to  $-70$  dB. Hence a 20 dB improvement has been achieved.

Bandpass filters used in the simulation eliminate the quantization noise and leave the desired signal and the image noise due to the mismatch untouched. But these bandpass filters are very difficult and expensive to implement in real time, because they work at very high speed (40 MHz in the example).

Recall the receiver structure shown in Fig. 2.6 of Chapter 2, in which the demodulator and



*Fig. 3.9 Output spectrum after the mismatch cancellation*

decimation filters are used for getting rid of quantization noise and bringing the IF signal to the baseband. Thus, we can remove the bandpass filters and take advantage of demodulator and decimation filters.

Demodulation, which is actually mixing here, is a process of shifting the frequency band of the received signal back down to the baseband. The digital quadrature demodulation scheme mentioned in Chapter 2 has been used.

Decimation is the process that digitally converts the sampling rate of a signal from a given rate to a lower rate [Crochiere83]. It has been used in sigma delta modulators to get rid of quantization noise and take the 1-bit data stream at a high sample rate and transform it into a higher resolution data stream at the Nyquist rate (twice the signal bandwidth).

If we can move the noise cancellation system after the decimation filters, the operating frequency can go down to 625 kHz in the example, and the complex bandpass filters shown in Fig. 3.8 are no longer necessary. This means the system is operating at same rate as DFE (Decision

Feedback Equalizer) [Lee94], which is in the system anyway. Thus, the novel correction system is a reasonable load for the receiver.

Decimation filtering for sigma delta modulators has been studied in [Candy92] [Kwentus97][Schreier90]. The simplest and most economical filter to reduce the input sampling rate is a cascaded integrator-comb (CIC) filter proposed by Hogenauer [Hogenauer81], because such a filter does not require a multiplier. A CIC decimation filter consists of two main sections: an integrator section, which is a cascade of  $L$  integrators with the transfer function

$$H_I(z) = \left( \frac{1}{1-z^{-1}} \right)^L$$

and a comb section, which is a cascade of  $L$  combs with the transfer function

$$H_C(z) = (1-z^{-1})^L$$

The integrator and comb sections are separated by a decimator with a decimation factor  $R$ . The

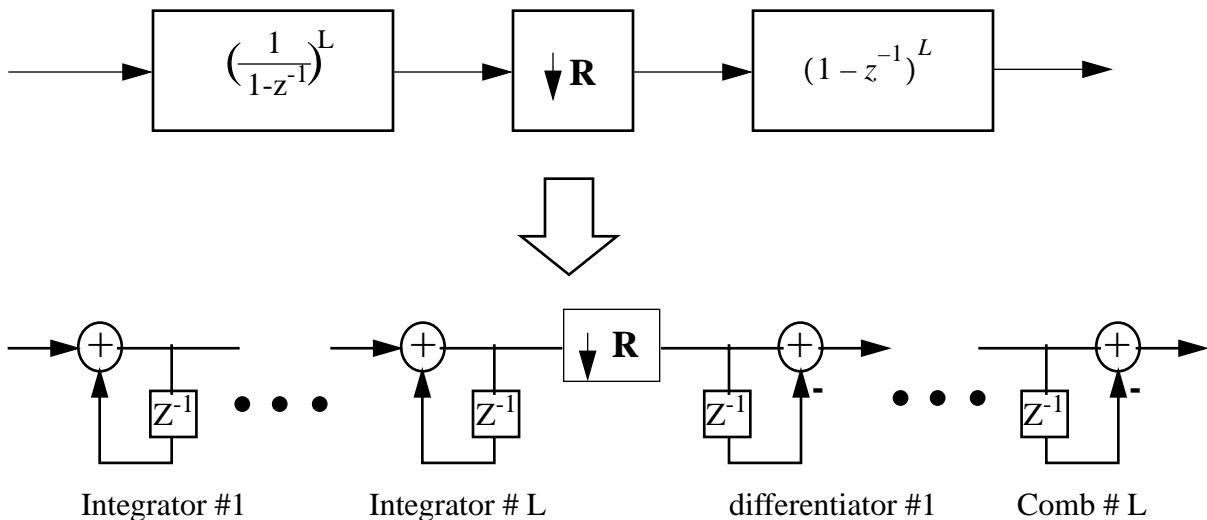


Fig. 3.10 Block diagram of a CIC decimation filter

structure of this filter is shown in Fig. 3.10. It is very suitable for VLSI implementation at high

data rates because of the simplicity of this filter and its efficient structure. Additionally, the comb section operates at the lower data rate, resulting in a smaller chip area and lower power dissipation.

Thus, the modified algorithm not only can improve the system performance by compensating the degradation due to mismatch, but can do so in a very efficient way.

### 3.6 A Simulink Model for the Complex A/D and the Modified Algorithm

Fig. 3.11 shows the MATLAB model and the spectrum at each stage. The desired signal generated from a GMSK random source is modulated to an RF frequency  $f_{RF}$ . The image interference generated from an FM source is modulated to  $f_{RF} + 2f_{IF}$ . After passing through the mixer shown in part II of Fig. 3.11, the signal and the image interference are located at  $f_{IF}$  and  $-f_{IF}$  respectively, which can be clearly seen from the spectra.

The output of the complex bandpass sigma delta modulator is an oversampled 1-bit data stream, which has a deep notch at  $f_{IF}$  and an asymmetric frequency response at  $-f_{IF}$  shown in Part III of Fig. 3.11. The image aliasing due to the mismatch can also be seen at this stage.

Part IV is a digital quadrature demodulator, of which the output is a baseband signal sampled at the oversampling rate. After the decimation, the sampling rate is back to the Nyquist rate. The magnitude responses of the outputs after the decimation, including the *primary input* and the *reference input* for the adaptive mismatch cancellation system, are shown in Part V.

The corrected signal is shown in Part VI.

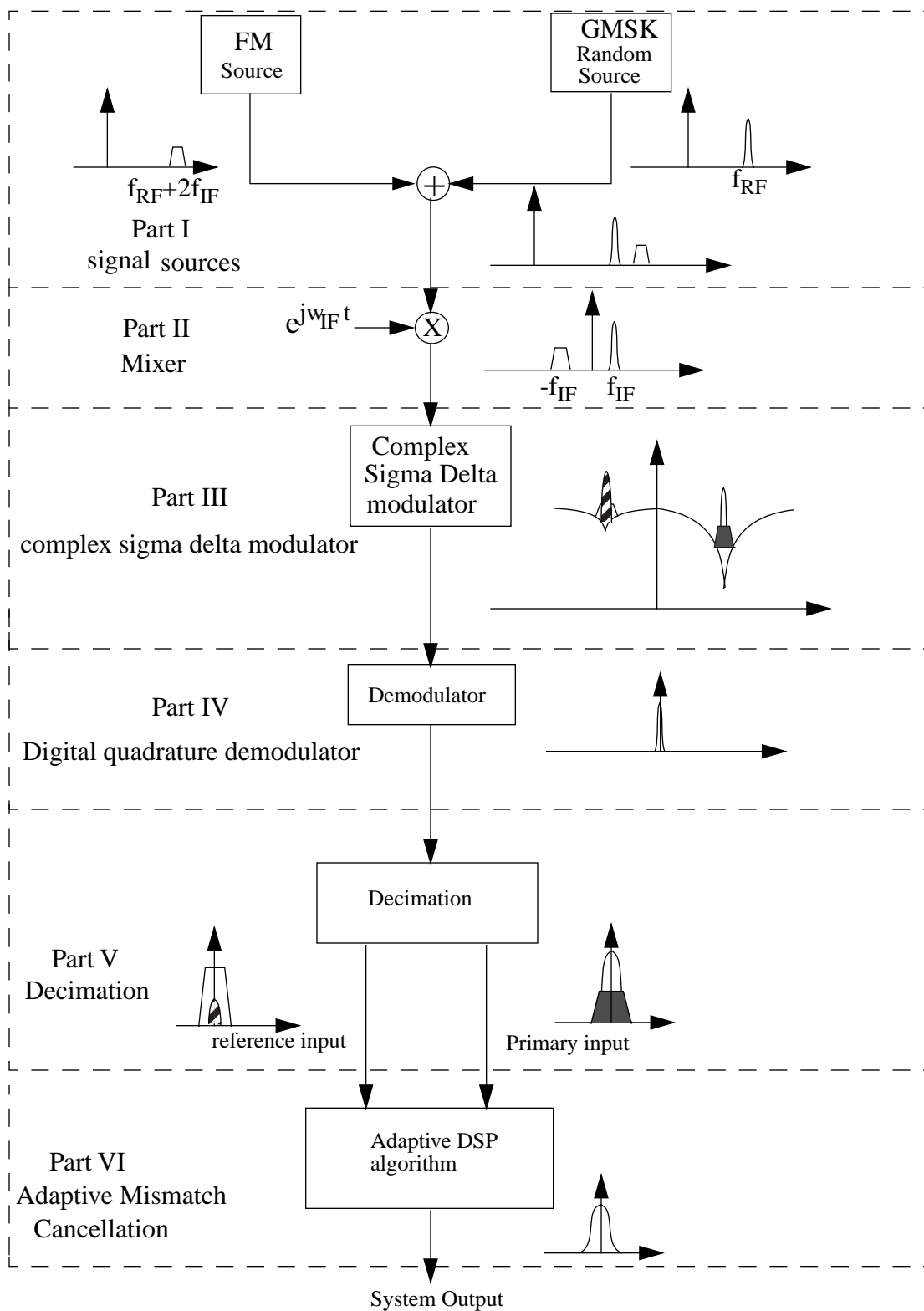


Fig. 3.11 Matlab module and signal spectrum in each stage

### 3.7 Simulation Results

This section will present results using the MATLAB model shown in Fig. 3.11 to prove the feasibility of the novel adaptive mismatch cancellation system. The adaptive mismatch cancellation system operates on the signal,  $I_5 + jQ_5$ . After applying the system, the improvements of  $I_5 + jQ_5$  are presented in this section. The magnitude response of  $I_5 + jQ_5$  in

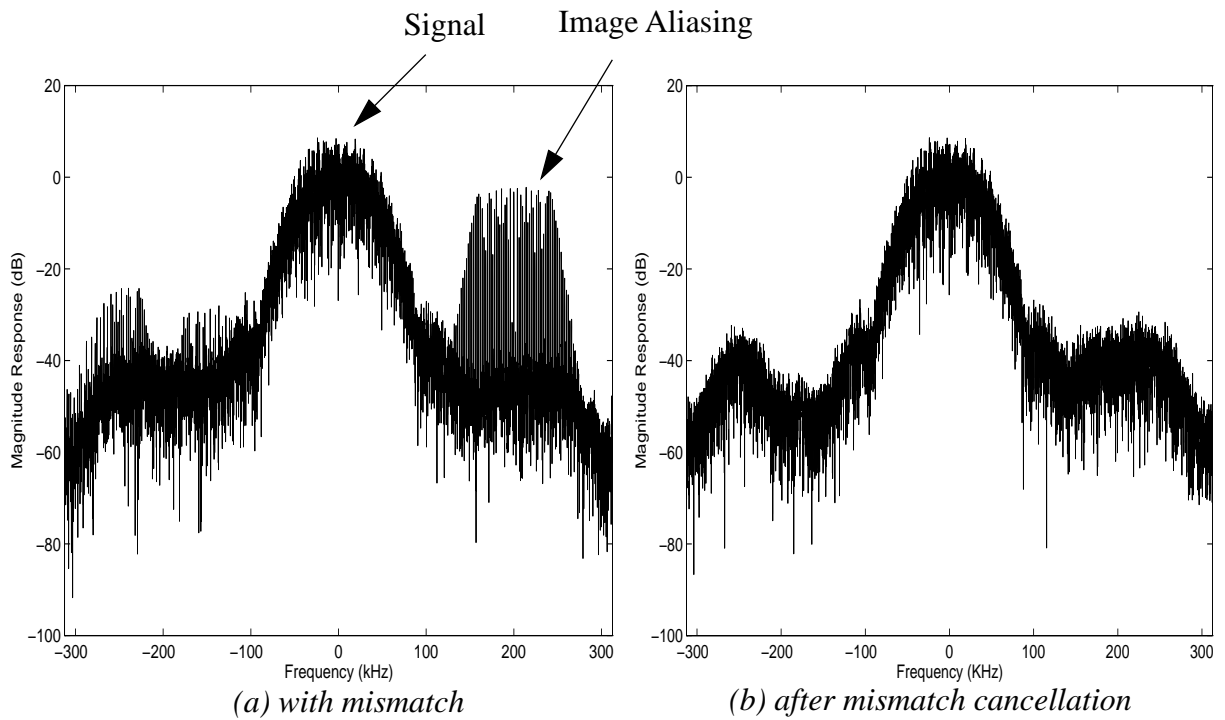


Fig. 3.12 Output spectra before and after using the mismatch cancellation system

the absence of the mismatch cancellation system is shown in Fig. 3.12(a). The image aliasing can be clearly seen. This is an artificial example with the FM interference moved 200 kHz off the image frequency so that the signal and interference can be visually separated. In this case, of course, conventional filtering would suffice. The SNR in this case is about 30 dB. Fig. 3.12(b) shows the output spectrum after the mismatch cancellation. It can be seen that the image aliasing

gets significant attenuation after applying the mismatch cancellation system. The SNR is increased to 52 dB which implies an SNR improvement of more than 20 dB. Fig. 3.13(a) shows a

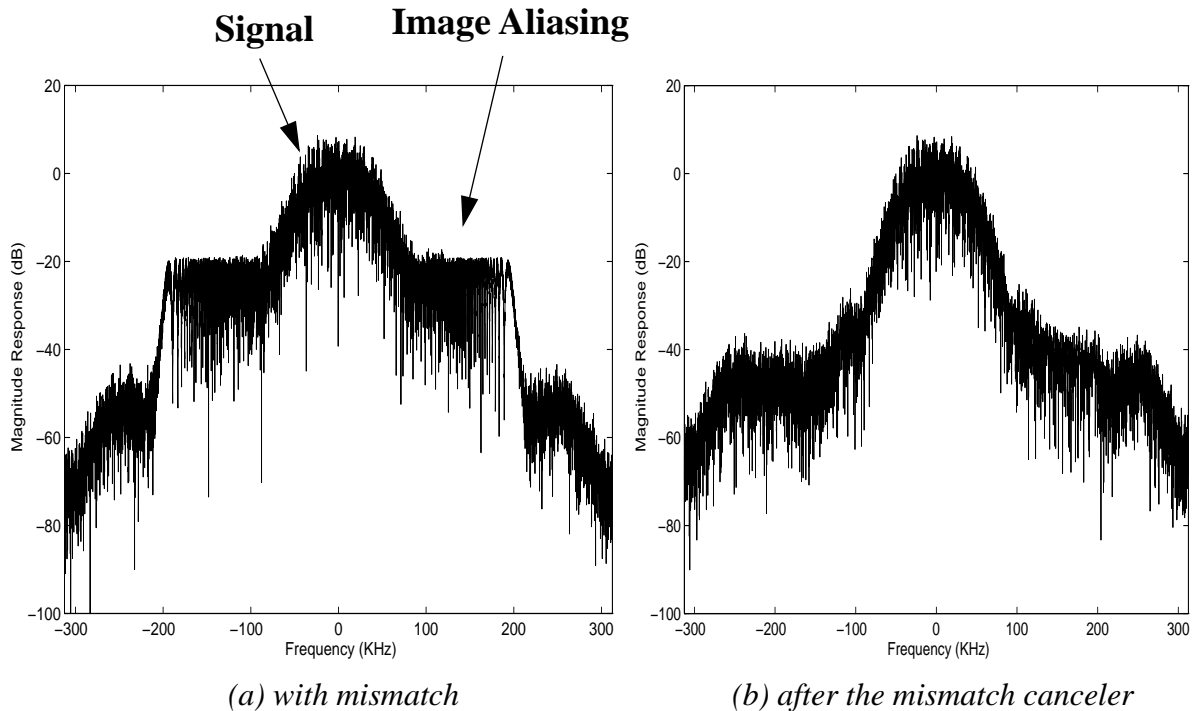


Fig. 3.13 Output magnitude responses before and after the mismatch cancellation system

more realistic scenario, with overlapped signal and image. Fig. 3.13(b) shows the improved output after applying the proposed mismatch cancellation system.<sup>1</sup>

Dramatic improvement can also be seen from comparison of the eye diagrams of the outputs in Fig. 3.12(a) and (b). Fig. 3.14(a) shows the eye diagrams of the I and Q outputs before applying the new mismatch cancellation system. We can see in the eye diagrams that the image interference (FM signal) has modulated the desired signal (GMSK signal). The eyes are only half-open and ambiguous. In Fig. 3.14(b) it can be seen that after using the presented adaptive system the eyes are wide open and clear, which means most of the image interference has been removed.

1. This figure shows an FFT of last 10k samples of a 200k-point simulation.

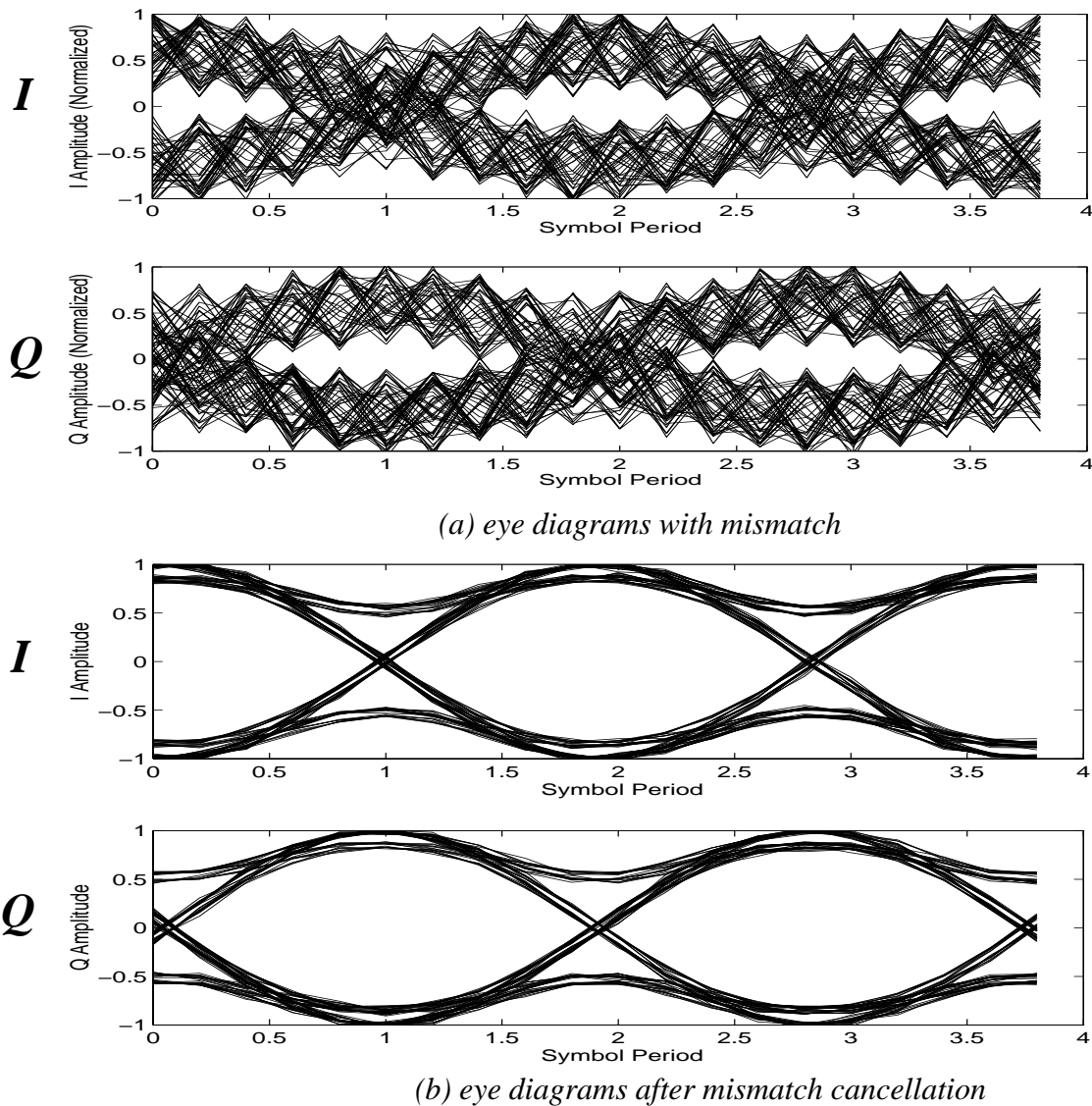
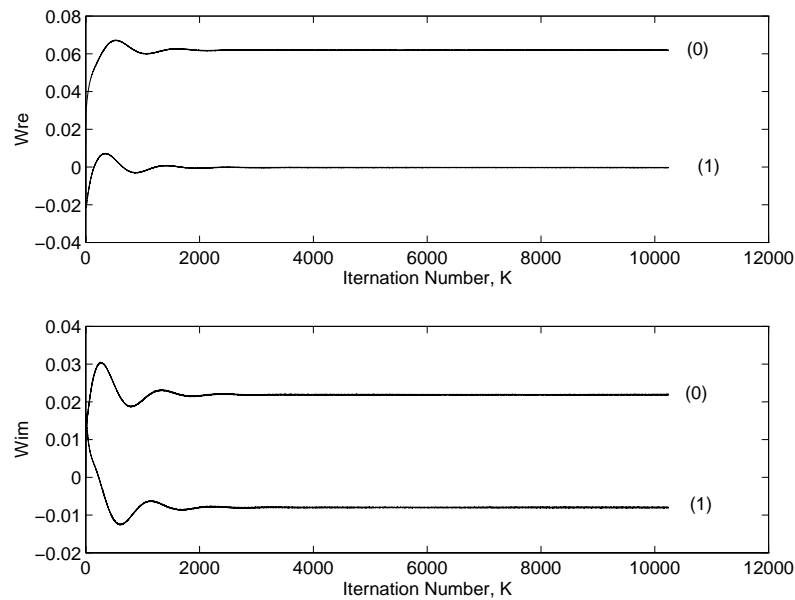


Fig. 3.14 Eye diagrams before and after mismatch cancellation

The convergence curves of coefficients of the adaptive filter are shown in Fig. 3.15. Only the coefficients of  $w_1(z)$  are presented because of the symmetric structure of the modified adaptive system in Fig. 3.7. In this example, the adaptive filter is a first order (two-tap) complex adaptive FIR filter. The upper part in Fig. 3.15 shows the real part of the coefficients, while the lower part shows the imaginary part of the coefficients.

From the simulation results shown in this section, it is clear that the novel system works

efficiently and powerfully.



*Fig. 3.15 Coefficients of the adaptive filter*

### 3.8 Further Application in Double Sampling Systems

The system discussed in this thesis is not restricted to complex receiver applications. It can also be used in double-sampled sigma delta modulators, a technique also used in digital IF receivers. Instead of having two complete identical paths, we can play some tricks with the clock and share hardware resources.

Double-sampled SC circuits are a subset of a class of circuits called N-path filters with N being equal to two. A diagram of a two-path circuit and its corresponding clock phases are shown in Fig. 3.16. In this circuit, the input signal is sampled every half clock period ( $T_s/2$ ) and appears at the output with a half-clock period delay. Therefore, the effective sampling frequency in this two-path sample-and-hold circuit is twice the clock frequency. The factor of two improvement in

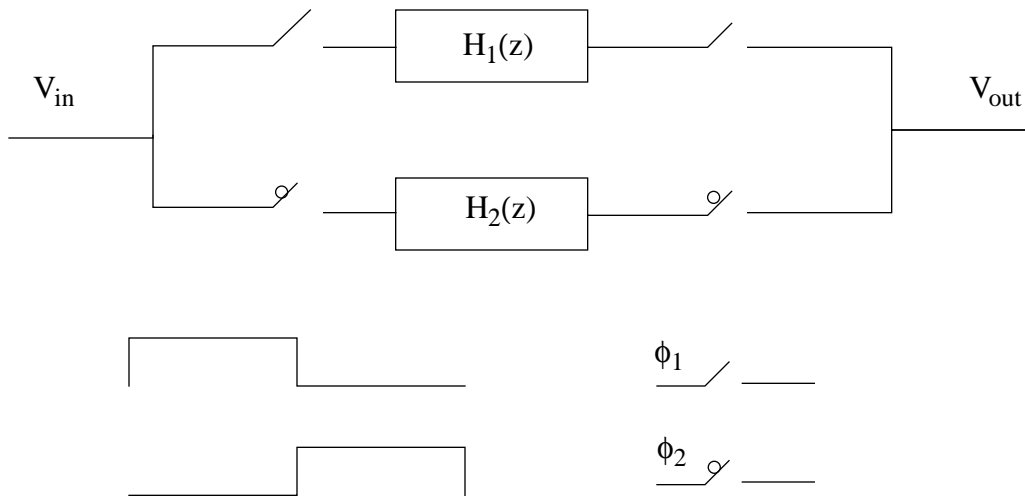


Fig. 3.16 Double sampling circuit model

the speed of the double-sampled SC delay cell is achieved without increasing the clock rate or requiring a fast opamp. In the quadrature system application, this double sampling technique can also be used in I/Q channels. The I and Q signals share the same path. Channel I is calculated in clock phase  $\phi_1$ , and channel Q is calculated in clock phase  $\phi_2$  [Bazarjani96].

However, double-sampled SC delay circuits suffer from image aliasing due to capacitor mismatches and uneven clock phases, which occur when clock phase  $\phi_1$  and phase  $\phi_2$  do not have the same length. The input  $V_{in}$  can be expressed as

$$V_{in}(z) = V_{in}^o(z) + V_{in}^e(z) \quad \text{Eq. (3.21)}$$

where the sequence of signals during  $\phi_1$  (odd samples) is denoted by an “o” superscript and the sequence of signals during  $\phi_2$  (even samples) is denoted by an “e” superscript.

Similarly, the output sequence is expressed as

$$V_{out}(z) = V_{out}^o(z) + V_{out}^e(z) \quad \text{Eq. (3.22)}$$

where odd and even sequences are related by

$$V_{out}^o(z) = H_1(z)V_{in}^o(z) \text{ and } V_{out}^e(z) = H_2(z)V_{in}^e(z)$$

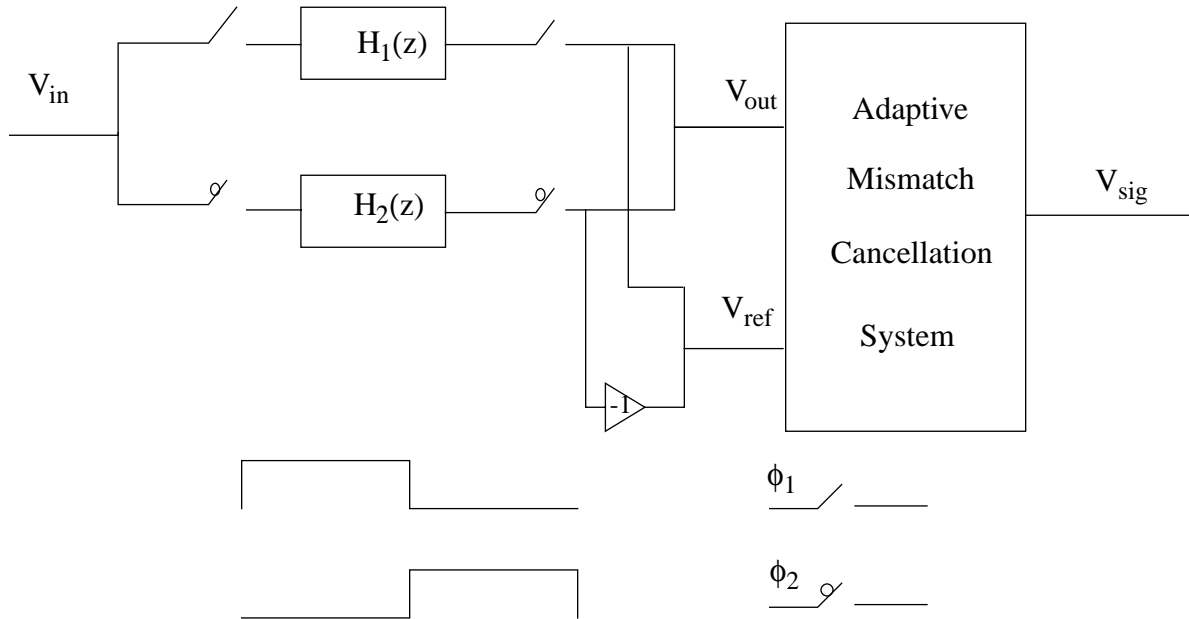


Fig. 3.17 Double sampling mismatch cancellation model

### 3.8.1 A Gain Mismatch in Double Sampling Systems

If the two paths are not symmetric and, for instance, there is a gain mismatch of  $\delta$  between them, which is  $H_1(z) = (1 + \delta)H(z)$  and  $H_2(z) = H(z)$ , the input-output relation is

$$V_{out}(z) = (1 + \delta)H(z)V_{in}^o(z) + H(z)V_{in}^e(z) \quad \text{Eq. (3.23)}$$

This equation can be expressed as

$$V_{out}^o(z) + V_{out}^e(z) = V_{out}(z) = H(z) \left[ \left(1 + \frac{\delta}{2}\right)V_{in}(z) + \frac{\delta}{2}(V_{in}^o - V_{in}^e) \right] \quad \text{Eq. (3.24)}$$

Obviously,  $H(z) \cdot \frac{\delta}{2}(V_{in}^o - V_{in}^e)$  is the image noise due to the gain mismatch. by using

$V_{out}^o - V_{out}^e$  as the reference signal, the image noise can be cancelled. Thus,

$$V_{ref} = V_{out}^o - V_{out}^e = H(z) \left[ \left(1 + \frac{\delta}{2}\right) (V_{in}^o - V_{in}^e) + \frac{\delta}{2} V_{in}(z) \right]. \quad \text{Eq. (3.25)}$$

$$\text{In this simple case, } V_{sig} = V_{out} - \frac{\delta/2}{1 + \delta/2} V_{ref} = H(z) \left(1 + \frac{\delta/2}{1 + \delta/2}\right) V_{in}.$$

Fig. 3.17 shows the double sampling mismatch cancellation system model. The reference signal can be obtained by taking odd and even samples from the double sampling A/D but flipping the sign of the even samples.

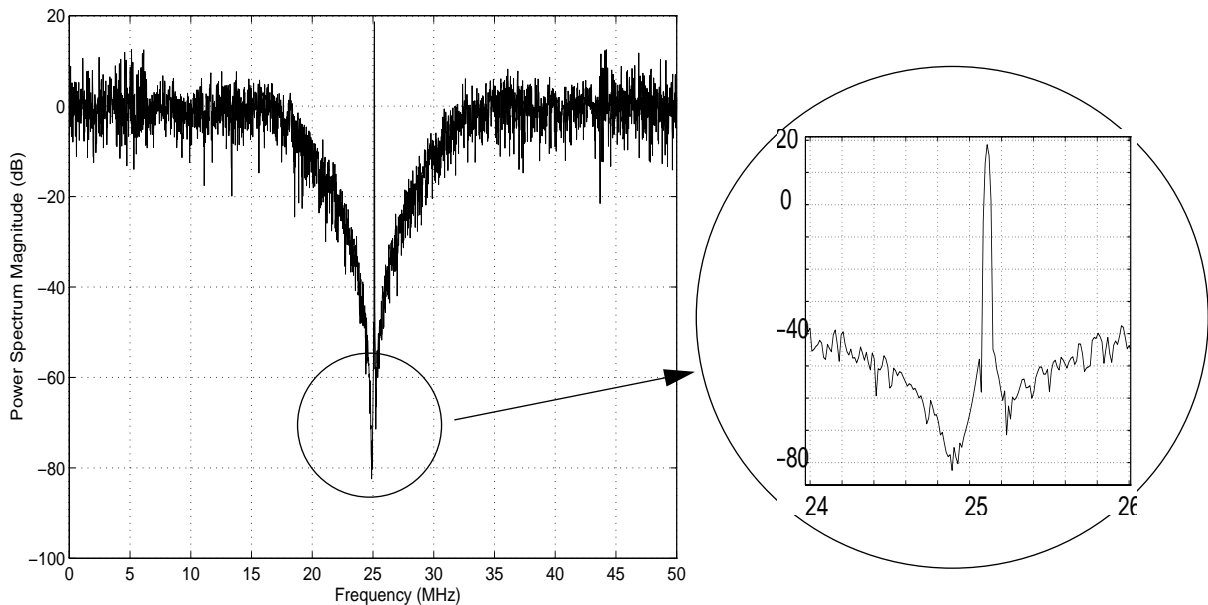


Fig. 3.18 Ideal case

Fig. 3.18 shows an ideal case output magnitude response when there is no mismatch between the two paths, where the signal is transmitted at  $25.1\text{MHz}$  and the clock rate is  $50\text{MHz}$ . The noise floor at the image frequency ( $24.9\text{MHz}$ ) is about  $-80\text{dB}$ . In Fig. 3.19, the output magnitude response is shown for the case when there is 5% gain mismatch between two paths. An interference tone can clearly be seen at  $24.9\text{MHz}$  with a power of about  $-15\text{dBc}$ . After applying

the double sampling mismatch cancellation system shown in Fig. 3.17, the power spectrum of the improved output is shown in Fig. 3.20. It can be seen that the interference tone is attenuated back to  $-80\text{dB}$ .

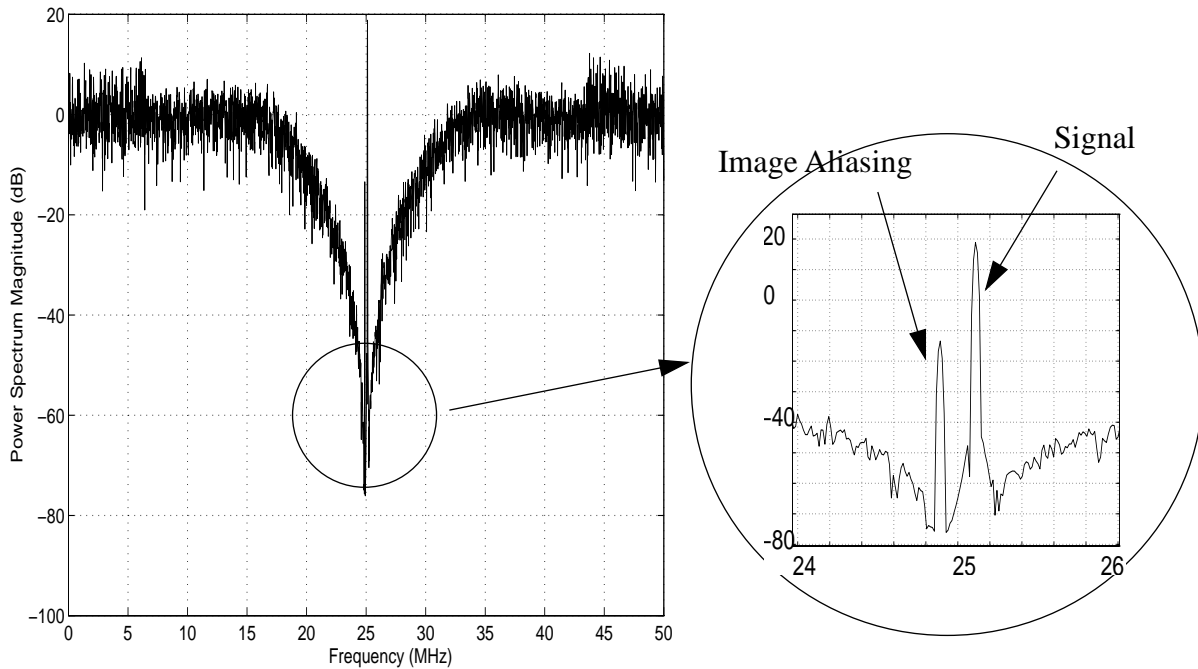
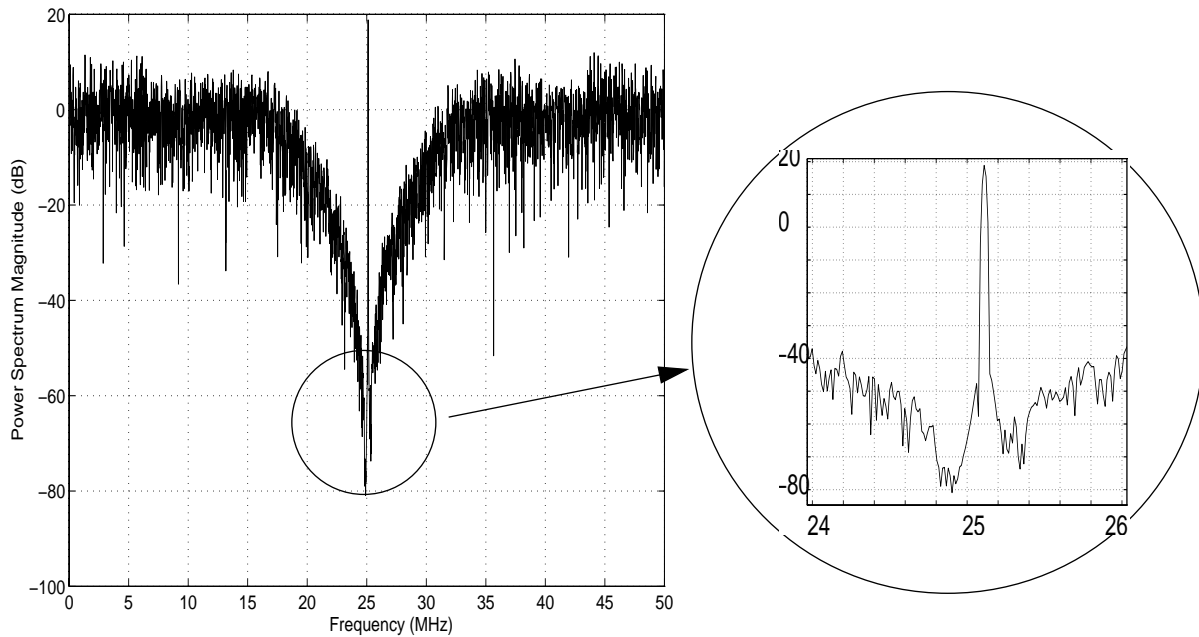


Fig. 3.19 Magnitude response with 5% gain mismatch in a double sampling sigma delta A/D

### 3.8.2 Uneven Clock Phases in Double Sampling Systems

Non-uniform sampling due to uneven  $\phi_1$  and  $\phi_2$  phases has a similar effect [Yang94]. If phase  $\phi_1$  is longer by an amount  $\tau$  compared to phase  $\phi_2$ , then it is like a phase error between the two channels.  $1 + \delta = e^{-s\tau} \approx 1 - s\tau$ , so  $\delta \approx -s\tau$ . The image noise due to this effect can be attenuated in the same way proposed in Section 3.8.1.



*Fig. 3.20 Magnitude response after mismatch cancellation system*

### 3.9 Conclusion

The image aliasing due to I/Q channel imbalance has been a big problem in realizing single IF receivers[41][31]. The complex single IF receiver introduced in Chapter 2 also suffers from the problem that there might be imbalance in the analog quadrature mixer or capacitor mismatch in the complex sigma delta modulator.

In this chapter, previous solutions for I/Q channel mismatch problems have been reviewed and the new adaptive DSP mismatch cancellation system has been presented and discussed.

This new system uses a new powerful complex LMS algorithm and modifies the classic adaptive noise cancellation system to get the best performance. The simplicity of the algorithm and its symmetric system structure make the system feasible and easy to implement.

In the simulation results presented in this chapter, improvements were observed from both power spectra of outputs and eye diagrams of the I and Q signals. A further application of the

mismatch cancellation system in double sampling systems is introduced. Simulation results for gain mismatch and clock phase offset are discussed in this chapter which further prove the applicability of the system.

The next chapter will present results obtained with experimental data which prove the algorithm and system discussed in this chapter can work in real conditions.

## *Chapter 4*

---

### *A Real Time Implementation and Further Applications*

#### **4.1 Introduction**

This chapter describes a real-time implementation of the novel DSP mismatch cancellation system proposed in Chapter 3. The target application is a complex IF receiver. This implementation proves that the technique works well in the presence of all of the impairments of a practical system, such as circuit noise, offsets, drifts and distortions.

Four main parts are presented in the real-time implementation: the RF front end, complex sigma delta modulator, decimation filtering and interfacing, and DSP for the adaptive mismatch cancellation.

#### **4.2 A real-time Implementation**

This thesis proposes a technique and analyzes, simulates and builds a prototype. The test example is based on DCS-1800 (GSM) in the receiver proposed by Swaminathan [Swaminathan96b]. The overall performance of this testing prototype is limited by the available components and restricted choice of IF. This thesis focuses on DSP correction of mismatch.

The technique chosen for the test hardware are not representative of an optimized design, which would probably have a higher IF, but were chosen for the system proposed by

Swaminathan which demonstrated a novel architecture with available components [Swaminathan96b]. Our work extends this to demonstrate the new correction technique.

The block diagram of the testing hardware is shown in Fig. 4.1. The details of each part will be presented in the following sections.

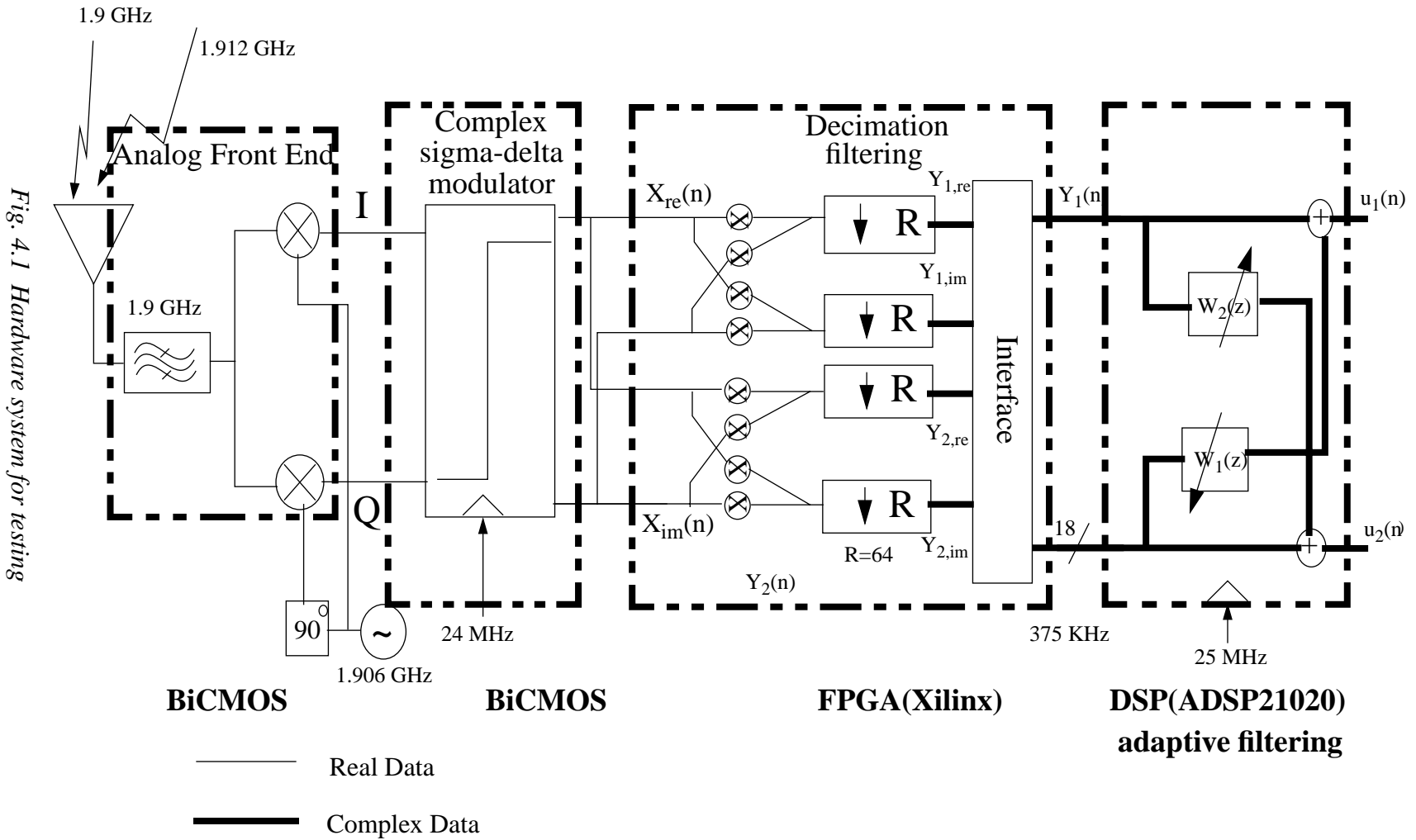
#### ***4.2.1 RF Front End***

The analog front end consists of a monolithic LNA [Long95], notch filter [Macedo96], and quadrature mixer. These were all implemented by Macedo [Swaminathan97] in a  $0.8\mu m$  BiCMOS process with on-chip inductors. These components have already been described in [Swaminathan97] and their specifications are shown in Table 2.1. The LNA is a tuned amplifier with an on-chip resonant LC tank [Long95]. The notch filter consists of a series LC resonator tuned to the image frequency to create the notch, cascaded with an on-chip LC tank tuned to the passband frequency (in this case, 1.9GHz) [Macedo96]. The quadrature mixer was simply a pair of Gilbert cells [Grebene84], one for each channel. The function of the RF front end is to mix the radio frequency signal down to the IF, and at the same time to generate I and Q signals.

This chip is design for the application with 300 MHz IF to let the notch operates properly. But this would need 1.2 GHz clock for A/D or filtering for subsampling.

#### ***4.2.2 Complex Sigma Delta Modulator***

The complex sigma delta modulator used in the implementation is a fourth order modulator which has three zeros in the real band and one zero in the imaginary band in order to attenuate the image noise before it aliases into the real band. This modulator was designed by Swaminathan [Swaminathan97].



Following are the poles and zeros for the NTF and STF of the fourth order complex sigma delta modulator:

$$Poles = \pm 0.8j, \pm 0.2 + 0.7j$$

$$NTF_{zeros} = j(\text{triple}), -j$$

$$STF_{zeros} = 0.8j$$

$$STF_{gain} = 0.5$$

These poles and zeros give the complex modulator a nominal notch depth of 90 dB (worst case of in-band relative to NTF out-of-band magnitude) within a bandwidth of 625 kHz for an OSR (oversampling ratio) of 64. The magnitude responses of these transfer functions are given in Fig. 4.2.

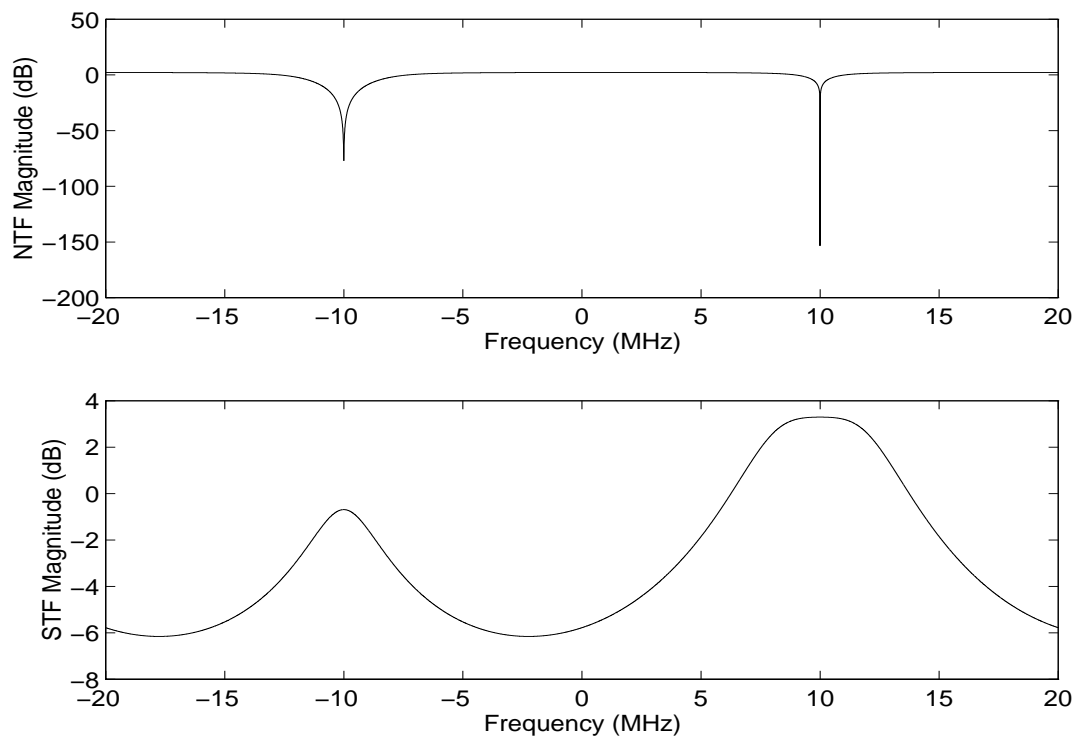


Fig. 4.2 STF and NTF magnitude responses of a fourth order complex modulator

### 4.2.3 Decimation Filters and Interface to the DSP Board

The sigma delta modulator is an oversampled one bit A/D converter. A decimation filter is needed to convert the one bit stream at the oversampling rate to an n-bit word at the Nyquist rate.

The proposed structure for the decimation filters was introduced in section 3.5.3. It can be implemented very simply using the sequence of accumulators and differentiators shown in Fig. 4.3(a).  $f_D$  is the sampling rate after decimation, and is the oversampling rate  $f_s$  (sampling rate of the modulator) divided by the decimation ratio  $R$ .  $D_{in}$  is the output from the modulator which is an oversampled one bit stream, and  $D_{out}$  is the n-bit output word, and  $N$  is the number of stages of the CIC filter. Yang has proposed polyphase techniques for implementing these filters in ASIC to GHz rates [Yang96]. In this testing example, it only requests 24 MHz.

According to Hogenauer [Hogenauer81], the required resolution in the CIC filter is:

$$B_{max} = \lceil N \log_2 R \rceil + B_{in} - 1$$

where  $B_{in}$  is the length of the input word (1 for  $D_{in}$ ).  $B_{max}$  is the maximum resolution possible for the output word  $D_{out}$ . Here we choose

$$R = 64, N = 3, B_{in} = 1$$

so the maximum resolution of the CIC filter is 18 bits.

This third-order CIC decimation filter was implemented on a Xilinx FPGA shown in Fig. 4.3(b).

$Y_{1, re}$ ,  $Y_{1, im}$  represents the in-phase and quadrature phase of the *primary input* for the adaptive mismatch cancellation system respectively.  $Y_{2, re}$ ,  $Y_{2, im}$  are the in-phase and quadrature phase of the *reference input*.

From the structure shown in Fig. 4.3, it can be seen that all the accumulators are operated

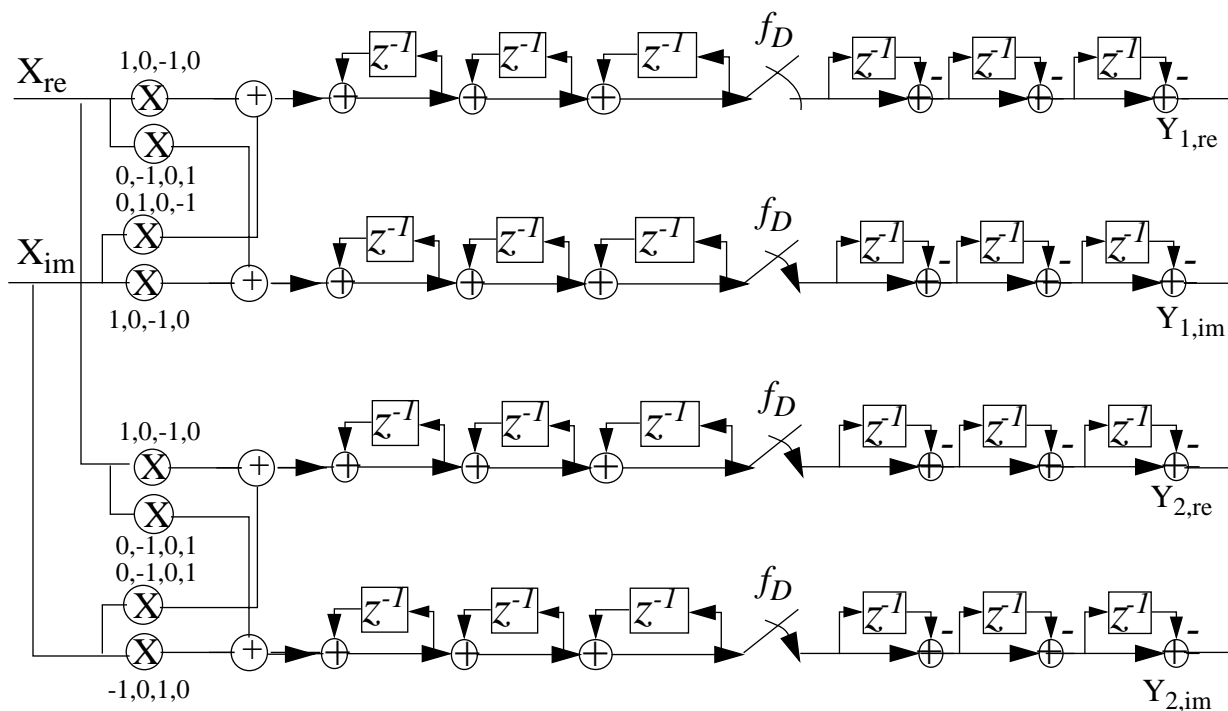
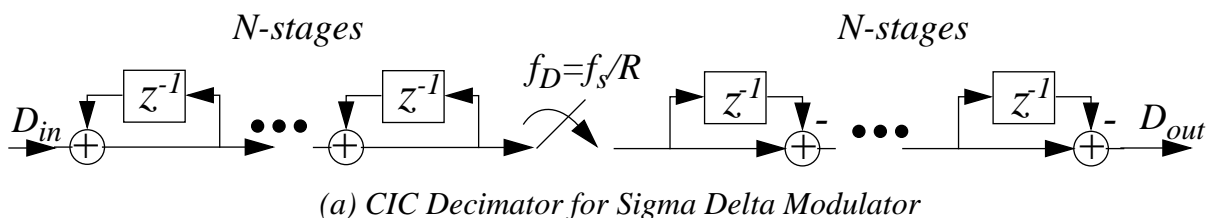


Fig. 4.3 Real time structure of the decimation filter

at the oversampling rate, which is 40 MHz in the receiver. These accumulators are crucial for the timing and area considerations for the FPGA design. The clock period in this structure should be longer than the propagation delay of the three adders because the latched value is accurate only if the last adder finishes the operation. On the Xilinx 4000 series FPGA, the speed can only get to 10MHz if we stay with the structure shown in Fig. 4.3.

If we use pipelining by moving latches (delay elements) following the adders on the main

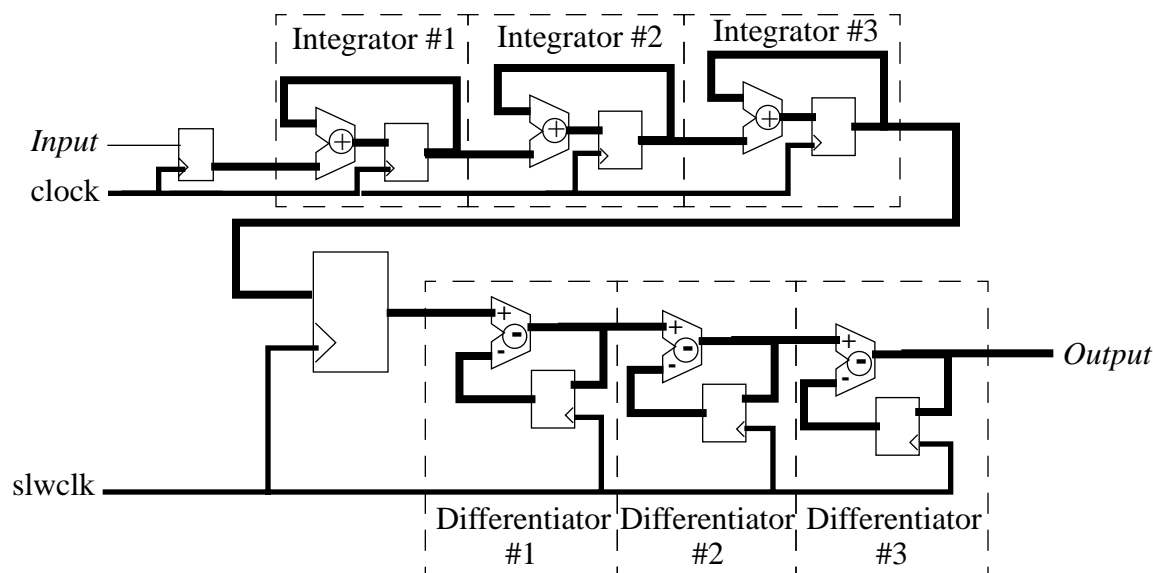


Fig. 4.4 Implementation of the decimation filter

path, the restriction on the clock becomes one adder delay instead of three. The modified implementation is shown in Fig. 4.4. The signal “clock” is at the oversampling rate, while the signal “slwclk” is at the Nyquist rate. The “Input” signal is a 1-bit data stream and “Output” is an 18-bit data stream.

In order to feed the *primary input* and *reference input* generated by the Xilinx FPGA into the DSP chip, an interface between the Xilinx FPGA and DSP chip is needed. The DSP chip used here is the Analog Devices ADSP-21020 floating-point DSP which provides the bus request/bus grant protocol allowing an external device to transfer data to the processor’s memory.

The memory reads in the DSP occur with the following sequence of events [ADSPb] (see Fig. 4.5):

1. The Analog Devices ADSP-21020 drives the read address and asserts a memory select signal to indicate the selected bank. A memory select signal is not de-asserted between successive

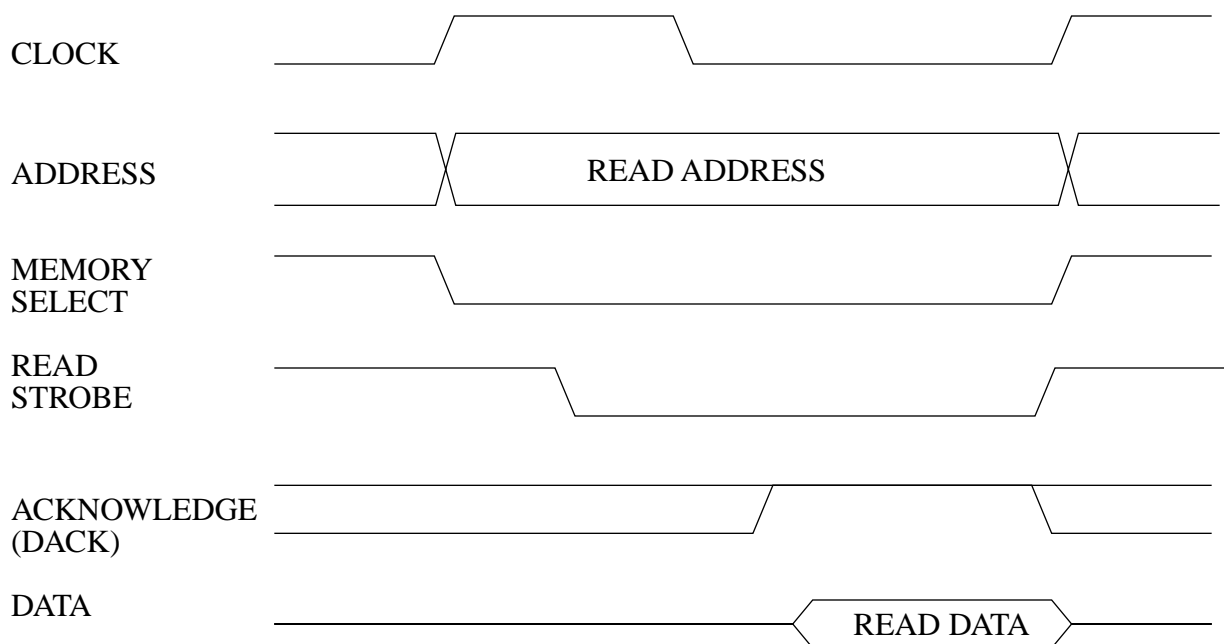


*Fig. 4.5 ADSP-21020 memory read cycle*

accesses of the same memory bank.

2. The Analog Devices ADSP-21020 asserts the read strobe.
3. The Analog Devices ADSP-21020 checks whether wait states are needed. If so, the memory select and read strobe remain active for the additional cycle(s). Wait states are determined by the state of the external acknowledge signal, the internally programmed wait state count, or a combination of the two. If the acknowledge signal is low, the Analog Devices ADSP-21020 inserts a wait state by holding strobes and address on the interface valid an additional cycle. If it is high, the Analog Devices ADSP-21020 completes the cycle.
4. The Analog Devices ADSP-21020 latches in the data.
5. The Analog Devices ADSP-21020 de-asserts the read strobe.
6. If initiating another memory access, the Analog Devices ADSP-21020 drives the address and memory select for the next cycle.

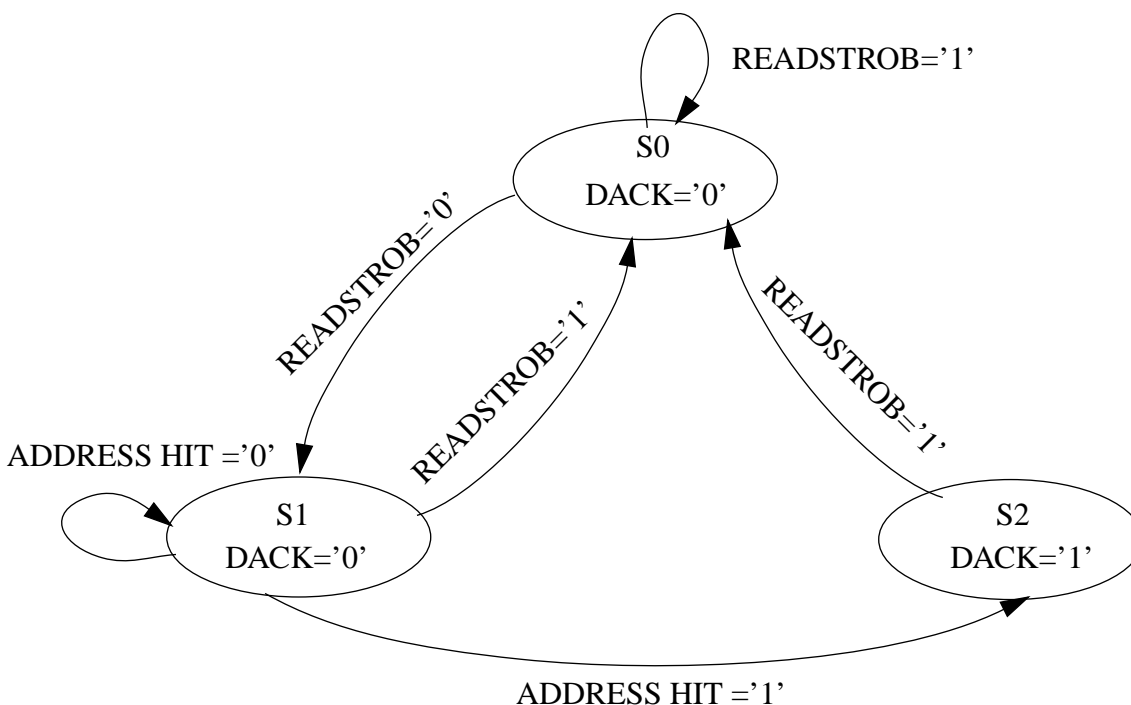


*Fig. 4.6 State diagram of the interface*

Based on the information above, a state diagram of the interface is shown in Fig. 4.6, where the signal READSTROB is the read strobe sent by the Analog Devices ADSP-21020, the signal ADDRESS HIT is true when the Analog Devices ADSP-21020 selects the Xilinx FPGA to read the data. The signal DACK is the acknowledge signal generated by the Xilinx FPGA to signal that the data on the bus are valid.

When the processor wants to read the data, it de-asserts the signal READSTROB. If the address given by the processor hits the Xilinx FPGA, the Xilinx FPGA sends the data to the data bus and at the same time, asserts the signal DACK.

#### **4.2.4 Analog Devices ASDP 21020**

The implementation of the novel adaptive mismatch cancellation algorithm uses an

---

evaluation kit [ADSPa] provided by Analog Devices, which has an Analog Devices ADSP-21020 32-bit floating point signal processor operating at 33 MHz, an in-circuit emulator and a PC.

The board has two 96-contact female Eurocard connectors which accommodate the external memory and extended capabilities. The data expansion connector has been used as the interface between the DSP and the Xilinx FPGA.

The algorithm is coded in the DSP's assembly language (see APPENDIX A). The parameters that can be changed in the algorithm are the stepsize and the order of the adaptive filters. The settings are shown at the beginning of the code.

#### **4.2.5 ASIC Option**

The algorithm proposed in section 3.5.2 can be implemented with ASIC technology. If two-tap complex adaptive filters are chosen, there are four multiplications and four additions for each complex adaptive filter. Thus there are 8 multiplications and 8 additions for each Nyquist sample. It can be seen that the reference path can be very simple because  $u_1$  is the desired output and the  $u_2$  is the image noise. Thus, the complex filter  $w_2$  can be of zero order and the multiplier does not need to be very accurate. Receivers usually have enough DSP power to do this anyway, because other modem functions need it.

### **4.3 Clock Rate Matching on the Interfaces**

In our design, clock rate matching has to be considered between two interfaces. One is the interface between the complex sigma delta modulator and the Xilinx FPGA, and the other is the interface between the Xilinx FPGA and the ADSP-21020.

The initial design of a receiver for the GSM standard requires a 40 MHz oversampling

---

rate for the modulator, followed by a lowpass filter having a decimation rate of 64. Unfortunately, the decimation filter implementation shown in Fig. 4.3 is an inherently low-speed implementation when it is put on an FPGA. Even with the improved structure shown in Fig. 4.4, the speed can only reach 24 MHz. Thus, in the presented real time implementation, the complex sigma delta modulator operates at a sampling rate of only 24 MHz, and after decimation, the signal bandwidth is about 187.5 kHz<sup>1</sup> which is the same rate and same order as the DFE in the system. The data rate of the GMSK signal used in the real time implementation is 100kb/s.

The data expansion port used in the ADSP-21020 can work at 25 MHz which is much higher than the Nyquist sampling rate of the baseband signal--375 kHz. So there is no problem at this interface.

## 4.4 Performance of the real-time implementation

### 4.4.1 Experimental Results

The main purpose of implementing the system shown in Fig. 4.1 is to prove that I/Q channel mismatch is no longer a problem in a practical complex single IF receiver even with interference at the image band of the desired signal. Implementing it in real time shows that the computational load is reasonable, driving it for long runs shows that the algorithm is stable, and using real components to generate the bit streams shows that it is robust under the presence of the wide variety of distortions, offsets, drifts, mismatches and noise sources encountered in a real system. In this testing prototype, the interference signals are actually introduced just after the mixers and before the modulator because of the limitation of the components and equipments.

---

1. Nyquist sampling rate  $f_{\text{Nyquist}} = (24/64)MHz = 375kHz$

---

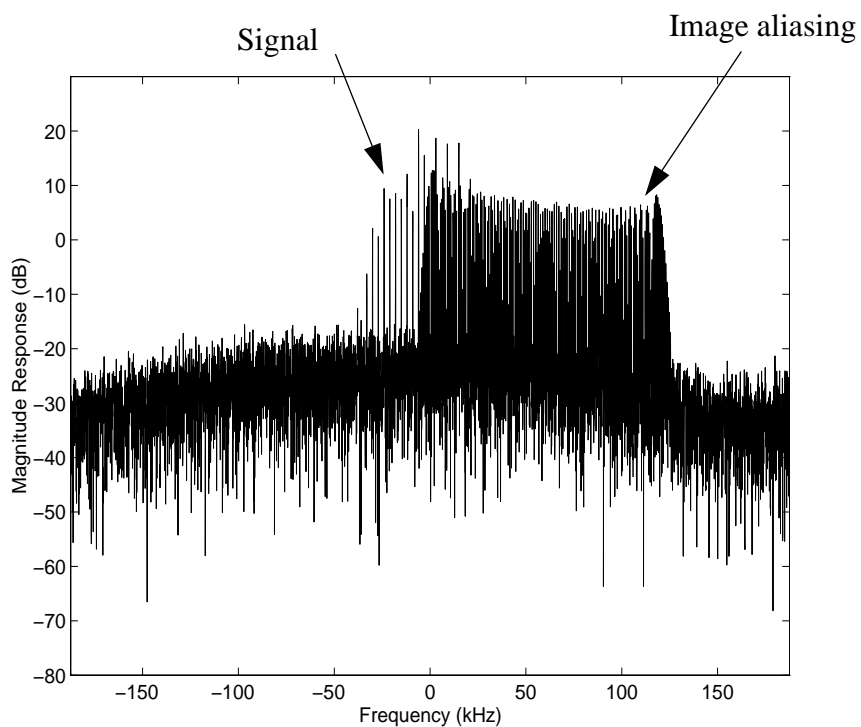
As mentioned in section 4.3, the desired signal used in this example is a GMSK signal with 100 *kb/s* data rate. The interference signal is an FM signal at 1.912 GHz, and its bandwidth is 100 kHz. After decimation, the image interference will alias into the baseband 0~100 kHz when there is a mismatch in the receiver. Fig. 4.7 shows the magnitude responses of  $Y_1$  and  $U_1$  (defined in Fig. 4.1). It can be seen that the image aliasing between 0~100kHz has been attenuated in Fig. 4.7(b).

The comparison has also been done with eye diagrams as shown in Fig. 4.8. The eyes are completely closed before applying the mismatch cancellation system. After the mismatch cancellation, we can see the eyes are open which means the receiver has a reasonable SNR, which in turn allows us to extract the desired information.

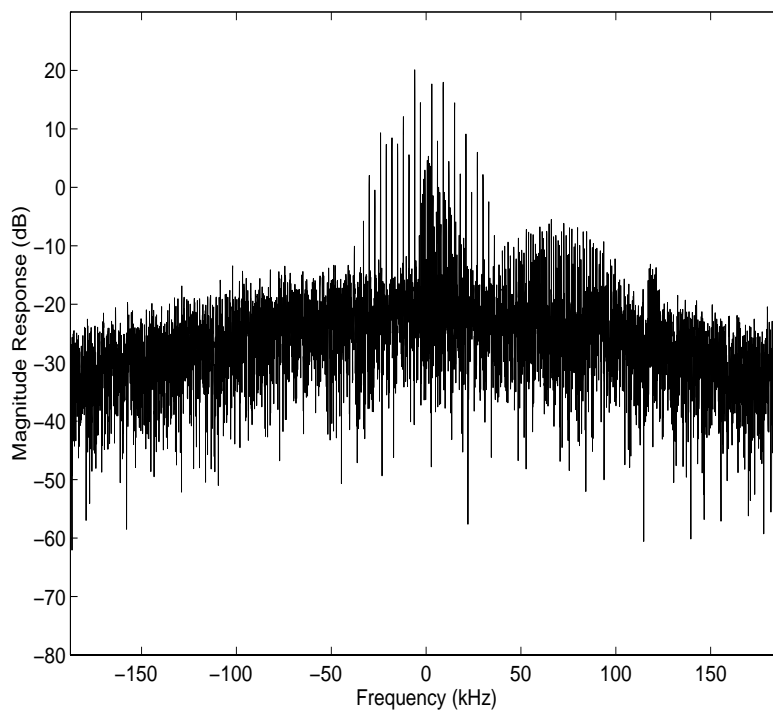
We can see from the eye diagrams that there is still some residual noise which makes the eyes unclear. The residual noise comes from two sources: signal leakage and circuit noise. Even though we use the modified version of the adaptive mismatch system, the signal component can not be completely eliminated in the *reference input*. This leakage can impair the performance of the adaptive system. Circuit noise is inherent in the circuits. This kind of noise is uncorrelated with the mismatch effect, thus, we can not use the mismatch cancellation strategy to attenuate it. So signal leakage in the *reference input* and the circuit noise both contribute to the residual noise.

#### ***4.4.2 Analysis of Experimental Results***

The adaptive mismatch cancellation system is a system that uses an adaptive algorithm to find an optimum filter which is capable of subtracting image noise from the corrupted signal input. The adaptive filter used in the modified noise cancellation system is a transversal FIR filter.

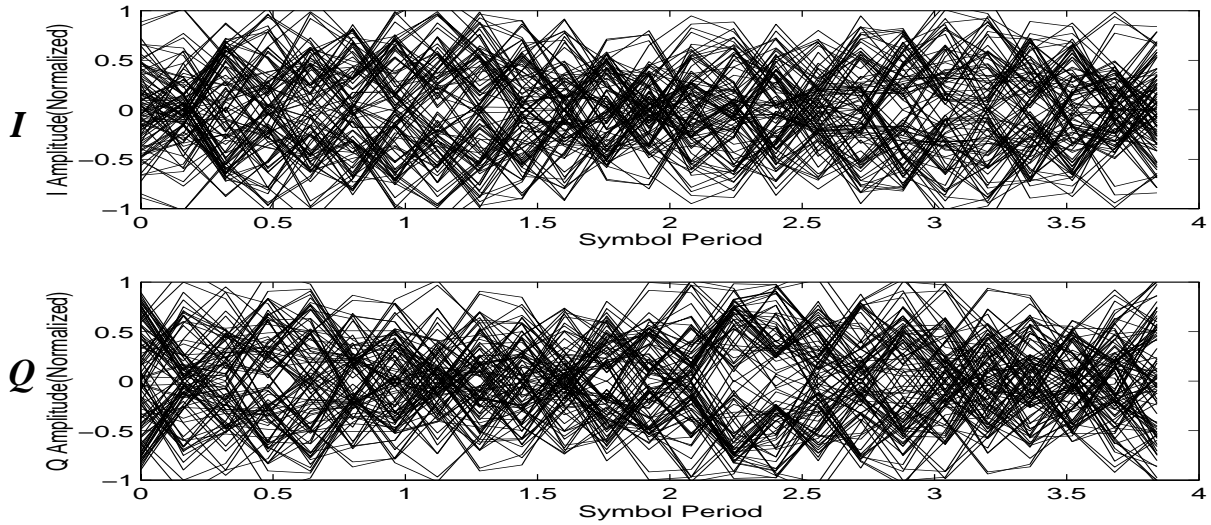


(a) *Magnitude Response of  $Y_1$*

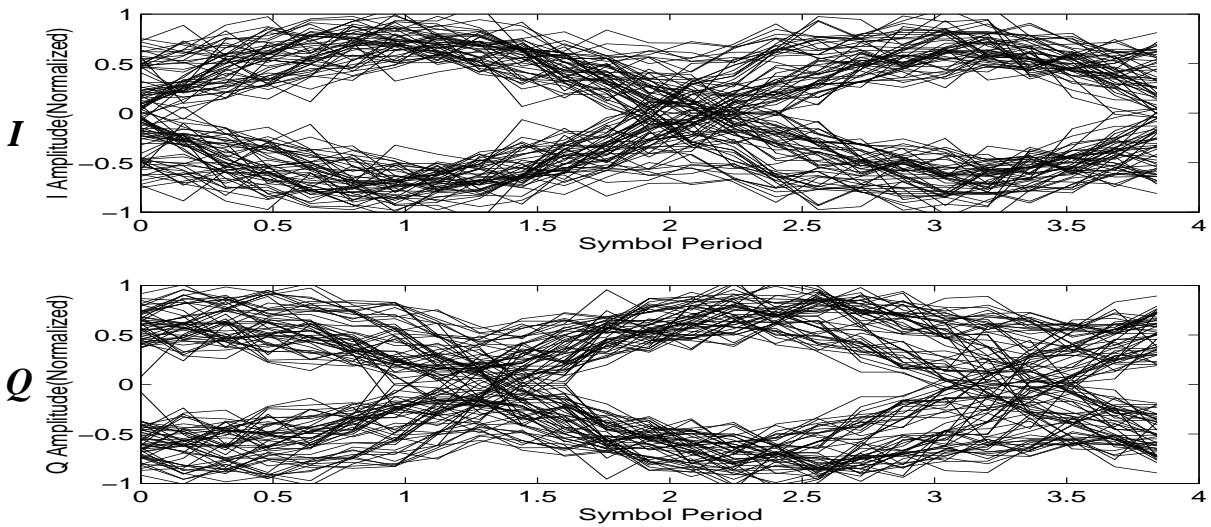


(b) *Magnitude Response of  $U_1$*

*Fig. 4.7 Magnitude responses of the receiver output- before and after mismatch cancellation (Experimental)*



(a) Eye diagrams of  $Y_{1,re}$  and  $Y_{1,im}$



(b) Eye diagrams of  $U_{1,re}$  and  $U_{1,im}$

Fig. 4.8 Eye diagrams for I and Q channels- before and after mismatch cancellation (Experimental)

Its structure is shown in Fig. 4.9 and it can be expressed as [47][Widrow85]:

$$H(z) = w_0 + w_1 \cdot z^{-1} + \dots + w_{L-1} z^{-(L-1)}.$$

In the adaptive algorithm used to find optimum filters  $\mathbf{w}_1$ ,  $\mathbf{w}_2$  in Eq. (3.19) and Eq. (3.20), there are two pairs of parameters that can determine how close we are to the optimum: stepsizes  $\mu$

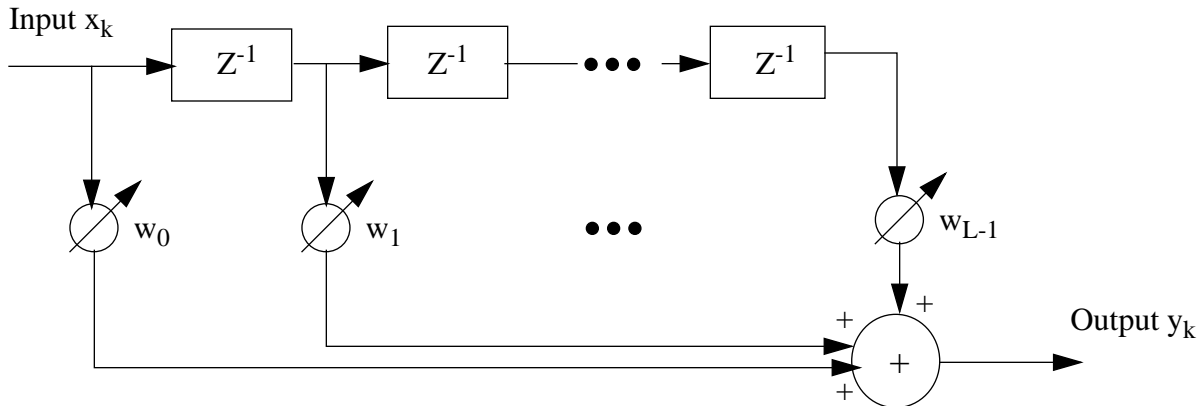


Fig. 4.9 The adaptive transversal FIR filter

$(\mu_1, \mu_2)$  and orders  $L$  ( $L_1, L_2$ ) of adaptive filters.

#### 4.4.3 SNR Versus Step size

The step size  $\mu$  in the LMS algorithm controls the speed of adaptation and also the residual noise in the signal after the noise cancellation system. The larger the step size, the faster the algorithm converges, but the more the residual noise.

Using the same data in section 4.4.1, we run the adaptive algorithm with different step size  $\mu$ . Fig. 4.10 shows the curve of the step size  $\mu$  and the SNR improvement. As the step size increases, the SNR improvement decreases. Fig. 4.11(a) and (b) show the coefficient convergence for  $\mu = 0.4$  and  $\mu = 0.0001$  respectively. It can be seen that it takes less than 100 iterations for the coefficients to converge when  $\mu = 0.4$  and takes more than 150,000 iterations when  $\mu = 0.0001$ .

In Fig. 4.11(a), when  $\mu = 0.4$ , the real part of the coefficient is oscillating around  $W_{re} = 0.0485$  with a peak amplitude of about 0.1, while the imaginary part is oscillating around

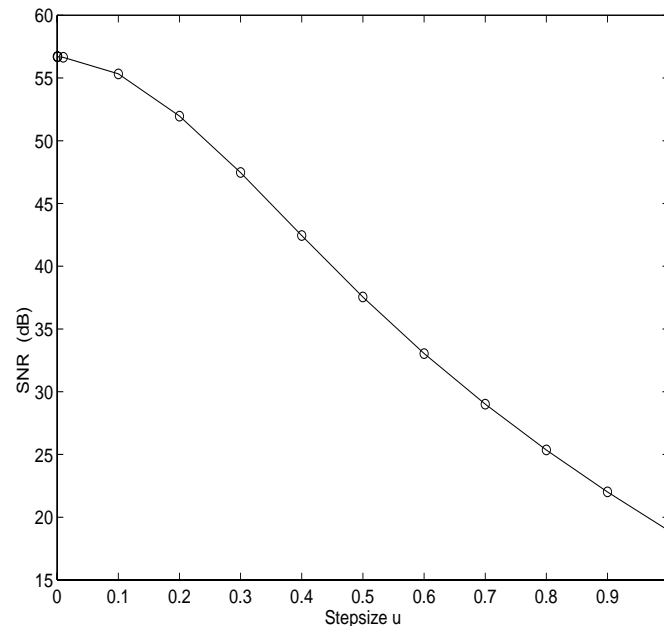


*Fig. 4.10 SNR versus stepsize (Experimental)*

$W_{im} = 0.0258$  with a peak amplitude of about 0.1 .

In Fig. 4.11(b), when  $\mu = 0.0001$ , the real part of the coefficient converges to  $W_{re} = 0.0495$  with a peak deviation of about 0.0002, while the imaginary part converges to  $W_{im} = 0.0256$  with errors less than 0.0002 .

With a bigger  $\mu$ , the coefficients can converge faster since they will take larger steps. But coefficients vary around the optimum solution with a bigger amplitude which prevents the system from getting maximum SNR improvement.

With a smaller  $\mu$ , each time coefficients can only move towards the optimum solution with a very small step, so it takes much longer time to get to the optimum. But coefficients will stay very close to the optimum, so more SNR improvement can be achieved. The samples come every  $1.6 \mu\text{s}$  after the decimation filtering (the baseband sampling rate is 625 KHz). 150,000 iterations therefore take only about 240 milliseconds. This power-up transient can easily be tolerated by the

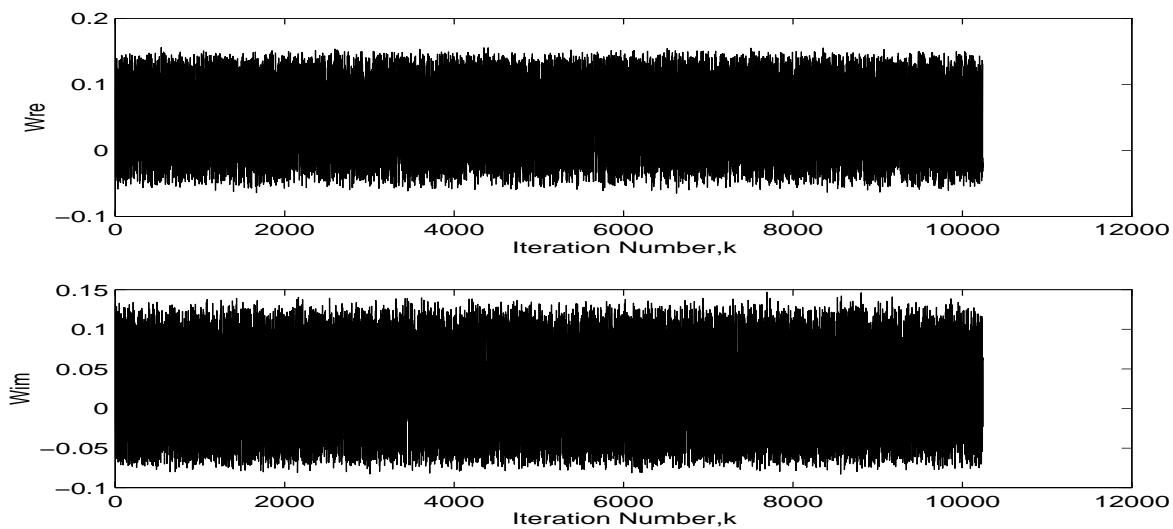
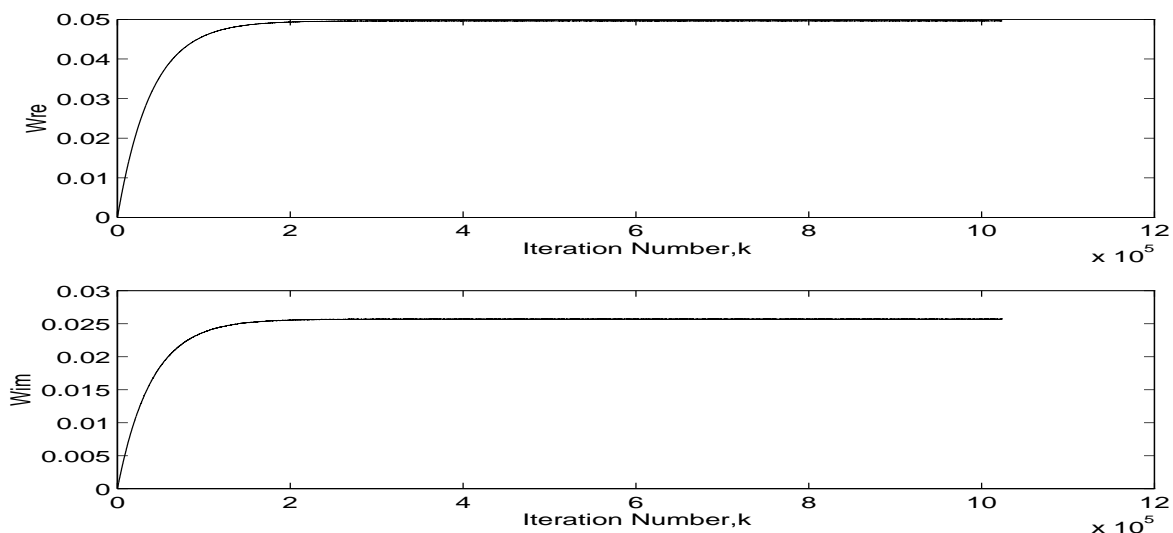
(a)  $\mu=0.4$ (b)  $\mu=0.0001$ 

Fig. 4.11 Coefficient convergencies for  $\mu = 0.4$  and  $\mu = 0.0001$  (Experimental)

communication system. Fig. 4.10 shows that little further improvement is obtained below  $\mu = 0.1$ . With  $\mu = 0.1$ , it takes 10,000 iterations (16ms) for the adaptive algorithm to converge. This is faster compared to the time constants of temperature variation that could cause drifts, and faster compared to power-up operations. So in fact, convergence rates can be very fast even with a simple LMS algorithm.

#### 4.4.4 Orders of Adaptive filters Versus SNR

Another pair of parameters that can be chosen in the modified algorithm is the orders of the adaptive filters,  $L_1$  and  $L_2$ . If the optimum filter is used in the mismatch cancellation system shown in Fig. 3.6 of Chapter 3, the noise component that is correlated with  $n_l$  will be completely eliminated in the system output  $e$ . The maximum SNR improvement is then achieved, but algorithm complexity and stability are compromised.

We will use an example to explain how the performance of the algorithm, i.e. the SNR improvement, is affected by the order of the adaptive filter. Assume it is known that the optimum filter is a third-order FIR filter expressed as

$$H_{opt}(z) = a_0 + a_1 \cdot z^{-1} + a_2 \cdot z^{-2} + a_3 \cdot z^{-3}.$$

We would get the best performance if we chose the order of the adaptive filter to be three. Coefficients of the adaptive filter will converge to coefficients of the optimum filter according to the LMS algorithm. The adaptation speed and the residual noise depend on the stepsize  $\mu$  in the algorithm.

If we underestimate the filter as first order (two-tap), which means we choose the adaptive filter  $H(z) = w_0 + w_1 \cdot z^{-1}$ , its coefficients will converge to the first two coefficients of the optimum filter,  $a_0$  and  $a_1$ , if the input is white noise. If the same stepsize  $\mu$  is chosen, the residual noise in this case will be larger than that in the case where the order is 3.

If we over-estimate the order of the filter, e.g. as  $\sum_{k=0}^5 w_k \cdot z^{-k}$ , then  $w_0, w_1, \dots, w_3$  will converge to  $a_0, a_1, \dots, a_3$  respectively. Theoretically,  $w_4, w_5$  should be zero, but the channel itself

---

does not place any constraints on these two coefficients. It is stable if noise-like inputs are applied. But if the input is a sinusoidal signal, over-modeling will cause a problem. The sudden perturbation to the channel will not have a dramatic effect on the adaptive filter if we choose the order to be less than 3, because if the perturbation causes the coefficients to move away from the optimum, the adaptation will gradually bring the coefficients oscillating around the optimum when the channel is stable. But when the filter has two more degrees of freedom, the unexpected perturbation destroys the dynamic balance because it has two more coefficients to trace the perturbation. Sometimes, the perturbation can destroy the whole system and coefficients will not converge. Even if there is no perturbation,  $w_4$  and  $w_5$  may oscillate around zero but not converge to zero, so additional noise will be added to the system.

If the optimum filter is an IIR filter, theoretically, we need an infinite order FIR filter to model the IIR filter. But practically, coefficients of the adaptive filter can only oscillate around optimum coefficients and will not be equal to the optimum. In this case, the noise due to this oscillation will increase as the order of the filter increases if we choose the same stepsize  $\mu$ . There will be a point where as the order increases, the performance will stop improving and even be degraded.

As demonstrated in section 4.4.3, a single-tap complex FIR filter can compensate the SNR degradation due to gain or phase mismatch in the mixer. When there is a coefficient mismatch in the complex sigma delta modulator, a larger order FIR filter is needed.

Next, let us look at another example for which the coefficient mismatch is considered. Fig. 4.11 shows the SNR in terms of the order of the adaptive filter, where the stepsizes  $\mu = 0.0001, 0.001, 0.01, 0.1, 0.2, 0.5, 1$  are used in the modified LMS algorithm. It can be seen that the best performance is achieved when the order is one (a two-tap complex filter). When the

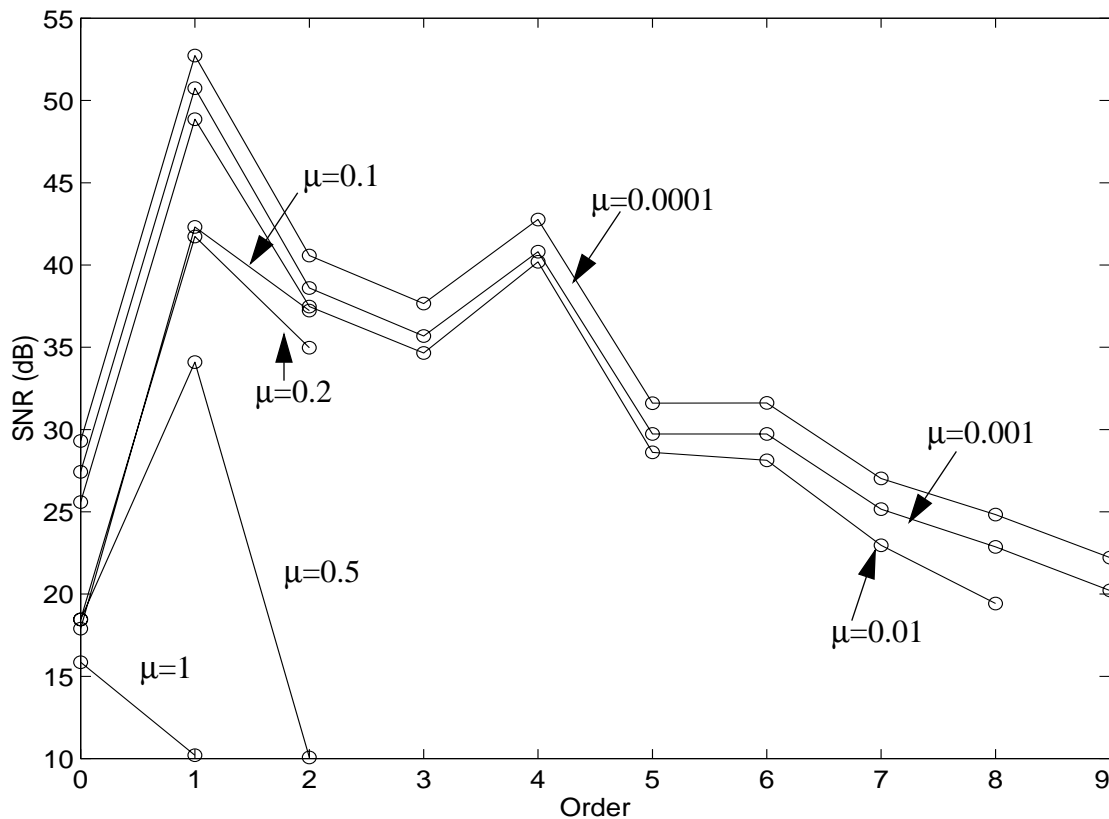


Fig. 4.12 SNR versus orders of adaptive filters (Experimental)

order of the adaptive filter is more than 5, the performance degrades because of over-estimation and the noise in the coefficients.

#### 4.4.5 Location of Interference

The effect of coefficient mismatch was analyzed in section 2.4.2.2. The frequency response of the image rejection was shown in Fig. 2.13 of Chapter 2. It can be seen that the worst of the image rejection happens at the image frequency of the band center. The complex sigma delta modulator used in the example is an improved complex modulator. The improved modulator places one of the NTF notches in the image band to attenuate the image noise before it aliases into the desired signal band. The magnitude response of the modulator is shown in Fig. 3.4 of

chapter 3 .

Fig. 4.13 shows that when the improved modulator is used in the receiver, the coefficients

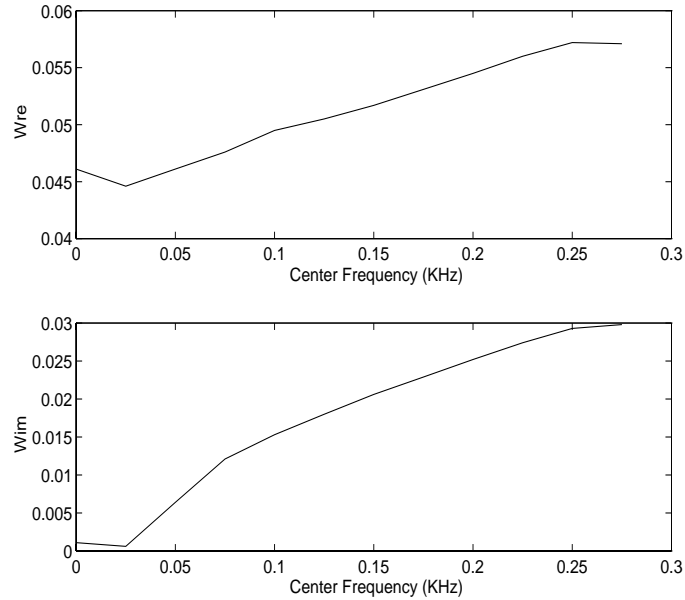


*Fig. 4.13 Coefficients of the adaptive filter with the image interference at different frequencies (Experimental)*

of the adaptive filter change as the frequency of the interference changes. As mentioned in 3.2.3, the output of the complex sigma delta modulator can be expressed as Eq. (3.10):

$$Y = GX + \Delta G_{diff} \bar{X} + HE + \Delta H_{diff} \bar{E}$$

where  $X$  is the input of the complex sigma delta modulator,  $E$  is the quantization noise,  $G$  is the STF (signal transfer function) and  $H$  is the NTF (noise transfer function). The frequency responses of its STF and NTF are shown in Fig. 4.2. When interference exists exactly at the image frequency, the error term  $\Delta G_{diff} \bar{X}$  plays the main role because it can be seen from Fig. 4.2 that the NTF has a notch at the image frequency, and STF has a small gain at that frequency. So the adaptive filter is mainly modeling  $\Delta G_{diff}$ . As the interference moves away from the image

frequency, the influence of the error term  $\Delta H_{diff} \bar{E}$  gets stronger and can not be ignored for large frequency offsets. The coefficient increases as the interference moves away from the image frequency.

## 4.5 Conclusion

In this chapter, an implementation of the adaptive mismatch cancellation system was presented. This system is included in a complex single IF receiver. The implementation of the receiver was also introduced. The analog front end was implemented with BICMOS technology by Macedo [Swaminathan97], and the complex sigma delta modulator was implemented by Swaminathan [Swaminathan97]. Decimation filters and the adaptive mismatch cancellation system were implemented using a Xilinx FPGA and an Analog Devices ADSP21020 floating-point signal processor respectively.

Comparison of results with and without the adaptive mismatch cancellation system shows that more than 20 dB SNR improvement can be achieved. Dramatic improvement in magnitude responses and eye diagrams is readily visible. The results also show the adaptation characteristics of the new algorithm.

These results prove that for a single IF complex receiver, the performance degradation due to the I/Q path imbalance can be corrected by adding the new algorithm and system. The SNR improvement can reach 20 dB. The work demonstrated that our algorithm and system can be implemented in real-time.

## *Chapter 5*

---

### *Conclusion and Future Work*

#### **5.1 Summary**

A novel approach for controlling the I/Q channel mismatch has been presented in this thesis. Results from simulations and a real time implementation indicated the feasibility of a complex single IF receiver using a real time DSP system to attenuate the image noise due to the I/Q channel imbalance.

The structure of a complex single IF receiver was introduced in chapter 2. It suffers from image aliasing due to the imbalance of the I and Q paths. This imbalance can be introduced not only by the analog quadrature mixer but also by the complex sigma delta modulator. The performance degradation of the receiver due to the image aliasing has been studied in detail in chapter 2.

A novel DSP solution was presented in chapter 3. The novel adaptive mismatch cancellation system is based on a new complex LMS algorithm and a modified classic adaptive noise cancellation system. The new algorithm adds another symmetric complex filter to separate the desired signal and the image interference, and this can achieve resulting good performance. Simulation results shown in chapter 3 demonstrated the performance of the new system.

Chapter 4 presented a real time implementation of the novel system using a DSP platform.

Experimental results further prove the feasibility of the adaptive mismatch cancellation system. This means a complex single IF receiver can get enough dynamic range even though there is imbalance between the I and Q paths. An extended application for this system in double sampling systems was presented.

## 5.2 Conclusion

This thesis presented a novel DSP solution for I/Q channel mismatch problems in complex single IF receivers. This thesis has shown how to use a modified adaptive algorithm to improve the SNR and enlarge the dynamic range without tedious correction procedures.

Image aliasing due to I/Q channel mismatch is always a big concern in realizing quadrature IF receivers. The imbalance between I and Q channels exists along signal paths in subsystems such as the mixer and the modulator. In this thesis quadrature systems were represented as complex systems, therefore, the theories of complex filters and transfer functions have been introduced.

The new DSP system proposed in this thesis uses a simple but powerful complex adaptive algorithm to correct the degradation due to the mismatch. A real time implementation of the new adaptive mismatch cancellation system and a whole complex single IF receiver were presented. The proposed system was implemented in a commercial DSP chip with an interface implemented on the Xilinx FPGA to the receiver front end.

Results from simulations and real time tests proved the new DSP system is feasible and stable. With the system, the SNR can reach 50 dB, as compared to about 30 dB without it. The dramatic improvement is visible in the magnitude responses and eye diagrams of the I/Q signals. Adaptation characteristics of the new algorithm were also shown in the results.

## 5.3 Future Work

### 5.3.1 ASIC Approach

As mentioned in section 4.3, the clock rate of the receiver shown in Fig. 4.1 is limited by the speed of Xilinx FPGA. Using ASIC technology, we can integrate the whole system in one chip.

### 5.3.2 N-path Systems

The algorithm and system to compensate the mismatch effects in complex circuits presented in this thesis can also be applied to double sampled circuits. It is very easy to further extend to N-path systems.

The N-path system model is shown in Fig. 5.1.  $\phi_1, \phi_2, \dots, \phi_N$  are N different phases of the

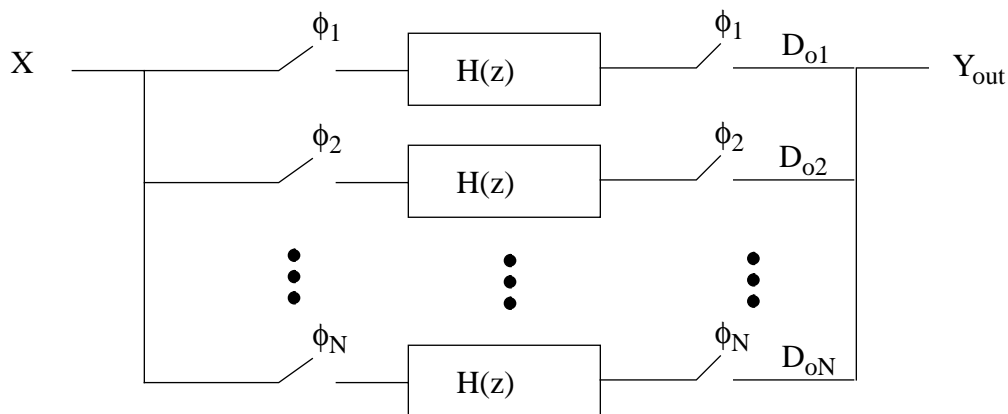


Fig. 5.1 N-path system model

clock. The output of the system  $Y_{out}$  can be expressed as

$$Y_{out} = \begin{bmatrix} 1 & 1 & \dots & 1 \end{bmatrix} \begin{bmatrix} D_{o1} \\ D_{o2} \\ \dots \\ D_{oN} \end{bmatrix} \quad \text{Eq. (5.1)}$$

We need  $N - 1$  noise references to extend the double sampling system to the N-path case. We can easily generate N-1 reference signals from combinations of  $D_{o1}, D_{o2}, \dots, D_{oN}$  which are orthogonal to  $Y_{out}$  using Walsh functions [Proakis89]. The problem is to get N vectors that are orthogonal to  $\begin{bmatrix} 1 & 1 & \dots & 1 \end{bmatrix}$ . The complex LMS algorithm can be easily extended to an N-path LMS algorithm which is widely used in beamforming systems.

Finally, we can see that the novel adaptive mismatch cancellation system presented in this thesis is not only a powerful solution for the I/Q channel mismatch problem in complex IF receivers but can be used to correct errors in a variety of multi-path analog structures. It makes a whole class of parallel analog approaches to high-speed operation practical.

---

## *References*

- [Abdennadher92] S. Abdennadher et al., "Adaptive Self-calibrating Delta-Sigma Modulators," *Electronics Letters*, vol.28, pp1288-1289, Jul. 1992.
- [ADSPa] *ADSP 21020 Evaluation Board Manual*, Analog Device Inc., 1992.
- [ADSPb] *ADSP 21020 User's Manual*, Analog Device Inc., 1992.
- [Allen85] Raymond H. Allen. "Complex Analog Filter Obtained from Shifted Lowpass Prototypes." Master Thesis, University of Toronto, 1985.
- [Aziz95] Pervez M. Aziz et al."Performance of Complex Noise Transfer functions in Bandpass and Multi Band Sigma Delta Systems" *Proceedings of the 1995 IEEE ISCAS*, vol.1, pg.641, May 1995.
- [Bazarjani96] Seyfi Bazarjani, "Mixed Analog-Digital Design Considerations in Deep Submicron CMOS Technologies.", Ph.D thesis, Carleton University, 1996.
- [Bollinger90] U. Bollinger and W. Vollenweider, "Some Experiments on Direct-Conversion Receivers," *Proceedings of the IEE Fifth International Conference on Radio Receivers and Associated Systems*, pg. 40-44, July 1990.
- [Candy92] James C.Candy, Gabor C. Temes."Oversampling Methods for A/D and D/A Conversion.", IEEE Press, 1992.
- [Carlson86] Carlson, A.B. *Communication Systems*, 3rd Edition New York, NY: McGraw Hill Book Co. 1986.
- [Cauwenberghs96] G.Cauwenberghs and G.C. Temes, "Adaptive Calibration of Multiple Quantization Oversampled A/D Converters," *IEEE Proc. ISCAS'96*,

- 
- Atlanta, pg.512-516, May 1996.
- [Churchill81] Churchill, F.E., Ogar, G.W., and Thompson, B.J.” The Correction of I and Q Errors in a Coherent Processor,” IEEE Trans. on Aerospace and Electronic Systems. Vol. AES-17, Jan. 1981, pg. 131-137.
- [Compernelle95] Dirk Van Compernelle and Stefaan Van Gerven. “Signal Separation in a Symmetric Adaptive Noise Canceler by Output Decorrelation”, IEEE Transactions on signal processing, vol.43, pg.1602, July 1995.
- [Crochiere83] Ronald E. Crochiere and Lawrence R. Rabiner, *Multi-rate Digital Signal Processing*, Prentice Hall, NJ, 1983.
- [Grebene84] A.Grebene. *Bipolar and MOS Analog Integrated Circuit Design*, Wiley, 1984.
- [Hogenauer81] E.B. Hogenauer, “An Economical Class of Digital Filters for Decimation and Interpolation,” IEEE Trans. Acoustic, Speech, Signal Processing, Vol. ASSP-29, Pg. 155-162, Apr. 1981.
- [Hurst90] P.J.Hurst and W.J. McIntyre, “Double Sampling in Switched-Capacitor Delta-Sigma A/D Converter.” Proceedings of IEEE International Symposium on Circuit and Systems, 1990. pg. 902-905.
- [Jantzi94] S. Jantzi, et al.”Complex Bandpass Sigma-Delta Converter for Digital Radio.” Proceedings of the 1994 IEEE ISCAS, vol.5, pg.453, May 1994.
- [Jantzi96] S.A.Jantzi, et al. ”The Effects of Mismatch in Complex Bandpass Sigma-Delta Modulators.” Proceedings of the ISCAS 1996,pg.227,May 1996.
- [Kiaei93] S.Kiaei et al., “Adaptive Digital Correction for Dual Quantization Sigma Delta Modulators,” IEEE Proc. ISCAS’93, Chicago, IL, pg.1228-1230,

- 
- May 1993.
- [Kwentus97] Alan Y. Kwentus et al. "Application of Filter Sharpening to Cascaded Integrator-Comb Decimation Filters", *IEEE Trans. on Signal Processing*, Vol.45, pg.457, Feb.1997.
- [Lee94] Edward A. Lee and David G. Messerschmitt, *Digital Communication*, 2nd Edition, Norwell, Massachusetts: Kluwer Academic Publishers 1994.
- [Leon94] Alberto Leon-Garcia, *Probability and Random Processes for Electrical Engineering*, Addison Wesley Publishing Company, 1994.
- [Long95] J.R.Long,et al. "A Low-Voltage Silicon Bipolar RF Front-End for PCN Receiver Applications." Proceedings of the 1995 ISSCC, pg.140, 1995.
- [Long96] J. R. Long, "A narrowband Radio Receiver Front-End for Portable Communications Applications" Ph.D. Thesis, Carleton University 1996.
- [Macedo96] J.Macedo, M.Copeland, P.Schvan."A 2.5GHz Monolithic Silicon Image Reject Filter." Proceedings of the IEEE CICC, 1996.
- [MATLABa] *MATLAB for Sun Workstations, User's Guide*, The Math Work Inc. 1990
- [MATLABb] *MATLAB for Sun Workstations, Simulink Manual*, The Math Work Inc. 1992.
- [Oppenheim83] A.V. Oppenheim and A.S. Willsky, *Signals and Systems*, Prentice Hall, Englewood Cliffs, NJ, 1983.
- [Oppenheim89] A.V. Oppenheim and R.W. Schaffer, *Discrete-Time Signal Processing*, Prentice Hall, Englewood Cliffs, NJ,1989.
- [Oppenheim94] Alan V. Oppenheim et al. *Computer-Based Exercises for Signal Processing Using MATLAB*. Prentice Hall, Englewood Cliffs, NJ, 1994.

- 
- [Proakis89] John G. Proakis, *Digital Communications*, Second Edition, McGraw-Hill, 1989.
- [Rappaport96] Theodore S. Rappaport, *Wireless Communications, Principles and Practice*. Prentice Hall, Upper Saddle River, NJ, 1996.
- [Sabin95] William E. Sabin and Edgar O. Schoenike, *Single Sideband Systems and Circuits*, McGraw Hill, 1995.
- [Saulnier90] Gary J. Saulnier et al. "A VLSI Demodulator for Digital RF Network Applications: Theory and Results", *IEEE Trans. on Selected Areas in Communications*, Vol.8, pg1500, October 1990.
- [Schreier90] R.Schreier and Martin Snelgrove. "Decimation for Bandpass Sigma Delta Analog to Digital Conversion." *Proceedings of the 1990 ISCAS*, pg.1801,1990.
- [Schultes90] G.Schultes et al., "Basic Performance of a Direct-Conversion DECT Receiver," *Electronics Letters*, vol.26, no.21, pg. 1746-1748, Oct.1990.
- [Schwartz90] Mischa Schwartz. *Information Transmission, Modulation and Noise*. 4th Edition: McGraw Hill Book Co. 1990
- [Shenoi95] Kishan Shenoi, *Digital Signal Processing in Telecommunications*, Prentice Hall, Upper Saddle River, NJ, 1995.
- [Snelgrove82] W. Martin Snelgrove, "Intermediate Function Synthesis:", Ph.D. thesis, University of Toronto, 1982.
- [Snelgrove97] W. Martin Snelgrove and Li Yu, preliminary disclosure of the patent is on file. August, 1997.
- [Stetzler95] T. Stetzler et. al. "A 2.7V to 4.5V Single-Chip GSM Transceiver RF

- 
- Integrated Circuit.” Proceedings of the 1995 ISSCC, pg. 150-151, 354, 114-115.
- [Swaminathan97] Ashok Swaminathan, “A Single-IF Receiver Architecture Using a Complex Sigma Delta Modulator”, Master thesis, Carleton University, 1997.
- [Swaminathan96a] Ashok Swaminathan, Martin Snelgrove et al.”A Monolithic Complex Sigma-delta Modulator for Digital Radio.” 1996 IEEE-CAS Region 8 Workshop on Analog and Mixed IC Design Proceedings, pg.83, September 1996.
- [Swaminathan96b] Ashok Swaminathan, Martin Snelgrove, “A Single-IF IR Radio for PCS.” Proceedings of the Biennial Symposium on Communications, Kingston, Ontario, 1996.
- [Trees68] Van Trees, H.L. *Detection, Estimation, and Modulation Theory.*, Part I, New York, NY: John Wiley & Sons, 1968.
- [Tsui95] James Tsui, *Digital Techniques for Wideband Receivers.* Artech House, 1995.
- [Vieria95] S.A. Vieria-Ribeiro, “Single-IF DECT Receiver Architecture Using a Quadrature Sub-Sampling Band-pass Sigma-Delta Modulator.” M.Eng Thesis, Carleton University, 1995.
- [Widrow85] B.Widrow et al. *Adaptive Signal Processing.* Prentice-Hall, 1985.
- [Widrow71] Bernard Widrow et al.”The Complex LMS Algorithm.” *Proceedings of IEEE*, pg.719, April 1971.
- [Wiesbauer96] A. Wiesbauer and G.C.Temes, “On-Line Digital Compensation of Analog

- Circuit Imperfections for Cascaded Sigma Delta Modulators”,  
Proceedings of the 1996 IEEE-CAS Region 8 Workshop on Analog and  
Mixed IC Design, pg.92, Sept.1996.
- [Yang92] Y.Yang et al., “On-line Adaptive Digital Correction for Dual-quantisation  
Delta Sigma Modulators,” Electronics Letters, vol.28, pg.1511-1513,  
July. 1992.
- [Yang94] H.K. Yang and E.I. El-Masry, “A Novel Double Sampling Technique for  
Delta Sigma Modulators.” Proceedings of 37th Midwest Symposium on  
Circuits and Systems. Lafayette, Louisiana, August 1994.
- [Yang96] H.K. Yang and W.Martin Snelgrove, “ High Speed Polyphase CIC  
Decimation Filters” ISCAS 96.
- [Yu97] Li Yu and Martin Snelgrove, “Mismatch Cancellation for Complex  
Bandpass Sigma Delta Modulators.” presented at 40th Midwest  
Symposium on Circuits and Systems. Sacramento, CA, August 1997.

## APPENDIX A

### Assembly Code for the Novel Adaptive Algorithm

{ CLMS.ASM performs the following Complex LMS algorithm implemented with a novel FIR filter structure

```

*****
* 1) yre(n)= wre.ure-wim.uim ( . = dot_product),
*   yim(n)= wre.uim+wre.uim ( . = dot_product),
*       yre(n)+j*yim(n)= FIR filter output
* where wre= [wre0(n) wre1(n) ... wreN-1(n)]= filter weights
* where wim= [wim0(n) wim1(n) ... wimN-1(n)]= filter weights
*
* and
* ure= [ure(n) ure(n-1) ... ure(n-N+1)]= input samples
* uim= [ure(n) ure(n-1) ... ure(n-N+1)]= input samples
* n= time index, N= number of filter weights (taps)
* 2) ere(n)= dre(n)-yre(n), ere(n)+j*eim(n)= error signal
*   eim(n)= dim(n)-yim(n), dre(n)+j*dim(n)= desired output
* 3) wire(n+1)= wire(n)+STEPSIZE1*ere(n)*ure(n-i)
*       +STEPSIZE1*eim(n)*uim(n-i), 0 =<i<= N-
*   wiim(n+1)= wiim(n)-STEPSIZE2*ere(n)*ure(n-i)
*       +STEPSIZE2*eim(n)*uim(n-i), 0 =<i<= N-
*****

```

Written by: Li Yu, March 18 1997

Calling parameters (inputs):

f0= ure(n) = input sample  
f1= uim(n) = input sample  
f2= dre(n) = desired output  
f3= dim(n) = desired output

Altered registers:

f0, f1, f2, f3, f4, f5, f6, f7, f8, f9, f10, f11, f12, f13

Results (outputs):

f4= ere(n)= filter error signal  
f5= eim(n)= filter error signal  
i8 -> Program Memory Data buffer of the filter weights real part  
i9 -> Program Memory Data buffer of the filter weights imag part

```

}

#define TAPS      2
#define STEPSIZE1 0.0005
#define STEPSIZE2 0.0005

.GLOBAL lms_init, lms_alg;

.SEGMENT/DM  dm_sram;
.VAR  xd[2*TAPS];
.VAR  yd[2*TAPS];
.VAR  u1[2*TAPS];
.VAR  u2[2*TAPS];
.VAR  w1d[2*TAPS];
.VAR  w2d[2*TAPS];
.ENDSEG;

.SEGMENT/PM  pm_data;
.VAR  wrep[TAPS];
.VAR  wimp[TAPS];
.ENDSEG;

.SEGMENT/PM  pm_sram;
lms_init:  b0=xd;
b1=yd;
m0=1;
l0=2*TAPS;
l1=l0;
m1=-3;{circular delay line buffer}
b2=u1;
b3=u2;
m2=1;
l2=2*TAPS;
l3=l1;
m3=-3;{circular delay line buffer}
b6=w1d;
b7=w2d;
m6=1;
l6=2*TAPS;
l7=l6;
m7=-1;
f0=0.0;
lcntr=2*TAPS, do clear_bufs until lce;
dm(i0,-1)=f0;
dm(i1,-1)=f0;
dm(i6,1)=f0;
dm(i7,1)=f0;
dm(i2,-1)=f0;
clear_bufs:  dm(i3,-1)=f0; {clear delay line & weights}
rts;

lms_alg:  dm(i0,m0)=f0;

```

```

dm(i0,m1)=f1;{store x(n) in delay line}
f8=dm(i6,m6);
f9=dm(i6,m6);{f8=w1re0, f9=w1im0(n)}
f10=f0*f8;
f11=f1*f9;      {f10= xre(n)*w1re0(n)}
f6=f10-f11;     {f11= xim(n)*w1im0(n)}
f6=f2-f6;      {yre-f6}
f12=f0*f9;
f13=f1*f8;     {f12= xre(n)*w1im0(n)}
f7=f12+f13;    {f13= xim(n)*w1re0(n)}
f7=f3-f7;     {yim-f7}

dm(i1,m0)=f2;
dm(i1,m1)=f3;{store y(n) in delay line}
f4=dm(i7,m6);
f5=dm(i7,m6);{f4=w2re0, f5=w2im0(n)}
f10=f2*f4;
f11=f3*f5;     {f10= yre(n)*w2re0(n)}
f14=f10-f11;   {f11= yim(n)*w2im0(n)}
f14=f0-f14;    {xre-f14}
f12=f3*f5;
f13=f2*f4;     {f12= yre(n)*w2im0(n)}
f15=f12+f13;   {f13= yim(n)*w2re0(n)}
f15=f1-f15;    {xim-f15}

lcntr=TAPS-1, do macs until lce;
f0=dm(i0,m0);
f1=dm(i0,m1);{f0,f1=x(n-i)}
f8=dm(i6,m6);
f9=dm(i6,m6);{f8=w1rei, f9=w1imi(n)}
f10=f0*f8;
f11=f1*f9;     {f10= xre(n-i)*w1rei(n)}
f10=f10-f11;   {f11= xim(n-i)*w1imi(n)}
f6=f6-f10;
f12=f0*f9;
f13=f1*f8;     {f12= xre(n-i)*w1imi(n)}
f12=f12+f13;   {f13= xim(n-i)*w1rei(n)}
f7=f7-f12;

f2=dm(i1,m0);
f3=dm(i1,m1);{f2,f3=y(n-i)}
f4=dm(i7,m6);
f5=dm(i7,m6);{f4=w2rei(n), f5=w2imi(n)}
f10=f2*f4;
f11=f3*f5;     {f10= yre(n-i)*w2rei(n)}
f10=f10-f11;   {f11= yim(n-i)*w2imi(n)}
f14=f14-f10;

f12=f3*f5;
f13=f2*f4;     {f12= yre(n-i)*w2imi(n)}
f12=f12+f13;   {f13= yim(n-i)*w2rei(n)}
macs: f15=f15-f12;
{u1re=f6= yre(n)-xre(n-i)*w1rei(n)+xim(n-i)*w1imi(n)}
{u1im=f7= yim(n)-xim(n-i)*w1rei(n)-xre(n-i)*w1imi(n)}

```

---

```

{u2re=f14= xre(n)-yre(n-i)*w2rei(n)+yim(n-i)*w2imi(n)}
{u2im=f15= xim(mn)-xim(n-i)*w2rei(n)-yre(n-i)*w2imi(n)}

dm(i2,m2)=f6;
dm(i2,m7)=f7;{store u1(n) in delay line}

dm(i3,m2)=f14;
dm(i3,m3)=f15;{store u2(n) in delay line}

dm(i4,m4)=f6;
dm(i4,m4)=f7;
dm(i5,m4)=f14;
dm(i5,m4)=f15;

f0=STEPSSIZE1;
f1=STEPSSIZE2;

f2=f0*f6;
f3=f0*f7; {f2= STEPSSIZE1*u1re(n),f3= STEPSSIZE1*u1im(n)}
f6=f1*f6;
f7=f1*f7; {f6= STEPSSIZE2*u1re(n),f7= STEPSSIZE2*u1im(n)}

f0=f14;
f1=f15;{f0,f1=u2(n)}

f10=f2*f0;
f11=f3*f1; {f10= STEPSSIZE1*u1re(n)*u2re(n)}
f10=f10+f11; {f11= STEPSSIZE1*u1im(n)*u2im(n)}
f12=f6*f1;
f13=f7*f0; {f12= STEPSSIZE2*u1re(n)*u2im(n)}
f12=f13-f12; {f13= STEPSSIZE1*u1im(n)*u2re(n)}

f8=dm(i6,m6);
f9=dm(i6,m7);{f8=w1re0(n), f9=w1im0(n)}
f8=f8+f10;
f9=f9+f12; {f8= w1re0(n+1) f9= w1im0(n+1)}
dm(i6,m6)=f8;
dm(i6,m6)=f9;{f8=w1re0(n), f9=w1im0(n)}

f0=STEPSSIZE1;
f1=STEPSSIZE2;

f4=f0*f14;
f5=f0*f15; {f4= STEPSSIZE1*u2re(n),f5= STEPSSIZE1*u2im(n)}
f14=f1*f14;
f15=f1*f15; {f14= STEPSSIZE2*u2re(n),f15= STEPSSIZE2*u2im(n)}

f0=dm(i2,m2);
f1=dm(i2,m3);{f0,f1=u1(n)}

f10=f4*f0;
f11=f5*f1; {f10= STEPSSIZE1*u2re(n)*u1re(n)}
f10=f10+f11; {f11= STEPSSIZE1*u2im(n)*u1im(n)}

```

---

```

f12=f14*f1;
f13=f15*f0; {f12= STEPSIZE2*u2re(n)*u1im(n)}
f12=f13-f12; {f13= STEPSIZE2*u2im(n)*u1re(n)}

f8=dm(i7,m6);
f9=dm(i7,m7);{f8=w2re0(n), f9=w2im0(n)}
f8=f8+f10;
f9=f9+f12; {f8= w2re0(n+1) f9= w2im0(n+1)}
dm(i7,m6)=f8;
dm(i7,m6)=f9;{f8=w2re0(n), f9=w2im0(n)}

lcntr=TAPS-1, do update_weights until lce;

f0=dm(i3,m2);
f1=dm(i3,m3);{f0,f1=u2(n-i)}

f10=f2*f0;
f11=f3*f1; {f10= STEPSIZE1*u1re(n)*u2re(n-i)}
f10=f10+f11; {f11= STEPSIZE1*u1im(n)*u2im(n-i)}
f12=f6*f1;
f13=f7*f0; {f12= STEPSIZE2*u1re(n)*u2im(n-i)}
f12=f13-f12; {f13= STEPSIZE1*u1im(n)*u2re(n-i)}

f8=dm(i6,m6);
f9=dm(i6,m7);{f8=w1rei(n), f9=w1imi(n)}
f8=f8+f10;
f9=f9+f12; {f8= w1rei(n+1) f9= w1imi(n+1)}
dm(i6,m6)=f8;
dm(i6,m6)=f9;{f8=w1rei(n), f9=w1imi(n)}

f0=dm(i2,m2);
f1=dm(i2,m3);{f0,f1=u1(n-i)}

f10=f4*f0;
f11=f5*f1; {f10= STEPSIZE1*u2re(n)*u1re(n-i)}
f10=f10+f11; {f11= STEPSIZE1*u2im(n)*u1im(n-i)}
f12=f14*f1;
f13=f15*f0; {f12= STEPSIZE2*u2re(n)*u1im(n-i)}
f12=f13-f12; {f13= STEPSIZE2*u2im(n)*u1re(n-i)}

f8=dm(i7,m6);
f9=dm(i7,m7);{f8=w2rei(n), f9=w2imi(n)}
f8=f8+f10;
f9=f9+f12; {f8= w2rei(n+1) f9= w2imi(n+1)}
dm(i7,m6)=f8;
update_weights: dm(i7,m6)=f9;{f8=w2rei(n), f9=w2imi(n)}

{ f8= wrei(n),f9=wimi(n)}
f0=dm(i0,m0);
f1=dm(i0,m0);
f2=dm(i1,m0);
f3=dm(i1,m0);
f0=dm(i2,m0);
f1=dm(i2,m0);

```

```
rts(db);  
f2=dm(i3,m0);  
f3=dm(i3,m0);  
  
.ENDSEG;
```

---

## APPENDIX B

---

### *Coefficient Mismatch Effects in Single-pole Complex Filters*

The real and imaginary part of the output can be expressed as

$$V_{\text{out},r} = \frac{1}{z-1} [V_{\text{in},r} + (a + \varepsilon_a - 1)V_{\text{out},r} - bV_{\text{out},i}] \quad \text{Eq. (C.2)}$$

$$V_{\text{out},i} = \frac{1}{z-1} [V_{\text{in},i} + (a-1)V_{\text{out},i} + (b + \varepsilon_b)V_{\text{out},r}] \quad \text{Eq. (C.3)}$$

From Eq. (C.2) and Eq. (C.3),  $V_{\text{out},r}$  and  $V_{\text{out},i}$  can be expressed as

$$V_{\text{out},r} = \frac{(z-a)V_{\text{in},r} - bV_{\text{in},i}}{(z-a-\varepsilon_a)(z-a) + b(b+\varepsilon_b)}$$

$$V_{\text{out},i} = \frac{(b+\varepsilon_b)V_{\text{in},r} + (z-a-\varepsilon_a)V_{\text{in},i}}{(z-a-\varepsilon_a)(z-a) + b(b+\varepsilon_b)}$$

$$V_{\text{out},r} + jV_{\text{out},i} = \frac{z - (a + \varepsilon_a/2) + j(b + \varepsilon_b/2)}{(z-a-\varepsilon_a)(z-a) + b(b+\varepsilon_b)} (V_{\text{in},r} + jV_{\text{in},i})$$

$$+ \frac{\varepsilon_a/2 + j\varepsilon_b/2}{(z-a-\varepsilon_a)(z-a) + b(b+\varepsilon_b)} (V_{\text{in},r} - jV_{\text{in},i})$$

$$T_{\text{nom}} = \frac{z - (a + \varepsilon_a/2) + j(b + \varepsilon_b/2)}{(z-a-\varepsilon_a)(z-a) + b(b+\varepsilon_b)} \approx \frac{1}{z-a-jb}$$

and

$$\begin{aligned}
\Delta T_{diff} &= \frac{\epsilon_a/2 + j\epsilon_b/2}{(z-a-\epsilon_a)(z-a) + b(b+\epsilon_b)} \\
&= \frac{\epsilon_a/2 + j\epsilon_b/2}{(z-a-\epsilon_a/2)^2 + (b+\epsilon_b/2)^2 - (\epsilon_a/2)^2 - (\epsilon_b/2)^2} \\
&\approx \frac{(\epsilon_a + j\epsilon_b)/2}{(z-a-j\sigma)(z-a+j\sigma)}
\end{aligned}$$

where  $\sigma^2 = b^2 - (\epsilon_a/2)^2 - (\epsilon_b/2)^2$

## APPENDIX C

### *Power Inversion*

Fig. C.1 shows an adaptive noise canceler which has the reference input containing signal

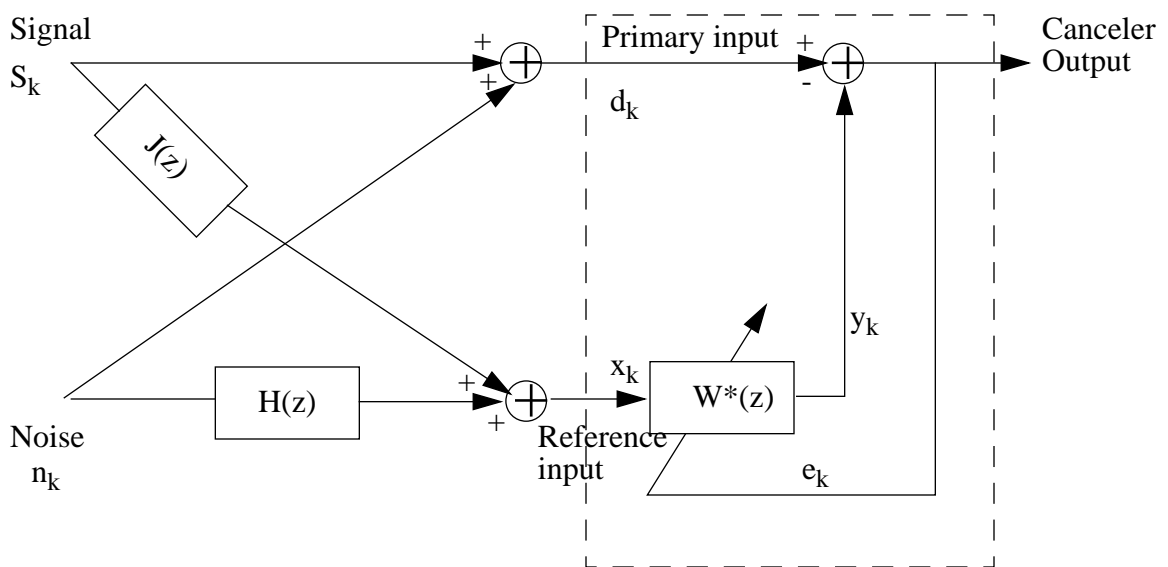


Fig. C.1 Adaptive noise canceler with signal components leaking into the reference input.

components and the primary and reference inputs containing additive correlated noises. The signal components leaking into the reference input are assumed to be propagated through a channel with the transfer function  $J(z)$ .

Suppose the input signal and noise power spectra in Fig. C.1 are  $\Phi_{ss}(z)$  and  $\Phi_{nn}(z)$ , respectively. The spectrum of the reference input, which is identical to the spectrum of the input

$x_k$  to the adaptive filter, is thus

$$\Phi_{xx}(z) = \Phi_{ss}(z)|J(z)|^2 + \Phi_{nn}(z)|H(z)|^2 \quad \text{Eq. (C.4)}$$

The cross-spectrum between the reference and primary inputs, identical to the cross-spectrum between the filter's input  $x_k$  and desired response  $d_k$ , is similarly

$$\Phi_{xd}(z) = \Phi_{ss}(z)J(z^{-1}) + \Phi_{nn}(z)H(z^{-1}) \quad \text{Eq. (C.5)}$$

When the adaptive process has converged, the unconstrained Wiener transfer function of the adaptive filter  $W^*(z) = \frac{\Phi_{xd}(z)}{\Phi_{xx}(z)}$ , is thus

$$W^*(z) = \frac{\Phi_{ss}(z)J(z^{-1}) + \Phi_{nn}(z)H(z^{-1})}{\Phi_{ss}(z)|J(z)|^2 + \Phi_{nn}(z)|H(z)|^2} \quad \text{Eq. (C.6)}$$

The first objective of our analysis is to find the signal-to-noise density ratio  $\rho_{out}(z)$ , at the noise canceler output. The transfer function of the propagation path from the signal input to the noise canceler output is  $1 - J(z)W^*(z)$  and that of the path from the noise input to the canceler output is  $1 - H(z)W^*(z)$ . The spectrum of the signal component in the output is thus

$$\begin{aligned} \Phi_{ss_{out}}(z) &= \Phi_{ss}(z) |1 - J(z)W^*(z)|^2 \\ &= \Phi_{ss}(z) \left| \frac{[H(z) - J(z)]\Phi_{nn}(z)H(z^{-1})}{\Phi_{ss}(z)|J(z)|^2 + \Phi_{nn}(z)|H(z)|^2} \right|^2 \end{aligned} \quad \text{Eq. (C.7)}$$

and that of the noise component is similarly

$$\Phi_{nn_{out}}(z) = \Phi_{nn}(z) |1 - H(z)W^*(z)|^2$$

$$= \Phi_{nn}(z) \left| \frac{[J(z) - H(z)]\Phi_{ss}(z)J(z^{-1})}{\Phi_{ss}(z)|J(z)|^2 + \Phi_{nn}(z)|H(z)|^2} \right|^2 \quad \text{Eq. (C.8)}$$

The output signal-to-noise density ratio is thus

$$\begin{aligned} \rho_{out}(z) &= \frac{\Phi_{ss}(z)}{\Phi_{nn}(z)} \left| \frac{\Phi_{nn}(z)H(z^{-1})}{\Phi_{ss}(z)J(z^{-1})} \right|^2 \\ &= \frac{\Phi_{nn}(z)|H(z)|^2}{\Phi_{ss}(z)|J(z)|^2} \end{aligned} \quad \text{Eq. (C.9)}$$

The output signal-to-noise density ratio can be conveniently expressed in terms of the signal-to-noise density ratio at the reference input,  $\rho_{ref}(z)$ , as follows. The spectrum of the signal component in the reference input is

$$\Phi_{ss_{ref}}(z) = \Phi_{ss}(z)|J(z)|^2 \quad \text{Eq. (C.10)}$$

and that of the noise component is similarly

$$\Phi_{nn_{ref}}(z) = \Phi_{nn}(z)|H(z)|^2 \quad \text{Eq. (C.11)}$$

The signal-to-noise density ratio at the reference input is thus

$$\rho_{ref}(z) = \frac{\Phi_{ss}(z)|J(z)|^2}{\Phi_{nn}(z)|H(z)|^2} \quad \text{Eq. (C.12)}$$

The output signal-to-noise density ratio (Eq. (C.9)) is, therefore,

$$\boxed{\rho_{out}(z) = \frac{1}{\rho_{ref}(z)}} \quad \text{Eq. (C.13)}$$

This result is exact and somewhat surprising. It shows that, assuming the adaptive solution to be unconstrained and the noises in the primary and reference inputs to be mutually correlated,

the signal-to-noise density ratio at the noise canceler output is simply the reciprocal at all frequencies of the signal-to-noise density ratio at the reference input. The process in Eq. (C.13) called power inversion.